X-RAY PHOTOELECTRON SPECTROSCOPIC STUDIES OF DILUTE TIN ALLOYS

A THESIS

SUBMITTED TO THE

UNIVERSITY OF POONA

FOR THE DEGREE OF

DOCTOR OF PHILOSOPHY

IN CHEMISTRY

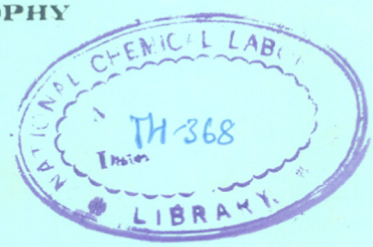

BY

R. I. HEGDE
M. Sc.

PHYSICAL CHEMISTRY DIVISION
NATIONAL CHEMICAL LABORATORY
POONA 411 008. (INDIA)

1983

Certified that the work incorporated in the thesis 'X-RAY PHOTOELECTRON SPECTROSCOPIC STUDIES OF DILUTE TIN ALLOYS' submitted by R.I. HEGDE has been carried out under my supervision. Such materials as have been obtained from other sources are duly acknowledged in the thesis.

[Dr. A.P.B. Sinha]
Supervisor

A C K N O W L E D G E M E N T

It is a pleasure to acknowledge my profound gratitude to Dr. A.P.B. Sinha, F.N.A., Distinguished Scientist, National Chemical Laboratory, Poona, for the immense help, guidance and constant encouragement offered to me throughout the course of my research.

It will be out of place if I don't record my high sense of appreciation for the invaluable assistance rendered by Dr. S. Badrinarayanan and Dr. S.R. Sainkar.

I am thankful to my young colleagues, friends and in particular to Mr. S.M. Joshi for their help and willing cooperation during the course of my research work.

Finally I end with a note of grateful thanks to the Council of Scientific and Industrial Research, New Delhi, for the award of Research Fellowship, and to the Director, National Chemical Laboratory, Poona, for allowing me to submit this investigation in the form of a Ph.D. thesis.

RIegde

[R.I. Hegde]
M.Sc.

Poona 411008
MARCH 1983.

DEDICATED TO

MY PARENTS

AND

YAJI BROTHERS

C O N T E N T S

contd. ...

Conts. ...

Contd. ...

***

CHAPTER I

INTRODUCTION

[A] STATEMENT OF THE PROBLEM

X-ray photoelectron spectroscopy (XPS) or electron spectroscopy for chemical analysis (ESCA) has proved to be a powerful tool for studying the electronic structure of metals and alloys[1]. An important property of the electron spectrum is that the core lines show binding energy shifts called 'Chemical Shifts', which depend on the chemical environment of the atom. Especially for molecular systems these chemical shifts have been found to be a very valuable tool for the study of the valence-electron structure. Various models[2-14] have been developed to calculate these shifts. Furthermore, for molecular systems a first interpretation of the chemical shift can often be given in terms of the so-called group shifts[15].

For metallic alloys relatively little has been done concerning the fundamental understanding and interpretation of the chemical shifts. One obvious complication is that these shifts in alloys are quite small ($\lesssim$ 2 eV) in contrast to molecular systems where they often are as large as 5-10 eV. Therefore, the accuracy of any model which is meant to deal with alloy chemical shifts must be very high. Secondly, there is no direct and simple relation between

the chemical shifts and properties such as charge transfer or electronegativity differences known so far.

We therefore undertook to investigate systematically the effects of different factors such as electronegativity, coordination number etc. on the chemical shift[16-18]. For this purpose, we selected several dilute tin alloys. Tin was selected because it shows relatively larger chemical shifts and is therefore easier to handle experimentally, and also its alloys fall in various crystal categories. It was also necessary in these cases to study only dilute alloys to avoid Sn-Sn proximity so that the effect of the host atoms surroundings could be clearly seen. We selected a group of alloys where the crystal structure was the same, but the electronegativities were different and another group where the electronegativity was the same but the coordination number was different. This way we hoped to see the effect of different contributing factors on the chemical shifts more clearly. A simple empirical model was developed to substantiate the correlations that we observed.

We used these alloy systems for surface segregation studies[19] as well. ESCA is a method well suited for the surface segregation studies because of its established surface sensitivity. Surface segregation in alloys[1] plays

a very vital role in industrially important subjects such as catalysis, corrosion, passivation, electrochemistry, optics and electronics. In addition, the understanding of physics of the surfaces and interfaces is of basic importance[20,21] in material sciences, because they have a severe influence on many materials properties as for example, catalytic activity of alloys, surface and grain boundary segregation in alloys, associated by the phenomena of temper brittleness, or intergranular corrosion cracking, to mention only a few.

At the present state of 'surface segregation theory', it is difficult to make predictions regarding this surface segregation in view of the profound influence of the impurities and the ambient gases etc. which can totally change the surface composition. So one has to rely on accurate experimental measurements. From this point of view ESCA plays a very important role in experimentally defining the surface composition under various experimental conditions.

The observed ESCA signal intensities can be converted into relative elemental concentrations provided that the so-called matrix effects[22-24] (e.g. changes in peak shape, sputtering, atomic density, surface roughness, escape depth and backscattering) do not cause significant errors. So to make it more quantitative an internal calibration method

is used. An investigation of the composition of three Cu-Sn intermetallics shows that the observed ESCA signal intensity ratio is proportional to the corresponding atomic ratio of the elements present, which would suggest that matrix effects do not play an important role, or to be precise, that any effect caused by a change in the chemical composition is neutralized when one considers the ratio of the ESCA signals. This result enables a quantitative determination of the average surface composition of dilute tin alloys under various conditions of treatment such as annealing in ultrahigh vacuum, cleaning by argon ion sputtering etc. Furthermore, the study of surface composition as a function of temperature predicts a quantitative approach to the surface segregation phenomena.

The results of these studies are presented in this thesis.

[B] ELECTRON SPECTROSCOPY

I. Introduction :

Electron spectroscopy has by now become a widely used technique for studying the properties of atoms, molecules, solids and surfaces. The technique involves the irradiation

of a sample with a beam of photons with energy $h\nu$. Electrons with a binding energy less than $h\nu$ are then ejected into vacuum, where their energy is carefully measured. The phenomenon was originally described as the 'photoelectric effect', since there is a measurable photo-current, but now a days the terms 'photoionization' or 'photoemission' are more commonly used. This phenomenon of 'photoemission' has a history dating back to Hertz's observation in 1887 of the initiation of sparks across a gap by exposure to ultraviolet light[25]. The explanation of the photo-electric effect by Einstein[26] and the early experimental studies by Robinson and Rutherford[27] on measuring β-ray spectra set the stage for major developments after the second World War. Although a lot of activity took place up to this period, major progress in studying the electronic structure of materials did not occur until the late sixties[28], primarily due to experimental difficulties.

The first application of photoemission to chemical analysis probably dates to Steinhardt[29] and Surfass[29,30], though this group never had the resources to bring the initial ideas to fruition. During the 1950s and 1960s, however, a major effort was undertaken by Professor Kai Siegbahn and his associates at Uppsala University in Sweden

to develop electron spectroscopy as a viable tool in electronic structure determination. With the development of strong X-ray sources to irradiate the sample, and the use of a high resolution β-ray spectrometer to measure the kinetic energy of the photoelectrons, to 1 part in 10^4 accuracy, these workers were able to work out many of the important applications of the technique. They then published their accumulated results in two definitive pieces of work devoted to solid state electronic structure[2] and to free molecule spectra[3]. Siegbahn also suggested in these studies that the acronym ESCA (electron spectroscopy for chemical analysis) referred to the specific application of the technique to problems of chemical interest.

With the rapid developments, both in technique and applications one can expect ESCA to rank among the top chemical research tools.

II. Basic Principles :

The basis of electron spectroscopy is the measurement of the energies of electrons emitted from a sample in vacuum following ionization by incident particles (usually photons or electrons). The binding energy of an electron, E_B, originating from a particular state is obtained by the

energy balance equation,

$$E_B = h\nu - E_k - \phi \qquad \ldots\ldots \quad [1.1]$$

where E_k is the kinetic energy of the electron, $h\nu$ is the energy of the incident particle and ϕ is the work function of the sample. For ionization by X-ray photons, the technique is known as X-ray photoelectron spectroscopy (XPS), while if the photons are in the vacuum ultraviolet region, the term ultraviolet photoelectron spectroscopy (UPS) is used. The UPS gives information only on the valence bands of solids, whereas XPS is a probe for both valence bands and core levels. In UPS one normally employs He I (21.22 eV) or He II (40.8 eV) radiation. In XPS, MgK_α (1253.6 eV), or AlK_α (1486.6 eV) radiation is generally employed. The escape depth of electrons in UPS is only 5-10 Å, whereas it is 20-40 Å in XPS.

In Auger electron spectroscopy (AES), X-ray (or beam of electrons) knocks out a core level electron and another electron comes out from any of the upper levels to fill the place vacated by the knocked-out electron. The difference in energy is used to eject a second electron in a non-radiative process. The Auger electron spectroscopy is particularly useful in the determination of surface composition.

III. Reference Level Problem in ESCA :

If the sample from which photoelectrons are to be emitted, is put in electrical contact with the spectrometer, charge flows to establish the contact potential, which is the work function difference $\phi_{sample} - \phi_{spect.}$, and the Fermi levels, E_F, of the sample and spectrometer are equalized. This is shown in Fig. 1.1. The kinetic energy, E_{kin}, of the electron when it enters the spectrometer chamber is thus slightly different from the energy E'_{kin} which it has on emerging from the sample. It is the kinetic energy, E_{kin}, that is measured. If we choose the Fermi level as a reference level for the electron binding energies, i.e. if we have zero binding energy at the Fermi level, conservation of energy requires that

$$E_B = E_{X-ray} - E_{kin} - \phi_{sp.} \qquad \ldots\ldots [1.2]$$

Here E_B is the electron binding energy and $\phi_{sp.}$ is the work function of the spectrometer material. It should be noticed that the term $\phi_{sp.}$ does not depend on the sample material and as long as it does not vary with time, one and the same work function correction can be applied to all the measurements. Thus the measured binding energy depends only on $\phi_{sp.}$, presumably a constant, even when

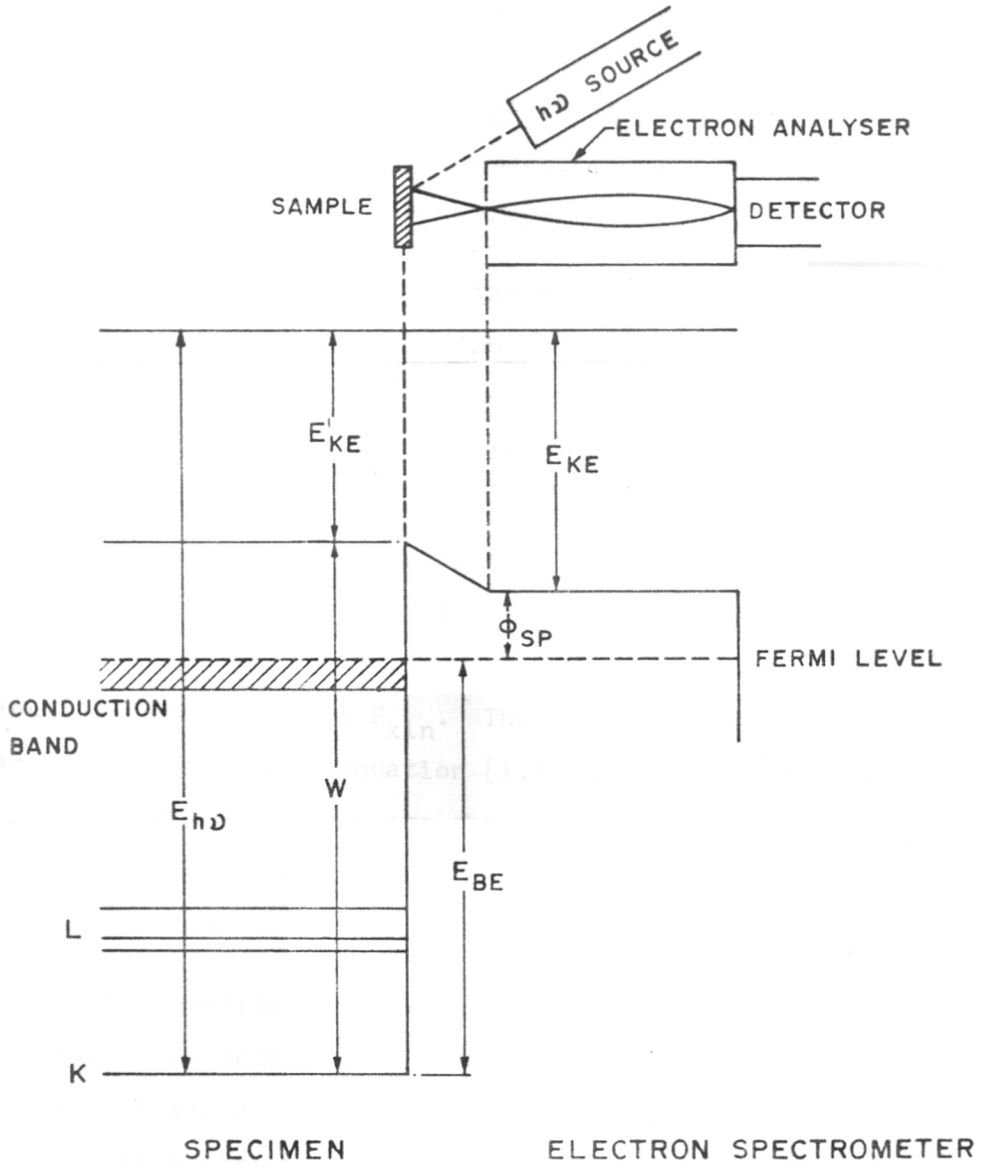

FIG. 1·1. PRINCIPLES OF AN ELECTRON SPECTROMETER FOR A METALLIC SAMPLE WHCH IS IN GOOD CONTACT WITH THE SPECTROMETER

different samples are used. The choice of the reference level as Fermi level has been made not only in the electron spectroscopy but also in X-ray spectroscopy.

In the above equation the recoil energy imparted by the ejected photoelectron which is very small (< 0.1 eV) has been ignored. For most commercial ESCA instruments $h\nu$ is either 1253.6 eV generated from a MgK_α anode or 1486.6 eV from an AlK_α source, although other energies are becoming available. Once the photon energy is known and analyzer work function $\phi_{sp.}$ is predetermined, a plot of spectrum can be made of the intensity of photoelectrons N(E) versus their kinetic energies E_{kin}. The binding energies (E_B) are calculated using equation [1.2] and as binding energies of electrons of an atom are characteristic of the atom, a plot of binding energies against number of electrons is a sure way of identifying elements.

The qualitative information is provided by peak positions and quantitative information by their peak heights (area). Moreover, with present instruments it is possible to measure shifts in energy levels to the extent of about 0.2 eV, so this becomes a very sensitive experimental technique for probing the effect of changes in chemical environment, coordination, bonding, charge density, etc. on the energy levels.

IV. Escape Depth :

At the outset of any discussion of X-ray photoemission from solids it should be noted that electron spectra can provide information about structure to a depth extending only a small distance from the emitting surface. X-rays may penetrate relatively far into the material (over 10 μm) but only those photoelectrons produced near the surface have only significant probability of escape without subsequent energy loss. What is important here is that at electron energies of 1253.6 eV and 1486.6 eV, corresponding to the MgK_α and AlK_α lines commonly employed in XPS, the escape depths are of the order of 20-40 Å.[31,32] Thus the XPS technique typically probes the first few angstroms of the solid surfaces. On one hand, the bulk is probed, on the other, XPS is a surface sensitive technique.

V. X-ray Photoelectron Line Shapes and Splittings :

Normally electron ejection by ESCA process will give rise to a single peak corresponding to the removal of an electron which yields a single final electronic state. However, the photoemission process is inherently a many electron event, that is during photoemission all of the other electrons in the system must readjust their

positions and energy since they are no longer in their ground electronic states. Thus, new electronic states become accessible to the final state electrons. These effects give rise to asymmetric peak shapes and various peak widths as well as peak splittings. It is very important for the electron spectroscopist to be aware of these effects to avoid mis-interpretation of spectra.

Spin-orbit splitting :

Spin-orbit splitting occurs due to coupling of spin and orbital angular momentum. Spin-orbit separation exists also in initial states and these are well characterized for inner shells. For a closed shell $l > 0$, two subshells arise with quantum numbers $l + \frac{1}{2}$ and $l - \frac{1}{2}$. The relative intensities of the two lines are the statistical weights $(2J + 1)$ of the two final states. The splitting increases with atomic number Z, roughly as a function Z^5. No spin-orbit splitting occurs with s subshells.

Multiplet splitting :

Multiplet splitting arises when interaction takes place between the unpaired electrons formed by photoelectron ejection and any unpaired electron already existing in the atom or molecule in any of its incomplete shell.

Multiplet splitting is found most intensely in 3s (and 4s) levels when unpaired electrons are present in 3d (and 4f) orbitals. Multiplet splitting has considerable potential as a diagnostic probe of oxidation/spin state, paramagnetic systems and distribution of unpaired electrons[33-35]. But its observation suffers from the practical limitation that the ns peak is inherently weak.

Jahn-Teller splitting :

If a molecule has complete symmetry e.g. CH_4, then a removal of an electron from one of its degenerate orbitals will remove the electronic symmetry and consequently its degeneracy and the molecular ion may be found in more than one final electronic state. This is known as the Jahn-Teller (JT) effect and the energy separation between the final states as the Jahn-Teller splitting.

Jahn-Teller broadening decreases with a decrease in the force constant[36] :

$$CH_4 > SiH_4 > GeH_4$$

The JT effect is small when heavier atoms are substituted for hydrogen e.g. CF_4, but when the central atom is substituted for any heavier atom, it increases, e.g. $Pb(CH_3)_4$[37]. For a linear molecule the corresponding

splitting is called the Runner-Teller splitting[38].

Satellites (electron shake-up and shake-off) :

Two other phenomena leading to a multiplicity of final electronic states are called electron shake-up and electron shake-off.

As a result of a sudden change in the central potential of an atom, (caused by the sudden removal of an electron from a core shell) an electron in a given orbital may go into an excited (electron shake-up) or continuum (shake-off) state.

$Ne(1s^2\ 2s^2\ 2p^6) \longrightarrow Ne^{+}(1s\ 2s^2\ 2p^5\ 3p)$ shake-up

$Ne(1s^2\ 2s^2\ 2p^6) \longrightarrow Ne^{2+}(1s\ 2s^2\ 2p^5)$ shake-off.

In photoelectron spectra the satellite structure occurs on the low kinetic energy side of the main peak as sharp peaks in the case of electron shake-up and a continuum in the case of electron shake-off[39-41]. Shake-up has been studied most for transition metal ions of the 3d series[42], strong satellites being observed on the 2p lines for paramagnetic species[43]. Satellites can be used as a reliable guide to oxidation state/spin state in several systems.

Plasmons :

Another final state effect which can influence the shape of the photoelectron spectra is the occurrence of various inelastic scattering events the electron experiences as it passes through the solid. The most common of these is the discrete energy loss due to plasmon excitation. These are usually observed on most solids[44], although their intensity is strongest on the free electron metals like Na and Al.

The above discussion covers most of the important features of the photoelectron line shape which may be of interest to the practising electron spectroscopist.

VI. Line Broadening :

Perhaps the most serious drawback to photoelectron spectroscopy of solids is line broadening. This broadening results from three main sources, in addition to the aberration of the spectrometer.

1. Width of the photon source,
2. Width of the subshell from which the electron is photoejected, and
3. Broadening due to charging.

1. The width of uv source is negligible (1 meV) compared to AlK_{α} and MgK_{α} X-rays. The widths are in part due to the lifetime of the K shell vacancy and in part due to spin-orbit splitting between the $2p_{1/2}$ and $2p_{3/2}$ levels. The net full-width at half-maximum is about 0.9 eV for $AlK_{\alpha_{1,2}}$ and 0.8 eV for $MgK_{\alpha_{1,2}}$. This source of broadening can be overcome by use of a monochromator.

2. Line broadening occurs as a result of the finite lifetime of the vacancy created in the atom of the material under study. The lifetime decreases with an increase in binding energy. The broadening in the $2p_{3/2}$ level in silicon has been measured to as low as 0.5 eV[45].

3. For non-conducting solids one of the most serious sources of line broadening is due to the uneven charging of the source as the result of photoionization. This line broadening seriously affects the resolution of the electron spectrometer.

This charging problem has been handled in a number of ways by many workers. In some spectrometers, a flood gun is available for bombarding the sample with additional electrons. Many have made use of a reference material, either added deliberately, such as evaporated gold or unavoidably present, such as the 'adventitious' carbon

present to some extent in most instruments[2]. It is then assumed, often implicitly, that this reference material is always the same and in electrical equilibrium with every sample regardless of its electrical properties.

VII. Sensitivity of ESCA :

ESCA is sensitive to almost all elements of the periodic table. The sensitivity of ESCA to different elements does not vary tremendously. ESCA is least sensitive to the very light elements such as Li and Be and most sensitive to the heavy elements such as Au or Hg. The difference however, is not greater than one order of magnitude.

The bulk sensitivity of ESCA is not high, it is generally limited to concentrations of approximately 0.1% based on bulk percentage. This means that ESCA will not be a sensitive technique for measuring trace material distributed through the bulk of the sample. The lack of bulk sensitivity exists because ESCA primarily samples the surface. Therefore, if the material is on the surface the actual number of atoms required to give an ESCA signal is small.

ESCA is a sensitive surface technique. Signals have been detected from as little as 0.2% of a monolayer of heavy metals which amounts to about 10^{12} atoms.

[C] REVIEW OF LITERATURE ON ESCA STUDY OF METALS AND ALLOYS

A brief and comprehensive review of literature on (1) core level binding energy shifts in alloys, (2) surface core level shifts in metals and (3) surface segregation in alloys has been discussed here.

(1) Core level binding energy shifts in alloys :

As is well known, the core XPS lines show binding energy shifts which depend on the chemical environment of the atoms. However, for metallic solids[46-51] comparatively little has been done as far as the interpretation of the chemical shift is concerned.

Measured core level binding energy shifts are listed in Table 1.1 for three Au-Sn alloys[52]. Negative values indicate that the levels are more tightly bound in the alloys and moreover substantial negative value for Au in $AuSn_4$ suggests that charge flows from Au to Sn sites.

Table 1.1 : Core level shifts of Au and Sn in the Au_xSn_y systems (Ref. 52)

Sample	Level energy shifts	
	Δ_{4f} (Au) eV	Δ_{3d} (Sn) eV
Au	0	-
$Au_{0.96}Sn_{0.04}$	-0.10 ± 0.14	-0.40 ± 0.14
AuSn	-0.45 ± 0.14	-0.40 ± 0.14
$AuSn_4$	-1.10 ± 0.14	-0.10 ± 0.14
Sn	-	0

The Mossbauer isomer shift data for these alloys indicate that there is a significant valence s-charge increase at Au sites and a somewhat smaller decrease at Sn sites upon alloying.

Watson et al.[53] observed Au $4f_{7/2}$ level binding energy shifts in a series of gold alloys; Au-Ag, $AuAl_2$ and $AuGa_2$. Two sets of observations are interpreted within the framework of band theory to mean that when Au is alloyed with Ag, Al and Ga the flow of s-charge on to Au sites is accompanied by a compensating depletion of d charge. The observed chemical shift is related to charge flow.

The high resolution XPS for Pt-Sn alloys[54] permitted the observation of chemical shifts in the line position (see Table 1.2). It is interesting to note that the Sn $3d_{5/2}$ peak is found at a B.E. which is about 1 eV less for the alloys than for pure Sn, whereas the Pt $4f_{7/2}$ peak is subject to much smaller effects. The excess net charge at the Sn atoms in the alloy indicated by the line shifts of 3d line is not in agreement with Knight shift and Mossbauer data[55] on Pt/Sn alloys which suggests a transfer of the Sn 5s electron to the Pt 5d band.

Table 1.2 : Core level binding energies of Sn $3d_{5/2}$ and Pt $4f_{7/2}$ in Sn/Pt alloys (Ref. 54)

Sample	Sn $3d_{5/2}$ eV	Pt $4f_{7/2}$ eV
Pt	-	71.8
Sn	486.6	-
Pt_3Sn	485.7	71.5
PtSn	485.5	72.0

A systematic series of ESCA measurements in Pt-Cu alloys[56,57] manifest observable shifts for only the Cu core levels. These shifts are linearly related to the corresponding centroids of the valence band spectra. The absence of any shift in the binding energy of any of the Pt core levels is consistent with negligible charge transfer.

Recently, some amount of work has been directed to interpret the core level binding energy shifts in alloys[58]. There are several major factors which can contribute to the shift of the XPS electron binding energies for an atom in a solid. Difference in valence electron density, crystal field potential, work function and relaxation energy have been considered as factors influencing the binding energy shifts. In general, the important contributions to the binding energy shift are included as follows :

$$\Delta E_B^F = \frac{\Delta q}{r} - \Delta V - \Delta E_R - \Delta \phi \qquad \ldots\ldots \quad [1.3]$$

where E_B^F is the binding energy referenced to the Fermi level, $\frac{\Delta q}{r}$ term represents the so called 'chemical shift' due to differences in valence electron density, ΔE_R is the difference in extra and intra-atomic relaxation energies, ΔV is the difference in crystal field potential energy and $\Delta \phi$ is the work function correction. The last three terms in equation [1.3] are strongly dependent on the host matrix.

Kim and Winograd[58] studied the core level binding energy shifts in the alloys; Au-Ag, Pt-Ag and Pt-C (see Tables 1.3 and 1.4). They interpreted the binding energy shifts to consist of a matrix shift and a chemical shift. They proposed a model to separate the chemical effect ($\frac{\Delta q}{r}$) from that of the matrix effect. By using an implanted noble gas where chemical effects are negligible[59] the matrix effect can be experimentally evaluated. The Au $4f_{7/2}$ B.E. shift of trace gold alloyed in Ag as compared to pure gold is 0.3 eV. The same shift has been observed from an(Au 5.3 at % - Ag 94.7 at %) alloy by Watson et al.[53]. When compared to the Ar B.E. shift, the chemical shift is

$$\frac{\Delta q}{r} = \Delta E_B^F \text{ (Au:Ag,Au)} - \Delta E_B^F \text{ (Ar:Ag,Au)}$$

$$= (84.1 - 83.8) - (241.9 - 240.5)$$

$$= 0.3 - 1.4$$

$$\frac{\Delta q}{r} = -1.1 \text{ eV} \qquad \ldots\ldots \quad [1.4]$$

This result clearly shows that although the measured B.E. of alloyed gold is higher than that of pure gold, indicating at first glance that a positive (partial) charge resides on the gold component, correction for the

Table 1.3 : XPS binding energies (eV) for the alloyed and implanted materials (Ref. 58)

Matrix	Implanted or alloyed material				
	Ar $2p_{3/2}$	Au $4f_{7/2}$	Ag $3d_{5/2}$	Pt $4f_{7/2}$	C 1s
Au	240.5	83.8	367.6	-	-
SiO_2	241.9	84.9	-	-	-
Ag	241.9	84.1	368.2	-	-
Pt	240.2	-	367.6	71.1	-
C	241.6	-	-	72.1	284.3

Table 1.4 : XPS binding energy shifts, estimated matrix shifts and chemical shifts for various implanted and alloyed systems (Ref. 58)

Matrix	Implanted or alloyed material (I)	ΔE_B^F (I:M,I) eV	ΔE_B^F (Λ:M,I) eV	$\frac{\Delta q}{r}$ eV
Ag	Au	0.3	1.4	-1.1
Au	Ag	-0.6	-1.4	0.8
Pt	Ag	-0.6	-1.7	1.1
SiO_2	Au	1.1	1.4	-0.3
C	Pt	1.0	1.4	-0.4

matrix effect reverses the sign of the $\frac{\Delta q}{r}$ term indicating that gold actually obtains a partial negative charge which is consistent with the Mossbauer results[60-63] on Au-Ag alloys and nullifies the need to invoke d-compensation of gold[53] electron density to explain the B.E. shift. A similar conclusion is reached for Ag-Pt and Pt-C alloys[58].

The shift in the core level binding energy in alloys from that in pure metals will have to be understood and interpreted by considering both chemical and matrix effects. In some publications this point seems to have been missed. Some apparent difference in conclusions of ESCA and Mossbauer results may also get resolved if the matrix effects are taken into account.

Recently Steiner et al.[64] have developed a procedure for calculating core level binding energy shifts in dilute alloys. This is essentially an application of the model developed by Martensson and Johansson[65,66] for arriving at the core level binding energy of a metal using a Born-Haber cycle. Thus, the difference between the binding energy of an atom A in its metallic state and when it is dissolved in another metal B as a dilute alloy (written as AB) is given by

$$\Delta E = E(A,B) + E(A+1, A) - E(A+1, B) \quad \ldots\ldots \quad [1.5]$$

where E(A,B) = energy of solution of A in B and so on, (A+1) stands for the element having the atomic number one higher than that of A.

The energy terms in the above equation [1.5] have been calculated by using the semi-empirical scheme developed by Miedema[67,68]. The results have been compared with experimental results obtained for forty dilute alloys (see Fig. 1.2). The agreement seems to be good except in cases of MnAg, MnCu, PdZr, PdTi and TiAl. One possible reason for this discrepancy is a shift in the d level occupancy at the transition metal leading to a change in the screening effect of these electrons. A point to keep in mind is that the small ΔE values are derived from the difference between two large quantities, i.e. E(A,B) and E(A+1, B) and even a small error in the calculation of these two terms can give a very large percentage error in ΔE. The other weakness is, as the authors themselves have pointed out, that the thermodynamic quantities refer to a situation when the lattice has relaxed to an equilibrium point which is not strictly so during the time interval of the electronic transition in XPS.

Martensson et al.[69] have carried out an ESCA study of core level binding energies in case of a series of Cu_xPd_{1-x} alloys ($0.1 < x < 0.9$). The results have been

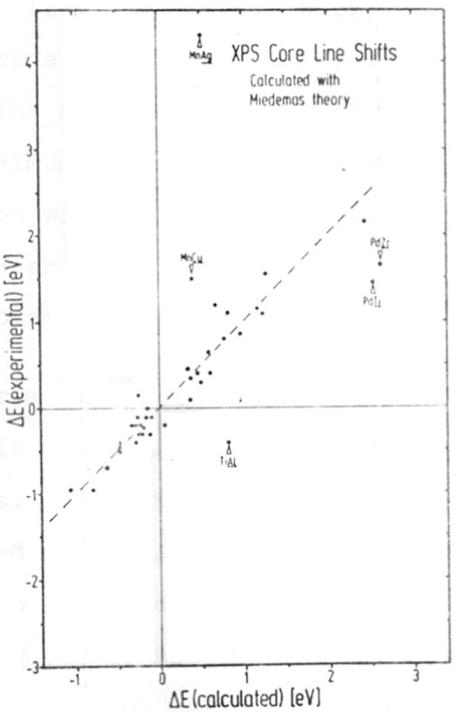

Fig.1.2:. Experimental core level binding energy shifts in dilute alloys as compared to those obtained from the semi-empirical calculations of solution energies of Miedema *al*.

analyzed using equation [1.5]. A = Pd, B = Cu_xPd_{1-x} and A+1 = Ag for $\Delta E^{(Pd)}$ and A = Cu, B = Cu_xPd_{1-x} and A+1 = Zn for $\Delta E^{(Cu)}$.

The $\Delta E^{(Pd)}$ is maximum ($\sim$ 0.8 eV) at low Pd concentration and it decreases systematically on increasing Pd concentration in the alloy as shown in Fig. 1.3. Similarly the $\Delta E^{(Cu)}$ is maximum ($\sim$ 1.0 eV) at low copper concentrations and decreases with increasing copper concentrations. The agreement between the experimental and calculated values seems to be good particularly in case of $\Delta E^{(Cu)}$ (see Fig. 1.4).

These experimental data have been used to calculate the heat of solution of a Zn atom in the Cu_xPd_{1-x} alloy for various 'x' values. The authors have shown another effective use of the measured chemical shifts of the two components in a binary alloy, namely, to determine the heat of formation of the alloy. An accurate measurement of chemical shifts may thus give a very useful method for rapid determination of thermo-chemical data.

A similar treatment of the Auger line gives results on double hole shifts.

Steiner and Hufner[70] studied XPS core level binding energy shifts for a large number of coevaporated Pd_xAg_{1-x}

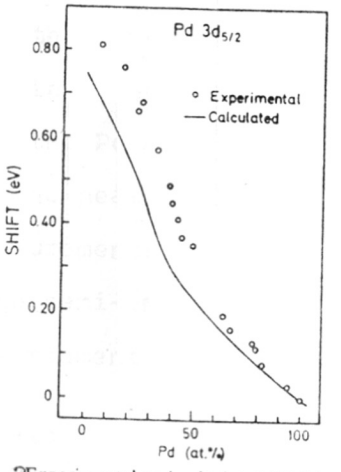

FIG. 1.3 Experimental and calculated Pd $3d_{5/2}$ chemical shifts.

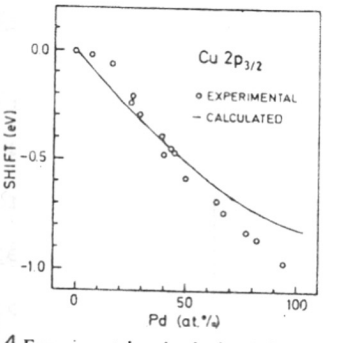

FIG. 1.4 Experimental and calculated Cu $2p_{3/2}$ chemical shifts.

alloys with $0 < x < 1$. The Ag $3d_{5/2}$ line shifts by -0.95 eV between Ag and dilute Ag in Pd. On the other hand, Pd $3d_{5/2}$ line shows a maximum shift of $\sim$ 0.5 eV and it decreases with increase in the Pd concentration. Using the experimental Pd $3d_{5/2}$ line shifts data, they calculated the heat of formation for the Pd_xAg_{1-x} system. They compared this result with (i) the heat of formation reported from standard calorimetric measurements[71] and (ii) also with the results obtained from the semi-empirical calculations of Miedema et al.[72]. The agreement seems to be good.

These XPS data of Ag $3d_{5/2}$ line shifts have been used to calculate the heat of solution of Cd in Pd_xAg_{1-x} system.

(2) Surface core level shifts :

In metals, core level binding energy seems to differ between surface and bulk atoms. There is a theoretical justification for this[73-81]; since the surface atoms experience a potential different from the bulk due to the lower coordination number, their core levels are expected to be shifted if one only considers initial state effects. However, many experimental results are not yet clearly understood and the significance of this problem is reflected by the several recent papers devoted to this subject.

The existence of a surface core level binding energy shift (SCS) was first noticed by Citrin et al.[82], for the Au $4f_{7/2}$ levels from the broadening of the XPS peak as grazing electron emission angle was approached. The surface atom 4f level is shifted to 0.40 $\pm$ 0.01 eV to lower binding energy relative to the bulk value. A model was proposed by Citrin et al.[82] to account for the SCS in terms of the modified surface density of states. The narrowing of the valence band, due to the reduced coordination of the surface atoms gives an overall net increase in the localized d states at the expense of the delocalized s and d states. Consequently the s-d charge redistribution decreases the energy between the center of the narrowed surface d band and the Fermi level. Since the Fermi level is fixed by the bulk, so that the surface density of states is pulled up to lower binding energy. The most of the valence charge occupies tightly bound (atomic like) states, the surface atom core levels feel this change in potential and is therefore shifted to lower binding energy.

Recently Heimann et al.[79] have measured 4f core level shifts and surface-to-bulk intensity ratios for surface atoms on the Au(111), (100) and (110) faces. These shifts show crystallographic dependences as well as dependences on surface reconstruction.

Direct observation of 4f splitting between (110) surface and bulk atoms of W was made by Duc[83] and his coworkers using the synchrotron radiation. High resolution spectra reflected two well resolved 4f lines separated by 0.30 eV, the low binding energy line being assigned to surface atoms. Thus in this study, the surface atom peak is clearly resolved from the bulk component. On the other hand the XPS of Au 4f exhibited only an enhanced shoulder[82] not a distinct surface peak.

Recently van der Veen et al.[84] have studied systematically the core level binding energy shifts for W(111) and Ta(111). They found that the surface shift for top most layer of Ta(111) is + 0.40 eV towards higher binding energy side, whereas for W(111) the shift is -0.43 eV towards lower binding energy. The change in sign in the surface core level shift between Ta(111) and W(111) is in agreement with recent theoretical predictions[76-78]. Ta(111) and W(111) surfaces show multiple surface core levels which corresponds to surface atoms with different coordination numbers.

Surface core level shift of 0.6 eV has been reported for Yb by Alvarado et al.[85]. The authors believe this to be due to surface contamination of oxygen on Yb surface.

However, a recent reinvestigation[78] of the Yb surface confirms that the observed shift is indeed a true surface effect.

Structure dependent 4f core level binding energies for surface atoms on Ir(111), Ir(100)-(5 x 1) and metastable Ir(100)-(1 x 1) phases were studied by van der Veen et al.[86] using synchrotron radiation (see Fig. 1.5). For the (1 x 1) surface, the shift of the $4f_{7/2}$ core level is 0.68 eV, whereas for the (5 x 1) reconstructed face, the shift is 0.49 eV towards lower binding energy in both cases. van der Veen et al. [86] found that the surface atom core level emission intensities give direct information on the number of surface atoms, while binding energies give information on the surface atom coordination number. These data show that the reconstructed Ir(100)-(5 x 1) face is described by a compressed hexagonal monolayer. Thus the measurement of surface core level binding energies and intensities shows promise as a 'site specific' tool to study surfaces of transition metals and is particularly interesting for catalytically active stepped surfaces.

Very useful information about the surface structure can be obtained for the surface core level data as has been nicely demonstrated by Himpsel et al.[87] and Brennan et al.[88]

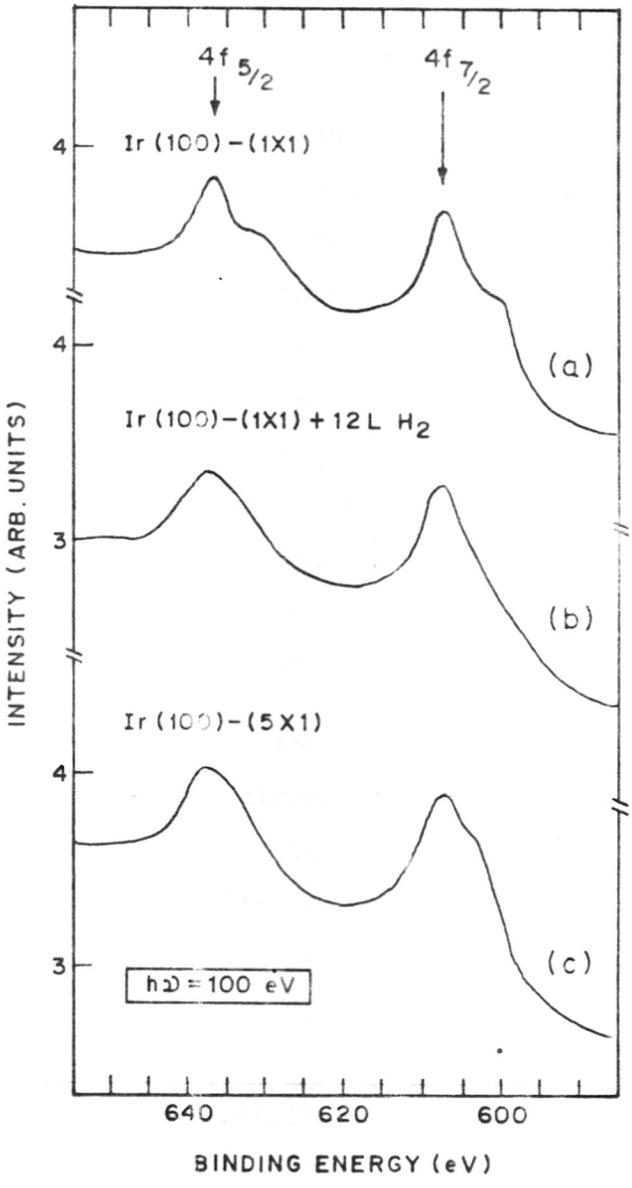

FIG. 1-5. PHOTOEMISSION SPECTRA OF Ir 4f CORE LEVELS FOR (a) Ir (100)-(1 X 1), (b) Ir (100)-(1 X 1) + 12 L H_2, AND (c) Ir (100)-(5 X 1).

for silicon samples. The former authors have found that for Si(100)-(2 x 1) surface the binding energy of $\sim$ 0.5 monolayer of surface atoms is shifted to a smaller value (-0.5 eV) relative to the bulk. This feature is interpreted to be consistent with an asymmetric dimer model, in which 1/2 layer of (100) surface atomsare shifted outwards and not with a symmetric dimer model, which would lead to a full outer layer of shifted atoms. The data from Si(111)-(2 x 1) surface support the buckled surface model with alternate rows of surface atoms raised and lowered. Si(111)-(1 x 1)H exhibits first layer (+0.26 eV) and second layer (+0.15 eV) shifts.

High resolution photoemission spectra[88] of the Si 2p level for freshly cleaved Si(111) reveal two additional core level structures which are shifted relative to the bulk. The observed shifts are 0.59 $\pm$ 0.04 eV to lower and 0.3 $\pm$ 0.03 eV to higher binding energy respectively. These shifted peaks which vanish with increasing contamination of the surface, are shown to be directly correlated with reconstruction on the Si(111)-(2 x 1) surface (buckling model).

Core level binding energy shifts of the Ni $2p_{3/2}$ and Au $4f_{7/2}$ lines have been measured by Steiner and

Hufner[89] for Ni on Au and Au on Ni overlayers down to mean coverages of less than 0.1 monolayers. The results show that these shifts are governed by the mean coordination number of the atoms in the overlayer.

Recently, Desjonqueres et al.[76] presented a model, in which the change of the binding energy of core levels at the surface is due to the displacement of the d band which arises from the narrowing of the surface density of d states.

Surface core level binding energy shifts for GaAs(110) and GaSb(110) have been studied recently by Eastman et al.[90] which give new information on semiconductor surface reconstruction. The shifts ($\sim$ 0.3 eV) are towards higher (lower) binding energies for the surface cations (anions) in agreement with a simple model involving the known surface relaxation of GaAs(110) with a geometry-dependent initial-state charge transfer.

Eastman et al.[90] have interpreted their results purely in intra-atomic terms to mean that the atomic charges in the surface are somewhat more positive on Ga and more negative on As than they are in the bulk. This interpretation is surprising, one would except on the contrary that

surface atoms having fewer neighbours than corresponding species in the bulk, are less ionic and on an intra-atomic basis alone should then exhibit shifts opposite in direction to those observed.

It is shown recently[91] that the difference between the Madelung potentials at the (110) surface and the bulk of GaAs is the major factor determining the core level shifts. The site charge difference between surface and bulk are such that Ga and As are less ionic at the surface than in the interior.

The Madelung potential[92,93] differs from that of the bulk not only because of any ionicity difference characterising the surface, but also because of the different coordination of neighbouring atoms. Thus because of the atomic constituents of a compound have lower coordination in the surface of a solid than in the interior one expects that compounds are less ionic at crystal surface than in the bulk, i.e. cations at surfaces are in lower states of oxidation. A general expression is obtained for a bound on such charge reduction at nonpolar surfaces. This shows that surface atoms, as a rule, have their ionic charge reduced relative to the value in the bulk by at most a factor of two.

From the given experimental results it follows that one would expect a core level shift between a bulk- and a surface-metal atom. Secondly, depending on the metal, the shift could be either towards higher or lower binding energies in accordance with theoretical calculations. Thirdly, it seems that the shift should be largest for the surface plane having the lowest coordination number. Finally, one would also expect a linear relationship between surface coordination number and the surface core level shift if one considers the simple bond breaking approach.

(3) Surface segregation in alloys :

3.1 Introduction

It is well known that the equilibrium composition at the surface of an alloy often differs from that in the bulk[1,21,94-98]. This behaviour was predicted by Gibbs[94] about a century ago, but was first observed experimentally in 1957 by Takeuchi et al.[95] in a Ni-Cu catalyst where the surface was found to be richer in Cu as compared to the bulk. During the last few years a large amount of evidence has been collected on the surface segregation in alloys[20,96-102].

3.2 Experimental techniques

As it is difficult to make ab initio predictions[102-119] regarding the surface segregation, particularly in view of the profound influence of the impurities and the ambient gases etc., which can totally change the surface composition, one has got to rely on accurate experimental measurements. From this point of view the surface analysis techniques such as AES[120], XPS/ESCA[2,3], Low energy ion scattering spectroscopy (LEIS)[121,122], Secondary ion mass spectrometry (SIMS)[123] and X-ray spectroscopy (SXS)[124] have played a very important role in experimentally defining the surface composition under various experimental conditions.

AES is a very powerful technique for surface composition studies. Its strengths are (i) depth resolution as small as 5-15 Å, (ii) high lateral resolution (a fraction of a micron), (iii) high light element sensitivity (only exceptions H and He), and (iv) fast analysis time. However in this technique the electron beam may cause some damage to the surface, particularly it can change the surface composition due to selective sputtering.

XPS/ESCA, is most commonly used when the determination of chemical state is of importance. In general XPS/ESCA will provide more quantitative chemical information

than AES, though analysis times are slower. This technique is non-destructive and no selective sputtering occurs in the case of multicomponent systems. Moreover vacuum requirements for XPS are less stringent than for AES. However the XPS gives weighted average values over some topmost atomic layers (thickness from 10-100 Å).

Detailed information is often obtained by a combination of techniques, such as AES, XPS/ESCA, high and low energy ion scattering spectroscopy, X-ray methods, SIMS, SEM, TEM, or other indirect methods which involve the measurements of changes in the sensitive properties that are affected by surface enrichment.

Changes in the work function can also be used as a sensitive probe for finding out differences in composition of the outer layers[125-128]. However in general there is no linear-relationship between surface concentration and work function[129,130].

3.3 Results

The following alloys have been studied by ESCA (XPS, AES) in recent years (see Table 1.5). The major component is written first, followed by the minor component (solute).

Table 1.5 : Surface segregation in alloys (exptl.)

Solvent (solute)	Segregating component (Exptl.)	Ref.
Ag (Au)	Ag	121,122,131,132
Ag (Cu)	Ag	133
Ag (Pb)	Pb	132
Ag (Zn)	Zn	114
Ag (Sn)	Ag	114
Au (Ag)	Ag	121,122,131,132
Au (Cu)	Au	134,135
Au (Pd)	Au	136-138
Au (Sn)	Sn	139,140
Au (Ni)	Ni	141-145
Au (Ca)	Ca	146
Au (In)	In	147
Cu (Ag)	Ag	132,133
Cu (Au)	Au	134,135
Cu (Ni)	None	95,113,148-158
Cu (Be)	Be	159
Cu (Zn)	Zn	160
Cu (Al)	Al	161

contd...

Table 1.5 (contd.)

Solvent (solute)	Segregating component (Exptl.)	Ref.
Cu (Fe)	Cu	162
Cu (Sn)	Sn	102,162,163
Cu (Pt)	Cu	162
Ni (Au)	Au	141-145
Ni (Cu)	Cu	95,113,148-158
Ni (C)	C	164
Ni (Pd)	Pd	165
Ni (Th)	Th	166
Ni (Sb)	Sb	167
Ni (Cr)	Cr	168
Ni (Mn)	Mn	169
Ni (Sn)	Sn	170
Fe (C)	C	171
Fe (Cu)	Cu	132
Fe (Mn)	Mn	172
Fe (Ni)	Ni	173,174
Fe (Zr)	Zr	175
Fe (Cr)	Cr	124,176
Fe (Sn)	Sn	177
Fe (Al)	Al	178

contd...

Table 1.5 (contd.)

Solvent (solute)	Segregating component (Exptl.)	Ref.
Pd (Ag)	Ag	129,136,179
Pd (Au)	Au	136-138
Pd (Ni)	Ni	162,165
Pd (C)	C	162
Pd (V)	None	180
Pt (Au)	Au	181
Pt (Cu)	Cu	182
Pt (Fe)	None	183
Pt (Ni)	None	183
Pt (C)	None	118,184,185
Pt (Rh)	Pt	162,186
Pt (Sn)	Sn	54,187,188
Pt (Cr)	None	183
Pt (Pd)	Pd	162
Rh (Ag)	Ag	189
Rh (Pt)	Pt	162,186
Zr (Fe)	Fe	175
Cr (Fe)	Cr	162
Th (Ni)	Th	162
Pb (Sn)	Pb	190
Pb (In)	None	191

contd...

Table 1.5 (contd.)

Solvent (solute)	Segregating component (Exptl.)	Ref.
Ir (Pt)	Pt	102
In (Pb)	None	191
Li (Na)	Na	192
Is (Pt)	Pt	162
Al (Ni)	Al	114,193
Pd (C)	C	185
Co (C)	C	185
Ni (C)	C	164,194
Fe (C)	C	171
Zr (Fe)	Fe	175

In most cases surface compositions have been found to be different from that of the bulk. The only exceptions are Pt(Fe)[183], Pt(Ni)[183], Pt(Cr)[183], Pt(C)[184], Pd(V)[180], Cu(Ni)[95,113,148-158], Pb(In)[191] systems where no segregation was observed. It has been observed that in most of the cases solute atoms are found to segregate preferentially on the surface as compared to the bulk.

However in some cases the solvent atoms are found to segregate on the surface e.g. Ag(Au)[121,122,131,132], Ag(Sn)[114], Au(Cu)[134,135], Au(Pd)[136-138], Cu(Fe)[162], Th(Ni)[162], Al(Ni)[114,193], Pt(Rh)[162,186], Pb(Sn)[190], Cu(Pt)[162], Cr(Fe)[162], since in these cases the solvent atoms have lower heat of sublimation and higher atomic radius as compared to solute atoms.

Disagreement amongst various investigators on surface composition can often be traced to (a) a temperature of annealing high above the miscibility gap[154,195-197], (b) a selective removal of one of the alloy components during the cleaning procedures such as Ar-ion sputtering[154-156,158,198-207] and (c) the presence of impurity stabilized surface complexes[191].

3.4 Theory

The segregation arises from the fact that the two types of atoms in solids have different free energy when located at the surface. Thus the one which has the lower

free energy at the surface tends to segregate on the surface.

According to Gibbs the excess concentration of the solute on the surface over the bulk concentration Γ is related to the surface free energy σ of the solution by the equation[208],

$$\Gamma = -\left(\frac{a}{RT}\right)\left(\frac{d\sigma}{da}\right) \quad \ldots\ldots \quad [1.6]$$

where 'a' is the activity of the solute. If σ decreases with addition of solute (i.e. $\frac{d\sigma}{da}$ is negative) then Γ is positive and the surface is enriched with solute. (Γ_i is defined as the (algebraic) excess of the i^{th} component in a 1 cm^2 cross section of surface region over the moles that would be present in a bulk region containing the same number of moles of solvent as does the section of surface region).

Here the problem is that very little is known about the composition dependence of the surface energy $\frac{d\sigma}{da}$. Therefore a number of attempts[105,107,191-193,209-211] have been made to develop expressions which would relate surface composition with some experimentally measurable quantity. For example, it is generally observed that the component which has a lower heat of sublimation, or which has a higher atomic radius gets concentrated on the surface. So theories have been developed correlating surface enrichment with heat of sublimation and atomic radius.

If there is no phase separation and no ordered phase in the bulk of the alloy, the surface concentration can be related to the bulk concentration through the following equation[98,102,107,109,113,209,212] :

$$\frac{X_A^S}{X_B^S} = \frac{X_A}{X_B} e^{\Delta F/RT} \qquad \ldots\ldots \quad [1.7]$$

where X_A and X_B are the concentrations of the two components constituting the alloy in the bulk and X_A^S and X_B^S are those on the surface, ΔF is the free energy decrease when one gm-atom of A in the bulk is moved to the surface (ΔF is the free energy of segregation). Assuming a negligible change in entropy,

$$\frac{X_A^S}{X_B^S} = \frac{X_A}{X_B} e^{Q/RT} \qquad \ldots\ldots \quad [1.8]$$

where 'Q' is the heat of segregation. This equation shows that for positive values of 'Q' the solute A will segregate to the surface than in the bulk. It also shows that the segregation decreases with increasing temperature and ultimately reaches the bulk value at very high temperature.

3.5 Heat of segregation

Burton, Hyman and Fedak[211] have obtained the following expression for ΔF, the free energy of segregation assuming that the interactions in the alloy are nearest neighbour interactions and the phase diagram of the bulk alloy is well described by regular solution theory.

$$\Delta F = \frac{\Delta Z}{2} (V_{AA} - V_{BB}) \quad \ldots\ldots \quad [1.9]$$

where ΔZ is the difference in coordination number between bulk and surface. V_{AA} is the energy of an A–A nearest neighbour bond, V_{BB} that of B–B bond.

The bond energies can be estimated approximately from the heats of sublimation of the constituents as

$$V_{AA} \simeq \frac{-2H_A}{Z} \quad \ldots\ldots \quad [1.10]$$

where Z is the bulk coordination number. Similarly,

$$V_{BB} \simeq \frac{-2H_B}{Z} \quad \ldots\ldots \quad [1.11]$$

Substituting the values of V_{AA} and V_{BB} in equation [1.9] we get

$$\Delta F = \frac{\Delta Z}{2} \left(\frac{-2H_A}{Z} + \frac{2H_B}{Z}\right)$$

$$\Delta F = \frac{\Delta Z}{Z} (H_B - H_A) \quad \ldots\ldots \quad [1.12]$$

again if we assume $\Delta S = 0$, i.e. ideal mixing, no ordering or no miscibility gap, then

$$Q = \Delta F = \frac{\Delta Z}{Z} (H_B - H_A) .$$

$$Q = \frac{\Delta Z}{Z} (H_B - H_A) \quad \ldots\ldots \quad [1.13]$$

where H_B and H_A are the heats of sublimation of B and A respectively.

Some work has been carried out to account for the entropy changes in the calculation of 'Q' using either Monte Carlo calculations, or exact formulations[213]. But the results are not fully satisfactory.

A second approach to calculate 'Q' uses the surface energies[104] rather than the heats of sublimation. The importance of using the surface energies is that surface enrichment is related to surface properties, and bond energies. Applying the same assumptions leading to equation [1.13] one can calculate 'Q' as

$$Q = \gamma_B a_B - \gamma_A a_A \quad \ldots\ldots \quad [1.14]$$

where γ_A and γ_B are the surface energies of the solute A and solvent B and 'a' is the area per surface atom.

A third approach is based on elastic strain energy effects[107]. In this approach a solute atom having a size different from that of solvent atoms exerts a stress on the lattice. Interchanging the solute atom with a surface atom reduces this stress in the lattice. 'Q' is then calculated as elastic lattice strain energy,

$$Q = \frac{24\ \pi\ KGr^3\epsilon^2}{3K + 4G} \qquad \ldots\ldots \quad [1.15]$$

where K is the bulk modulus of the solute, G is the shear modulus of the solvent, r is the average radius of a solute and a solvent atom, $r = \frac{r_A + r_B}{2}$ and $\epsilon = \frac{r_A - r_B}{r_A}$.

The predicted 'Q' values are compared with the experimental results. But none of the theories give satisfactory agreement with experiment.

A more comprehensive theory for surface segregation has been developed recently by Seah[21,98]. The free energy of segregation per atom

$$\frac{E}{N} = \frac{1}{2} Z_v (\epsilon_{BB} - \epsilon_{AA}) + 2\omega [Z_1(X_A^B - X_A^S) + Z_v (X_A^B - \tfrac{1}{2})] \qquad \ldots\ldots \quad [1.16]$$

where N is Avagadro's number ϵ_{AA}, ϵ_{BB} are bond energies assigned to AA, BB neighbours respectively. Z_1 is the atomic coordination number in the layer and Z_v is the atomic coordination to one of the adjacent layers. The parameter ω is defined as

$$\omega = \epsilon_{AB} - \frac{1}{2} (\epsilon_{AA} + \epsilon_{BB}) \quad \ldots\ldots \quad [1.17]$$

From the equation derived by Seah[21], it can be seen that dilute solute with low surface energy or low enthalpy of segregation gets enriched at the surface of the alloy solution in addition if the enthalpy of mixing H_m is positive. In other words A--B bonds are not stable or when solute atom has size larger than the solvent atom then the segregation of the solute atom is enhanced. Seah's[21] further analysis shows that the surface energies are more closely related to melting temperature T^m (^oK) than to the sublimation enthalpy.

$$\gamma_A^S = 37\ T_A^m \text{ (Joules/gm-at)} \quad \ldots\ldots \quad [1.18]$$

He also added the strain term

$$- \frac{24\ \pi\ KGr_o r_1\ (r_o - r_1)^2}{3Kr_1 + 4Gr_o} \quad \ldots\ldots \quad [1.19]$$

to take into account the strain arising due to differences in the atomic radius of solute (r_1) and solvent (r_o).

Recently Tomanek et al.[162] have derived an expression for 'Q' using an expression derived by Miedema[214], for dilute alloys.

They considered alloy surface as average crystal plane where one-third of the bonds are broken. Now clearly exchange of a solute A and solvent B atoms will involve two terms :

(i) A heat of solution term due to modification of the surface;

(ii) A surface energy term due to difference in the surface energies of the exchanged atoms.

Taking into account these two terms, they obtained an expression for 'Q' as

$$Q = \frac{1}{3} [f \Delta H_{sol}(A,B) - g (\gamma_A - \gamma_B) V_A^{3/2}] \quad \ldots\ldots [1.20]$$

The factor f takes into account the deviation from the average crystal plane due to atomic relaxation and its value is 0.71, $g = 4.0 \times 10^8$ and V_A is the molar volume of

the solute. $\Delta H_{sol}(A,B)$ is the heat of solution of the solute in the solvent and $\gamma_{A(B)}$ is the surface energy of A(B). Thus the above equation [1.20] takes into account the corrections due to the relaxation of atoms in the surface layer and the strain energy arising due to the difference in atomic sizes of the constituents.

Using the above equation, authors[162] have calculated the heats of segregation 'Q' for a number of dilute alloys (see Table 1.6). 'Q' can be experimentally determined by measuring the surface concentration as a function of temperature (see Table 1.7).

3.6 Effect of third species

In a binary system the surface enrichment is controlled by the bulk concentration of the solute and its enthalpy of segregation, while in ternary system the segregation of the solute not only depends on these two, but also on the bulk concentration and the segregation characteristics of the other solute. If a strongly segregating solute is present even in a minute quantity it may depress the segregation of other constituent present in a much larger quantity, because of the competition for the available surface sites. For example, the segregation of sulphur supresses the segregation of copper in $AuCu_3$ alloy[215].

Table 1.6 : Heats of segregation 'Q' using equation [1.20] (Ref.162)

Alloy Solvent (solute)	Segregating element (Exptl.)	Q (KJ/mole)
Au (Ag)	Ag	+ 14.5
Cu (Ag)	Ag	+ 38.8
Pd (Ag)	Ag	+ 47.4
Rh (Ag)	Ag	+103.0
Cu (Au)	Au	+ 11.9
Ni (Au)	Au	+ 64.6
Pd (Au)	Au	+ 34.5
Pt (Cr)	None	- 13.0
Ni (Cu)	Cu	+ 35.5
Cr (Fe)	Cr	- 8.8
Cu (Fe)	Cu	- 20.3
Ni (Fe)	Ni	- 6.4
Pt (Fe)	None	- 11.1
Pd (Ni)	Pd	- 16.8
Pt (Ni)	None	+ 0.8
Th (Ni)	Th	- 86.7
Pt (Pd)	Pd	+ 27.7

contd...

Table 1.6 (contd.)

Alloy Solvent (solute)	Segregating element (Exptl.)	Q (KJ/mole)
Au (Pt)	Au	- 54.6
Cu (Pt)	Cu	- 48.6
Ir (Pt)	Pt	+ 32.7
Os (Pt)	Pt	+ 55.3
Rh (Pt)	Pt	+ 10.1
Au (Sn)	Sn	+ 60.8
Cu (Sn)	Sn	+ 94.2
Fe (Sn)	Sn	+170.3
Pt (Sn)	Sn	+130.3
Fe (Zr)	Zr	+ 18.5

Table 1.7 : Experimental heats of segregation 'Q'

Alloy Solvent (solute)	Segregating element (Exptl.)	Q kcals/mole (Exptl.)	Ref.
Ni (Au)	Au	12.0	142
Zr (Fe)	Fe	17.0	175
Fe (Zr)	Zr	30.0	175
Pt (Ni)	None	0	183
Pt (Fe)	None	0	183
Pt (Cr)	None	0	183
Pt (Au)	Au	10.0	181
Ni (Th)	Th	4.5	166

Gupta and Perraillon[111] have analyzed the segregation behaviour of ternary system theoretically. The important results are :

(i) The segregation behaviour of a solute A can be strongly modified by the presence of a second solute B. Thus the segregation does not only depend on its own bulk concentration and enthalpy of segregation, but also on the concentration and enthalpy of segregation of the second solute (Fig. 1.6).

(ii) This effect is more pronounced at low temperatures (Fig. 1.7).

(iii) The temperature at which the segregation of the solute A is maximum (peak temperature) rises with bulk concentration of impurity B (Fig. 1.8).

(iv) The peak temperature mentioned above, rises linearly with the heat of segregation of the impurity B (Fig. 1.9).

Some times, the opposite effect is also observed, i.e. the presence of impurity atoms can enhance the segregation of the solute and an interactive cosegregation results[216-219]. For example alloying elements such as

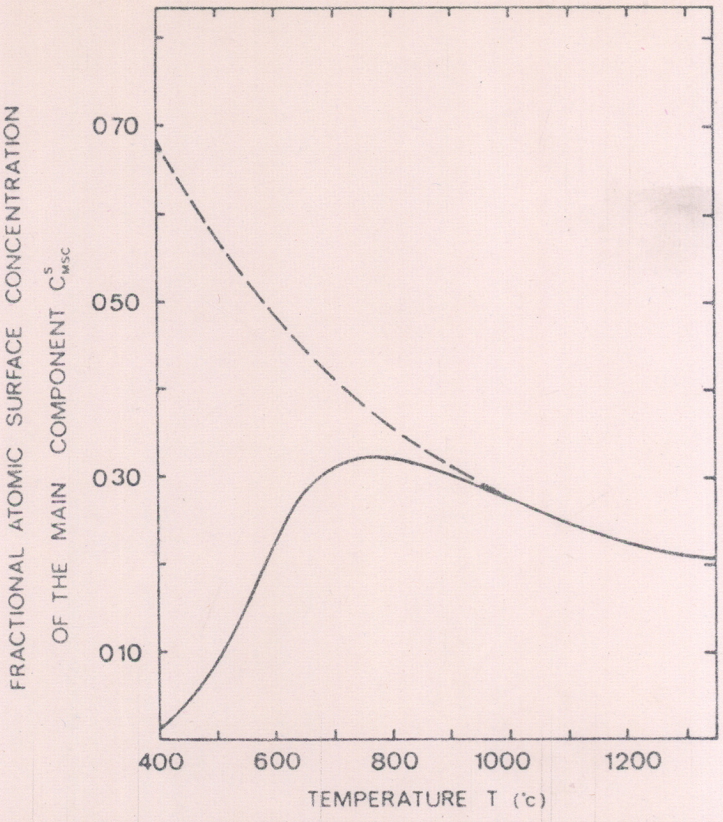

Fig.1.6: Variation of the surface concentration of the main segregation component with temperature.

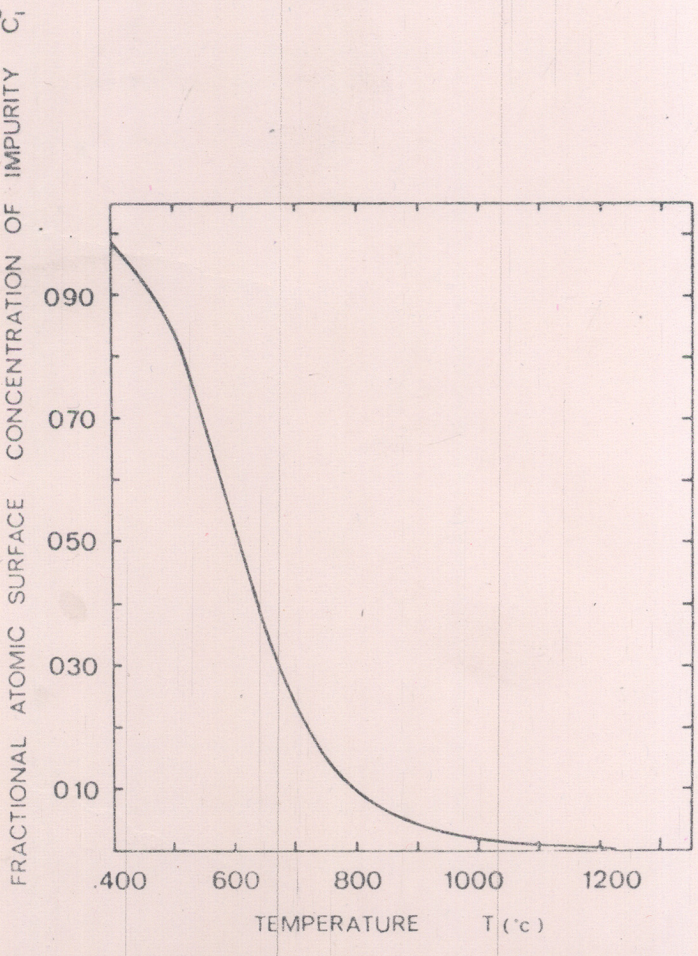

Fig.1.7: Variation of the surface concentration of the impurity with temperature.

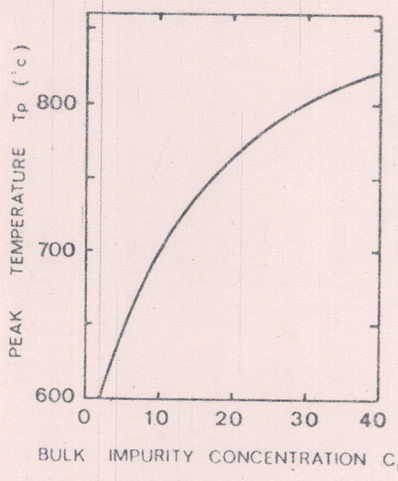

Fig.1.8:. Variation of the peak temperature (the temperature where the segregation of the main component is maximum) with bulk impurity concentration.

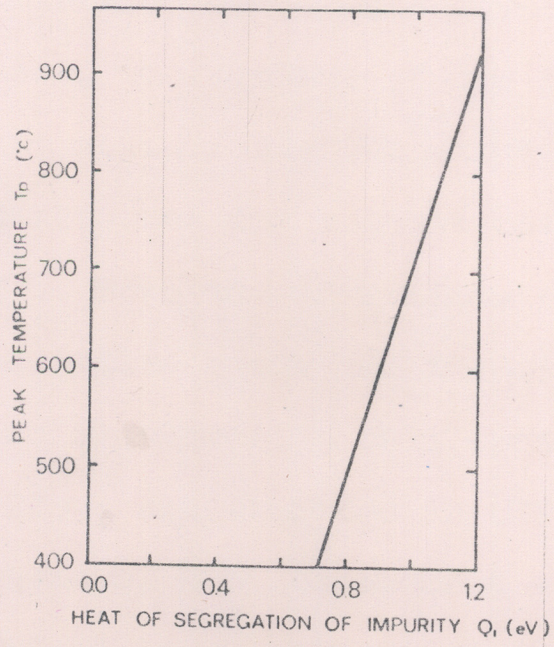

Fig.1.9: Dependence of the peak temperature on the heat of segregation of the impurity.

Mn, Cr, Ni etc. segregate more to the free surface of iron when impurities such as P, Sb, N, S, C are made to segregate[216,220]. This is because the impurities involved (Sb, P, N, S, C, ...) interact more attractively with classical alloying elements (Mn, Cr, Ni, ...) than with iron. Similarly the segregation of sulphur to the surface of nickel enhances that of calcium[112].

3.7 Effect of external agencies

The element which interacts with the solute at the alloy surface can also originate from outside. In this case an interaction may exist between the segregating solute and an adsorbed gas. As a result of interaction with active gases, the surface of the alloy is enriched with that constituent which forms the strongest chemical bond with the gas (which has the highest heat of formation) (see Table 1.8). Here the affinities of the individual elements to the active gases and the diffusion rates of the constituents are important in this connection e.g. Pt-Au[108,181] alloys equilibrated in UHV shows significant surface enrichment by Au. Subsequent exposure to CO, however resulted in an enrichment of the surface of the alloys by Pt[108,181]. The enrichment by Pt, at surfaces gives rise to more Pt-CO bonds and thus decreases the

Table 1.8 : Effect of gaseous surroundings

Alloy	Expected surface enrichment	Treatment	Observed surface enrichment	Ref.
Pd-Ag	Ag	Prolonged contact with CO gas at 293-373 K	Pd	221
Pd-Ag	Ag	Heated in air	Pd	198
Pd-Au	Au	Direct oxidation	Pd	137
Pd-Au	Au	Interaction with O_2 up to 600°C	Pd (PdO)	222
Pd-Au	Au	Hydrogen treatment at 350°C	Reduction of PdO without re-equilibrium of the surface	222
Sn-Pt	Sn	Direct oxidation	Sn (SnO_2)	54, 187, 188
Sn-Te	Te	Oxidation in air	Sn (SnO_2)	223
Sn-Te	Te	Thermal desorption after oxidation	Sn (SnO_2)	223
Sn-Pb	Pb	Influence of adsorbed oxygen	Sn (SnO_2)	112

contd...

Table 1.8 (contd.)

Alloy	Expected surface enrichment	Treatment	Observed surface enrichment	Ref.
Pb-Te	No segregation	Oxidation in air	Pb (PbO_2)	223
Pb-Te	No segregation	Thermal desorption after oxidation	Pb (PbO_2)	223
Pb-Bi	Bi	Influence of adsorbed oxygen	Bi (Bi_2O_3)	112
Th-Ni	Th	Oxidation	Th	166
Au-Pt	Au	Prolonged contact with CO gas	Pt	108, 181
Au-Ni	Au	Direct oxidation	Ni (NiO)	141-144
Au-Si	Au	Annealed in air	Si (SiO_2)	224
Cu-Ni	Cu	Exposed to NaCl solution at different impressed potentials	Ni (NiO)	225
Cu-Ni	Cu	Direct oxidation	Ni (NiO)	226, 227
Fe-Cr	No segregation	Oxidation	Cr (Cr-oxide)	176

surface free energy. This type of segregation in a Pt_3Sn alloy[228] in the presence of oxygen and hydrogen is illustrated in Fig. 1.10.

Gryaznov[229] pointed out that the XPS of Pd-Rh foils showed that the alloy surfaces were enriched in Rh after use as catalysts for cyclohexane dehydrogenation.

Treatment with acids or alkalis which dissolve specifically one constituents of the alloy from its surface causes the alloy to become enriched with that constituent (see Table 1.9) which is more difficult to dissolve or, which is not soluble at all[114,160]. Holm and Storp[114] found the surface of a freshly polished Ni-Al alloys to be enriched in Al. Storage in air (H_2O) especially at elevated temperature greatly increased the thickness of the aluminium oxide (or aluminium hydroxide) layer and reduced the Ni intensity correspondingly. Treatment with NaOH dissolved Al out from the surface which was thus left with a high Ni content.

On the other hand, Asami et al.[230] found that even when Fe-Cr alloys were polished in Cl_2CCHCl for a long time, the composition of the alloys in the layer immediately under the surface film was the same as that of the bulk.

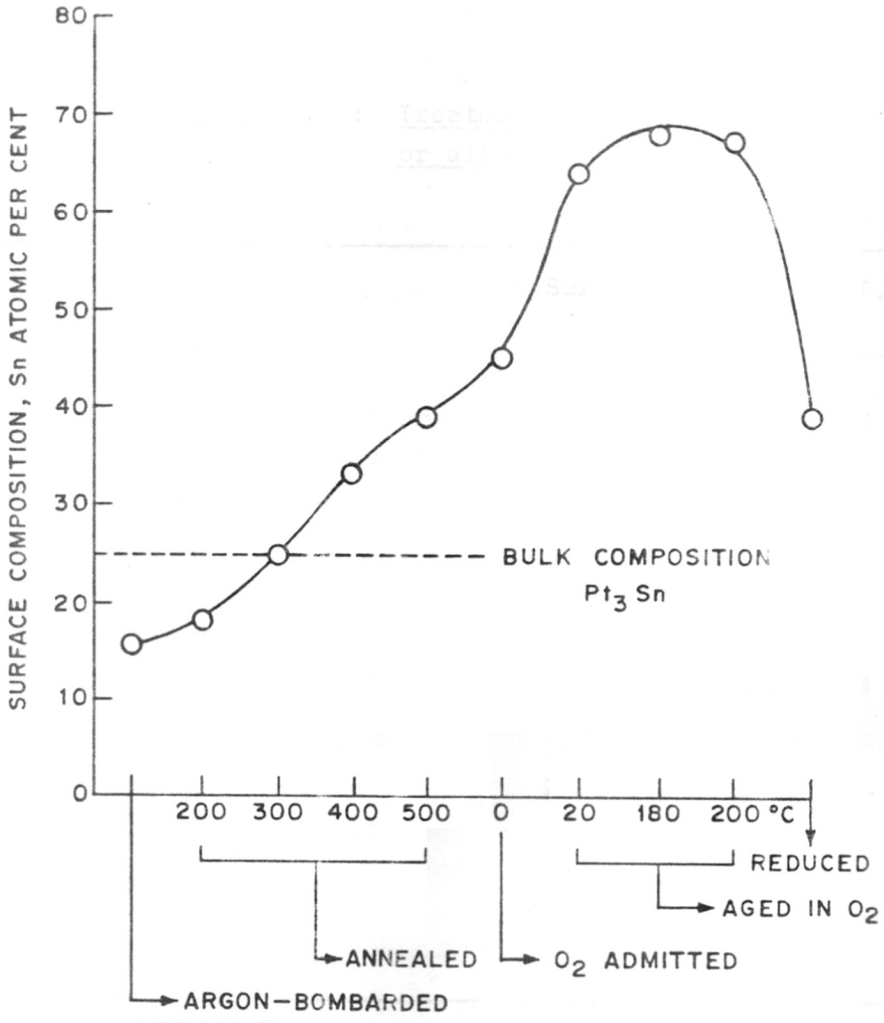

FIG. 1-10. THE EXTENT TO WHICH SURFACE SEGREGATION MAY OCCURE IN ALLOY SYSTEMS IS ILLUSTRATED BY THIS DIAGRAM OF THE CHANGES IN SURFACE COMPOSITION OF Pt_3Sn THROUGHOUT ANNEALING AND CHEMISORPTION TREATMENT DURING WHICH THE CONCENTRATION OF TIN IN THE SURFACE LAYERS WAS OBSERVED TO VARY FROM 15 TO 70 PER CENT

Table 1.9 : Treatment with acids or alkalis

Alloy	Treatment	Surface enrichment	Ref.
Ni-Al	i] Storage in air or H_2O especially at elevated temperature.	Al-oxide (Al-hydroxide)	114
	ii] Treatment with NaOH	High Ni content	114
	iii] Further oxidation	NiO predominates	114
Cu-Zn	i] Instantaneous heating in air	Zn enrichment	160
	ii] Treatment with HNO_3	Cu enrichment	160

3.8 Effect of crystal face

So far we have seen the selective enrichment of one of the components at the alloy surface, and examples for equilibrium surface segregation have been established for a great variety of binary alloy systems.

As far back as early 1970, Ollis (see in Ref. 104) drew attention to the crystallographic face dependence of surface enrichment. Recently Wandelt and Brundle[113] presented experimental evidence of crystal face specificity with regards to surface segregation in Ni(Cu) (single crystal) binary alloy.

According to the bond-breaking theory, the element which has the lower surface energy segregates to the surface, on the other hand elastic strain theory demands the segregation of odd-size solute atoms in dilute binary alloys.

In fact, Wandelt and Brundle found enhanced Cu segregation on the more open and lower coordinated (100) face as compared to the (111) face by using XPS Cu $2p_{3/2}$ to Ni $2p_{3/2}$ intensity ratio of clean Ni(Cu) alloy measured at grazing ejection angle.

On the basis of ideal solution model, heat of segregation Q_{seg} can be approximated by

$$Q_{seg} = \frac{\Delta Z}{Z} (H_B - H_A)$$

where ΔZ, Z, H_A and H_B have their usual significance. Now ΔZ (100) = 4 is larger than ΔZ (111) = 3 resulting in a higher Q_{seg} value for (100) face than towards (111) face.

CHAPTER II

EXPERIMENTS AND TECHNIQUES

EXPERIMENTS AND TECHNIQUES

The dilute tin alloys studied in the present investigations are as follows:

$Pb_{98}Sn_2$ - (Pb 98 wt % - Sn 2 wt %)
$Ag_{95}Sn_5$ - (Ag 95 wt % - Sn 5 wt %)
$Cu_{95}Sn_5$ - (Cu 95 wt % - Sn 5 wt %)
$Sb_{95}Sn_5$ - (Sb 95 wt % - Sn 5 wt %)
$In_{95}Sn_5$ - (In 95 wt % - Sn 5 wt %)
$Cd_{99.6}Sn_{0.4}$ - (Cd 99.6 wt % - Sn 0.4 wt %)

In addition three Cu-Sn intermetallic compounds viz. Cu_3Sn, Cu_4Sn and Cu_5Sn have also been studied. These alloys have been prepared by the usual metallurgical technique and examined by different techniques such as electron spectroscopy (ESCA) and powder X-ray diffraction (XRD).

The preparation and measurement procedures are given in detail in this Chapter.

2.1 Preparation of samples

As starting materials for the preparation of the samples spectroscopically pure metals were used. Except Pb and Sn (Chemistry Division, Bhabha Atomic Research Centre, Trombay, Bombay), all metals were purchased from

Johnson and Matthey Chemical Company, U.K.

We brought together the accurately weighed amounts of the metals in quartz tubes which were evacuated (pressure in the quartz tube was $< 10^{-6}$ Torr) and sealed under vacuum. The reaction was started by melting the constituents and the melts were heated to 50°C above their melting points for some time to render them homogeneous. Annealing was performed with the alloy ingots still in the closed container.

They were rolled into thin sheets, cleaned and polished to a mirror finish, and preserved properly to avoid any surface oxidation till they were used for recording the XP spectra.

For the various alloys, the highest temperature we reached in the melting procedure, the annealing temperatures and annealing times are given in Tables 2.1 and 2.2. Weight losses were found to be negligible in these alloy systems.

2.2 X-ray diffractometer

All the alloys were first characterized by powder X-ray diffraction technique. The alloy samples were directly mounted on the sample holder of a Philips X-ray diffractometer model PW 1730 for the structure identification. The diffracted X-ray intensities were recorded as a function of

Table 2.1 : Data on the preparation procedures of the various dilute tin alloys

Alloys	Crucible material	Highest temperature ^{o}C	Annealing temperature ^{o}C	Annealing time (days)	Results of X-ray analysis
$Pb_{98}Sn_2$	Silica	350	200	5	Single phase
$Ag_{95}Sn_5$	Silica	1000	725	8	Single phase
$Cu_{95}Sn_5$	Silica	1100	750	8	Single phase
$Sb_{95}Sn_5$	Silica	650	425	6	Single phase
$In_{95}Sn_5$	Silica	150	100	4	Single phase
$Cd_{99.6}Sn_{0.4}$	Silica	350	160	5	Single phase

Table 2.2 : Data on the preparation procedures of three Cu-Sn intermetallics

Intermetallics	Crucible material	Highest temperature °C	Annealing temperature °C	Annealing time (days)	Results of X-ray analysis
Cu_3Sn	Silica	1100	650	15	Single phase
Cu_4Sn	Silica	1100	700	15	Almost single phase
Cu_5Sn	Silica	1100	750	15	Single phase

2θ by using a copper target (CuK_α, $\lambda = 1.5404$ Å). The values of the interplanar spacing 'd' were calculated using the Bragg's relation,

$$n\lambda = 2d\sin\theta$$

where λ is the wavelength of the X-ray used, and θ is the Bragg's angle.

The expressions used to calculate lattice parameters for alloys of different crystal systems are as follows:

Cubic System : $$d_{hkl} = \frac{a}{\sqrt{h^2 + k^2 + l^2}}$$

$$a = b = c.$$

Tetragonal System : $$d_{hkl} = \frac{1}{\sqrt{h^2/a^2 + k^2/a^2 + l^2/c^2}}$$

$$a = b \neq c.$$

Hexagonal System : $$d_{hkl} = \frac{1}{\sqrt{(\frac{4}{3}a^2)\ (h^2+k^2+l^2) + (l^2/c^2)}}$$

$$a = b \neq c.$$

Rhombohedral System : $$d_{hkl} = \frac{1}{\sqrt{a\left[\frac{(h^2+k^2+l^2)\sin^2\alpha+2(hk+hl+kl)(\cos^2\alpha-\cos\alpha)}{1+2\cos^3\alpha-3\cos^2\alpha}\right]}}$$

$$a = b = c.$$

2.3 Electron spectrometer

All the tin alloys prepared in the present work are characterized on a commercial electron spectrometer marketed by M/s Vacuum Generators Scientific Ltd., U.K., ESCA-3, Mk II model and the same is described in detail here.

An electron spectrometer may conveniently be considered to consist of three main parts; (i) the excitation source (X-rays, ultraviolet photons, electrons or ions) to irradiate the sample, (ii) the energy analyzer to disperse the ejected electrons according to their energy and (iii) the detector for a quantitative estimation of the electron intensity and to provide a suitable output signal proportional to intensity as a function of electron binding energy.

Fig. 2.1 shows a block diagram of an electron spectrometer divided into its essential components.

The VG Scientific ESCA-3, Mk II is a high resolution electron spectrometer shown in Fig. 2.2 and it has been

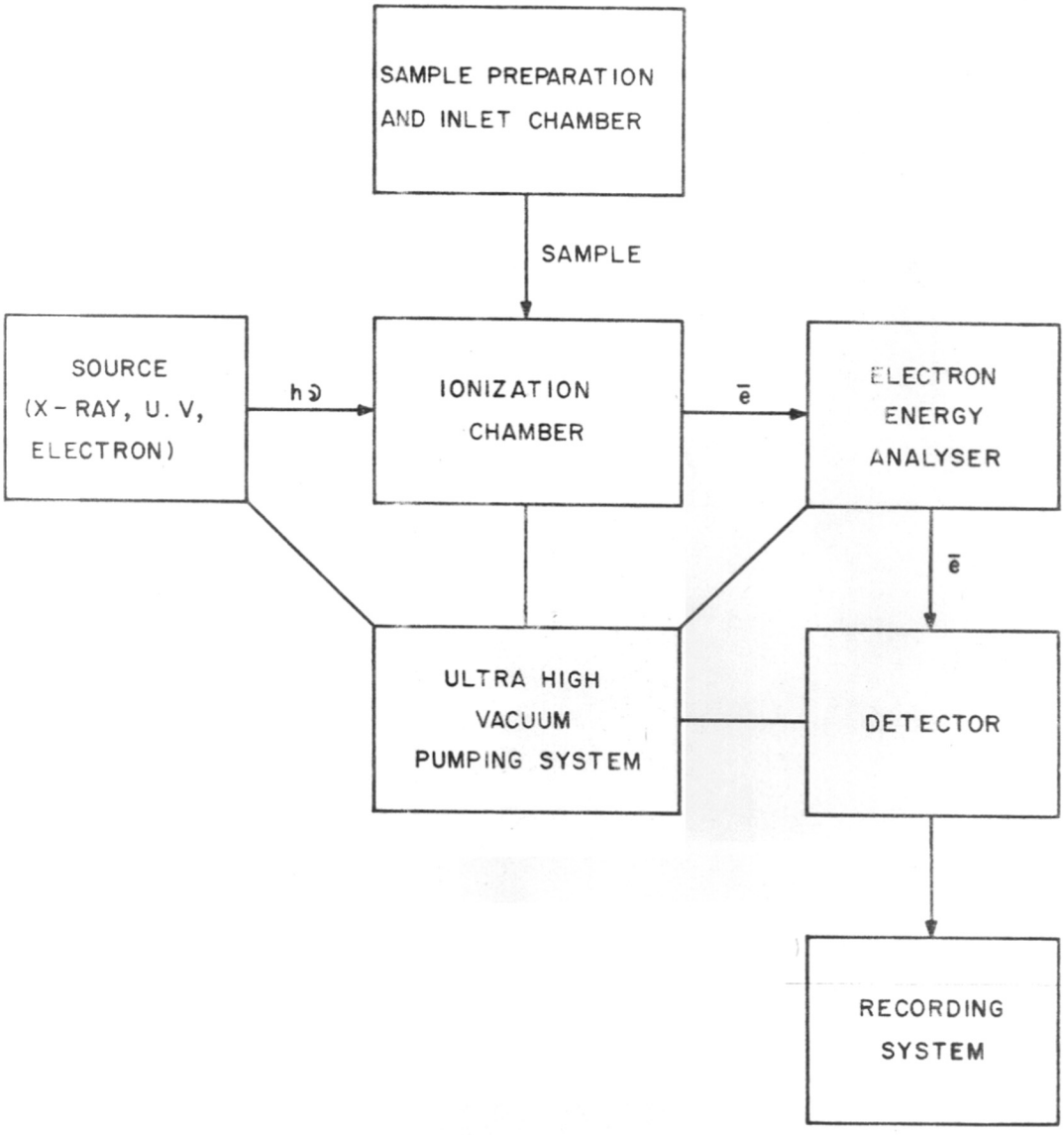

FIG. 2·1 : BLOCK DIAGRAM OF AN ELECTRON SPECTROMETER.

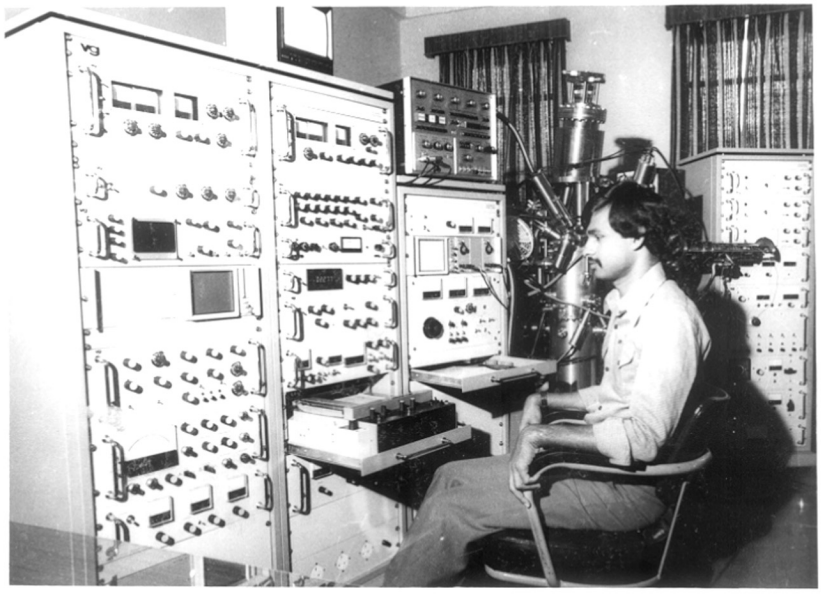

Fig. 2.2 : High resolution electron spectrometer marketed by M/s Vacuum Generators Scientific Ltd., U.K.

designed so that a variety of radiation sources can be accommodated simultaneously. The electron spectrometer at our laboratory (National Chemical Laboratory, Pune, India) has been fitted with the following radiation sources:

1. A twin anode (Al and Mg) X-ray source for X-ray photoelectron spectroscopy (XPS).
2. An ultraviolet helium lamp for ultraviolet photoelectron spectroscopy (UPS).
3. A small spot electron gun for electron initiated Auger electron spectroscopy (AES). The same gun is used for scanning Auger microprobe facility (SAM).
4. An argon ion gun to etch out the specimen for the depth profiling (DP).
5. Low ion density argon ion gun for secondary ion mass spectrometry (SIMS).

2.3.1 X-ray source

The simplest type of X-ray source used in XPS to probe atomic core levels is the standard X-ray tube. In this device, a heated filament provides electrons which are accelerated to a potential of between 10 and 20 keV toward a water cooled solid anode. The electrons create core holes in the anode atoms, which are filled by relaxing electrons from higher levels. The relaxation process is then accompanied by X-ray fluorescence. The anode material can be constructed from a wide variety of solids so that

the desired X-ray energy can be selected by choosing the appropriate material. The radiation is generally most intense from a single, sharp line providing a reasonably monochromatic X-ray source, although weaker lines and background continuous Bremsstrahlung radiation is also observed. A thin Al window usually serves to separate the X-ray tube from the rest of the spectrometer.

The K_{α} lines from elements like Mg and Al are probably the most suitable sources for XPS studies. As shown in Fig. 2.3 for the Al X-ray, a doublet arises from the $2p_{1/2}$, $2p_{3/2} \longrightarrow$ 1s electronic relaxation. Other bothersome spectral lines observed on spectrometers that do not provide additional energy selection include the $K_{\alpha_{3,4}}$ lines at $\sim$ 6% intensity, and a broad K_{β} line at 45 eV above $K_{\alpha_{1,2}}$ at $\sim$ 1% intensity[231]. The $K_{\alpha_{3,4}}$ lines arise from the $2p \longrightarrow$ 1s transition when the 1s level has been doubly ionized and from valence band to 1s transition results in K_{β} lines. A few of the other common anode materials[232] are given in Table 2.3.

Several important factors limit the choice of anode and explain why Mg and Al are the ones found on most commercial instruments. First, a narrow natural linewidth of the X-ray transition is important to obtain the desired

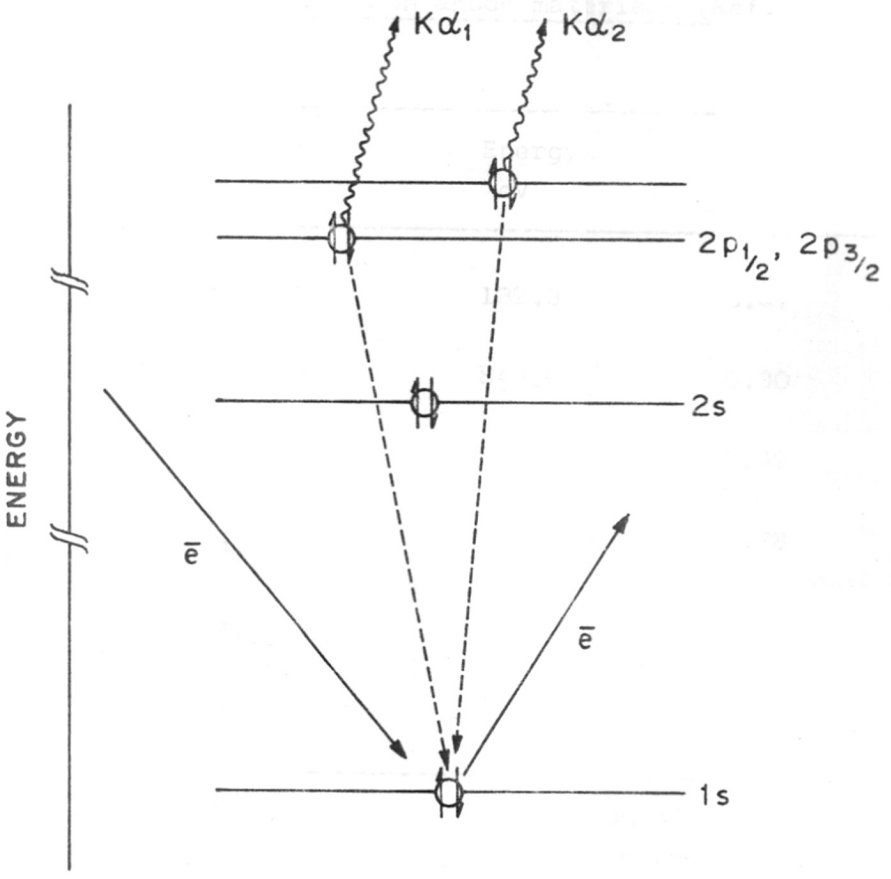

FIG. 2·3. ORIGIN OF THE Al Kα X-RAY LINES

Table 2.3 : Some common anode materials (Ref. 232)

Source	Transition	Energy eV	FWHM[a] eV
Y	$M\zeta$	132.3	0.47
Ne	$K_{\alpha_{1,2}}$	849.0	0.30
Na	$K_{\alpha_{1,2}}$	1041.0	0.42
Mg	$K_{\alpha_{1,2}}$	1253.6	0.78
Al	$K_{\alpha_{1,2}}$	1486.6	0.85
Cr	$K_{\alpha_{1,2}}$	5415.72	2.10

FWHM[a] is the full width at half maximum of a Goussian peak. The FWHM increases with increasing atomic number due to the 1s hole lifetime and to the increase in spin-orbit splitting of the $2p_{1/2}$ - $2p_{3/2}$ peaks.

energy resolution of 1 eV since any spread in $h\nu$ will result in an equivalent spread in the observed E_B. Anodes like CrK_α with a natural width of 2.1 eV would not be effective for high resolution studies. Second, the energy of the characteristic X-ray should be sufficient to excite photoelectrons from all the elements. The YMζ anode for example has good resolution but does not have sufficient energy to excite the 1s electron from C, a very commonly used transition. A photon energy of 1000-1500 eV seems most suitable as a general probe, although higher energies may be necessary to reach some important core level transitions like Pt 3d, and lower energies might be desirable to enhance surface sensitivity.

Our instrument has an additional monochromator device to reduce background from the Bremsstrahlung, eliminate extraneous spectral lines, and improve resolution. The AlK_α lines can be effectively monochromatized by reflection from a bent quartz crystal although the intensity is significantly reduced. This monochromatization improves the resolution up to 0.2 eV.

The twin anode is useful to differentiate between XPS peaks and X-ray excited Auger peaks. Since the Auger peaks remain unchanged in position on the kinetic energy

scale with change in excitation energy whereas photoelectron peaks will shift by 233 eV.

For the XPS study the alloy samples are irradiated by AlK_{α} with 15 KV, 20 mA anode voltage and emission current respectively and MgK_{α} with anode voltage 12 KV and emission current 20 mA and electrons from different orbits are ejected. These ejected electrons are analyzed energy-wise by a spherical sector analyzer.

2.3.2 Electron energy analyzer

The function of the energy analyzer is to disperse the ejected photoelectrons from a sample as a function of their energy.

For the electron spectrometer, it is desirable that both the spectral resolution as well as the sensitivity of photoelectron detection be as high as possible. Unfortunately however, both cannot be simultaneously increased, and compromises need to be made. The energy resolution is limited by the width of the photoelectron lines and is determined by several factors such as the inherent width of the ionizing radiation, the intrinsic width of the level which is responsible for photoelectron emission, and the finite resolving power of the electron energy analyzer used.

A resolution requirement for XPS is around 0.2 eV at 1000 eV i.e. resolving power ($E/\Delta E_{1/2}$) of 5000 where $\Delta E_{1/2}$ is the peak width at half maximum and E is the electron energy. This resolution is sufficient for normal electron spectroscopic applications. For high sensitivity application it is necessary to be able to degrade the resolution in order to achieve the necessary sensitivity increase. A reasonable upper limit is about 2.5 eV at 1000 eV, or a resolving power of 400.

There are two basic types of analyzers using the principles of (1) retarding potential and (2) dispersion respectively. Dispersion instruments are generally used for high resolution work and the same is used in ESCA-3, Mk II Electron Spectrometer.

An electron energy analyzer must be placed in a suitable vacuum environment, (pressure < 10^{-10} torr) to minimize the electron scattering through collision with the residual gas molecules. Similarly, since electrons are influenced by stray magnetic fields (including the earth's magnetism), it is necessary to cancel these fields within the enclosed volume of the analyzer. The cancellation of external magnetic field is done by using mμ-metal shield combined with Helmholtz coils.

2.3.3 Spherical sector analyzer

The spherical sector analyzer used for electron energy analysis in ESCA-3, Mk II electron spectrometer is shown in Fig. 2.4. It consists of two hemispheres (actually 150°), inner and outer, of 100 mm mean radius of curvature, mounted so as to provide a constant separation between them. A positive voltage is applied to the inner hemisphere and negative voltage to the outer one.

Electrons emitted by the sample enter the analyzer through the entrance slit and come under the influence of the electrostatic field (V) applied between the hemispheres, so that they now follow a curved path of constant radius.

High energy electrons moving at a relatively high speed are not deflected very much by the electrostatic field between the hemispheres, so they strike the outer hemisphere. Conversely low energy electrons moving at a relatively low speed are easily deflected and they strike the inner hemisphere. High energy electrons can then be detected by retarding them before they reach the analyzer until their energy is equal to the pass energy of the analyzer. Low energy electrons are detected in a similar way by accelerating them. The plate in front of analyzer hemispheres which contains the entry and exit slits is

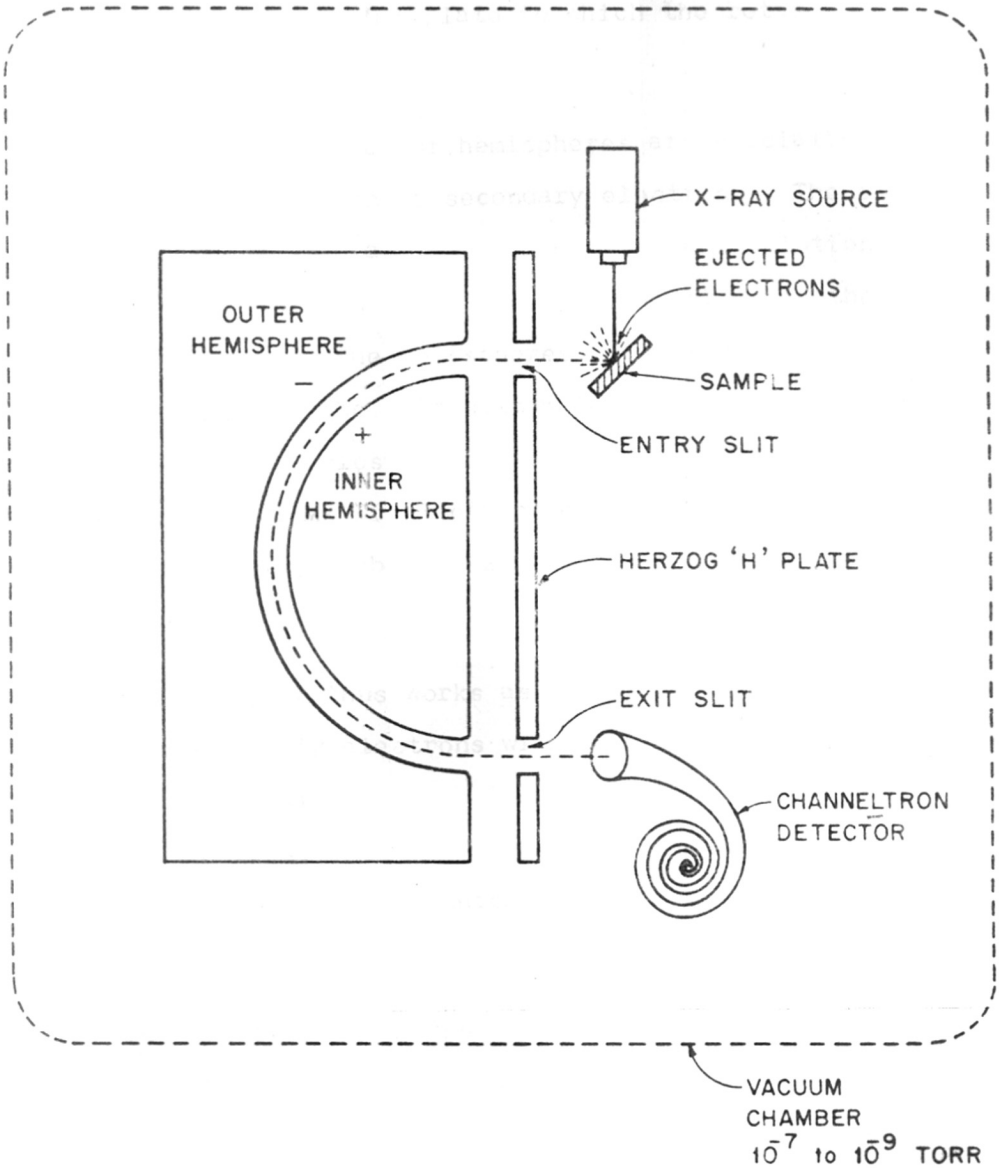

FIG. 2·4 : HEMISPHERICAL ANALYSER.

called the 'Herzog' or 'H' plate to which the retarding potential is applied.

The inner surfaces of hemispheres are specially treated to minimize the emission of secondary electrons. The slit at the entrance to the analyzer improves the resolution by ensuring that electrons enter the analyzer close to the neutral axis between the hemispheres. The resolution is further improved by the exit slit which allows only those electrons which are close to the neutral axis to reach the detector. ESCA-3, Mk II electron spectrometer is provided with externally adjustable 4, 2, 1 and 0.5 mm entrance and exit slits.

The analyzer thus works as a narrow pass filter letting through only electrons with an energy 'HV' where V is the potential difference between the inner and outer hemispheres and H is a constant determined by the physical dimensions of the analyzer which is equal to 2.64 for our instrument.

The electrons from the sample are retarded to a pass energy 'HV' by the scanned retarding potential 'R' applied between the specimen and the electrical centre point of the hemispheres. If E_{KE} is the kinetic energy of ejected electron (conventionally referred to the Fermi level) then

$$E_{KE} = R + HV + W$$

where W is a constant arising from the work function of the spectrometer material and is equal to 4.2 for our instrument.

The spectrometer control unit incorporates a switch for setting the pass energies of the analyzer at 2, 5, 10, 20, 50, 100 or 200 eV by varying the value of 'V' corresponding to about 0.7, 1.9, 3.8, 19, 38, 76 volts. It can provide energy scans of 1, 3, 10, 30, 100, 300 and 1000 volts in 30, 100, 300, 1000 and 3000 seconds.

The ability to select the energy with which electrons are transmitted around the analyzer and the ability to change entry and exit slit widths, provides a great flexibility in choosing the optimum sensitivity or resolution to suit a particular application.

2.3.4 Detector

The electron current emerging from the exit slit of the analyzer is very small of the order of 10^{-16} to 10^{-13} amperes. To detect this very weak current, a channel electron multiplier is used.

A channel electron multiplier is a small curved glass tube as shown in Fig. 2.4. The inside wall of this glass tube is coated with a high resistivity material. If a

potential is applied between the ends of the tube the resistive surface becomes a continuous dynode, electrically analogous to the separate dynodes of a conventional photo-multiplier together with the resistive chain used to establish the separate dynode potentials.

An electron entering the low potential end of the channel electron multiplier generates secondary electrons on collision with the wall of the tube. These secondary electrons are accelerated along the tube until they strike the wall again, where they generate further secondary electrons. This process produces a large number of electrons at the positive end of the tube. A channel electron multi-plier tube thus responds to an input of one electron by producing an output pulse of charge containing upto 10^8 electrons and its duration (full width at half maximum) is about 10 nanoseconds. The output electron beam charges a capacitor in the anode circuit of the multiplier which produces a voltage pulse. These pulses are fed to an amplifier and a discriminator. These pulses are then converted into NIM standard pulse of 5 volts amplitude and 500 nanoseconds duration and fed to the ratemeter which reads out the counts (pulses per second).

The X-axis of the X-Y recorder is connected via dividing resistors to scan the amplitude supply. The

Y-axis is fed from the recorder output of the ratemeter. A spectrum of total number of ejected electrons versus kinetic energy is thus plotted on the X-Y recorder.

Binding energies are obtained by substracting the kinetic energies from the energy of the X-ray source ($h\nu$).

2.3.5 Vacuum system

The heart of the electron spectrometer is its ultra high vacuum (UHV) console. Ultra high vacuum (better than 10^{-10} torr) is required for two reasons: (i) the ejected electron should pass through the analyzer without making any collisions with residual gas molecules and (ii) the partial pressure of reactive residual gases must be reduced to such a level that they will not unduly contaminate the sample surface and interfere with the study of that surface.

ESCA-3, Mk II vacuum console is designed to accept a variety of radiation sources simultaneously thereby allowing sequential analysis by a range of complementary surface techniques. The UHV system is divided into two parts, one is the sample preparation chamber and the other is the sample analyzer chamber.

The analyzer chamber is fabricated from mμ-metal with fourteen copper gasket-sealed-flanged ports fitted

with the electron analyzer assembly, the twin anode X-ray source, the UV source, the electron source, the ion source, the chaltron electron multiplier detector, the secondary electron detector, the glass view port, the sample manipulator and the X-ray monochromator source.

The 150 mm diameter x 340 mm long stainless steel specimen preparation chamber has 16 flanged ports sealed with copper gaskets and fitted with gate valve, sample transfer mechanism, argon ion cleaning gun, gas admission system, SIMS quadrupole detector, ion source, charge neutralising gun, view port and evaporation source.

Both the chambers are independently pumped by oil diffusion pumps fitted with water cooled chevron baffle and liquid nitrogen cold traps and backed rotary pumps. In addition titanium sublimation pumps (TSP) are fitted to both the chambers to reduce the pressure down to 5×10^{-11} torr.

The preparation chamber is isolated from the analyzer (or spectrometer) chamber at all times except when the specimen is being moved between them. The spectrometer and its channeltron multiplier is therefore protected against contamination from specimen preparation procedures. The sample preparation chamber also acts as a vacuum lock facility permitting relatively quick specimen change-overs.

The vacuum monitoring and protection system incorporate Pirani and ion gauges. The roughing line pressures are measured by Pirani gauges which incorporate facilities for protecting the diffusion pumps against failures in the rough vacuum system. Ultra high vacuum pressures are measured by ion gauges fitted separately to both chambers.

2.3.6 Sample handling

The electron spectrometer can handle samples which may be either solid with a regularly defined surface or a powder and may be a conductor, semi-conductor or non-conductor. Powders may be pelletized, compressed into suitable holder or dusted onto a carrier such as double sided adhesive tape.

The mounted sample holder is attached to the sample probe which is moved in the preparation chamber and to the analyzer chamber by means of a transfer mechanism consisting of edge welded stainless steel bellows giving a movement of approximately 13 inches. A heating and cooling facility enables the temperature of the sample to be varied between 600^{o}C to the liquid nitrogen temperature. The sample probe is mounted on a precision rotary motion drive with 360^{o} movement to allow the specimen to be accurately positioned for the appropriate analysis.

2.4 ESCA analysis of the alloy samples

X-ray photoelectron spectra of the alloy samples were recorded on this instrument. Before analysing the alloy samples the spectrometer was calibrated with the help of standard metallic samples. The spectroscopically pure foils of gold, silver, copper and platinum (obtained from M/s Johnson and Matthey Chemical Company, U.K.) were mounted on the standard sample holder assembled on to the sample transfer mechanism and finally located in the sample preparation chamber. The preparation chamber was then evacuated upto 10^{-2} torr by rotary pump and then upto 10^{-7} torr by the oil diffusion pump. The whole vacuum system was then baked at 150°C for 12 hours so that any contamination on the internal surface was removed and the system was cleaned. After removing the bakeout shrouds, the system was cooled to room temperature. The ion gauge heads, X-ray anode and filaments were outgassed for 30 minutes.

The liquid nitrogen traps of both the oil diffusion pumps were filled by sufficient liquid nitrogen. The titanium sublimation pump was fired for 1.5 minutes and vacuum better than 10^{-10} torr was achieved.

The samples were cleaned by argon ion etching followed by heating at 150°C in the sample preparation chamber to

remove all the surface contaminations. After opening the sample preparation and analyzer chamber isolation gate valve, samples were transferred to the analyzer chamber. One of the four samples was positioned exactly under the X-ray source and in front of the entry slit of the analyzer with the help of the X,Y,Z sample manipulator.

The ratemeter, channeltron multiplier power supply, X-ray source power supply, X-Y recorder, digital voltmeter and spectrometer control units were switched on for half an hour to stabilize before the spectra were taken.

The spectrometer control unit comprising programmed power supply, the ramp generator, hemisphere voltage, HV + W circuit, and pedestal supply were calibrated by adjusting the calibrating potentiometers. The XP spectra were then recorded. The other three samples were also analyzed in the same way. The binding energy values are given in Table 2.4. The best available standard binding energy values[233] are also given in the same Table for comparison. Our experimental binding energy values are in good agreement with the literature values.

After switching off the X-ray source, the analyzer and the detector power supply, the samples were brought back to the preparation chamber and the isolation gate valve

Table 2.4 : Binding energies suitable for use as standards for calibration of X-ray photoelectron spectrometer

Metal	Level	Binding energy eV (Literature value)*	Binding energy eV (Our experimental value)
Silver	$3d_{5/2}$	368.2 ± 0.2	368.3
Gold	$4f_{7/2}$	83.8 ± 0.2	84.0
Platinum	$4f_{7/2}$	71.0 ± 0.2	71.0
Copper	$2p_{3/2}$	932.8 ± 0.2	932.4

* Ref. 233

was closed. Then dry nitrogen was let in the sample preparation chamber upto atmospheric pressure. The sample probe was then removed from the sample transfer mechanism by unbolting the flange.

The tin alloy samples were mounted on the sample holder and were examined in the same way as described above.

For comparative study the spectrometer parameters were kept constant while analysing all alloy samples. All the spectra were taken at 50 eV pass energy of the analyzer, with 4 mm entry and exit slit. The total effective voltage to the channeltron multiplier was kept at 3.5 KV to avoid its damage.

The surface of the alloy was first examined by XPS. Then its pure constituents were examined. The recorded XP spectra and their analysis are given in the next Chapter.

CHAPTER III

CORE LEVEL BINDING ENERGY SHIFTS IN DILUTE TIN ALLOYS

CORE LEVEL BINDING ENERGY SHIFTS IN DILUTE TIN ALLOYS

3.1 Introduction

Near-neighbour interactions have a significant influence on the energy levels of core electrons, primarily from charge transfer effects due to differences in the electronegativities of the atoms involved. This charge transfer is also expected to depend on the coordination number and the surrounding geometry, although this effect has not been so clearly established. X-ray photoelectron spectroscopy is a powerful tool for obtaining information about electron energy levels in metals and alloys.

A survey of the available literature on photoelectron spectroscopy indicates that very few attempts have been made to determine the effect of different coordinations of an atom on its core electron energy levels. Watts and Huheey[234] reported a binding energy difference of 0.6 eV between the Sn $3d_{5/2}$ levels of α-tin (diamond structure) and β-tin (tetragonal structure). This was attributed to the change in coordination number as well as to decrease in the Sn-Sn distance. Porte and Maire[235] recorded the XP spectra of thallous iodide at various temperatures and noted an abrupt change in binding energy separation between the iodine and

thallium core levels when the structure changes from orthorhombic to simple cubic. On the contrary, Brundle et al.[236] in their study on iron oxides concluded that octahedrally coordinated Fe^{III} is not distinguishable from the tetrahedrally coordinated species by using Fe $2p_{3/2}$ core level spectra.

The core level binding energy dependence on coordination number has been observed recently by some other workers. The core level binding energy of surface atom in Au[79,82], Yb[85], and in single crystals of W[83,84], Ta[84], Ir[86], Si[87,88], GaAs and GaSb[90,91] has been found to depend on the coordination number of the surface atoms (or special geometry of the surface). Theoretically, it is also expected that binding energy should depend on coordination number. Steiner and Hufner[89] in their studies on the binding energy shift in Ni on Au and Au on Ni overlayers have concluded that the binding energy shifts are governed by the mean coordination number of the atoms in the overlayer.

In order to investigate systematically the effects of different factors such as electronegativity, coordination number etc. on the chemical shift we selected several dilute tin alloys[1,16-18]. Our main aim was to study the effect of change in coordination number on the Sn core

electron binding energy. However, it is not possible to obtain Sn surrounded by Sn in very many different crystal structures. It was therefore necessary to study Sn alloys with different crystal structures. At the same time care had to be taken to see that the new element added had nearly the same electronegativity as Sn, to avoid electronegativity effects. The following systems appeared attractive from these considerations: α-Sn, β-Sn, Ag-Sn, and Cu-Sn (the electronegativities of Ag, Cu and Sn are nearly equal). The work was further extended to determine the effect of changes in the electronegativity. For this purpose, the alloys compared had to have Sn in the same surroundings. The following systems were selected for this investigation; Pb-Sn, Ag-Sn, Cu-Sn, Cd-Sn and In-Sn (all are close-packed with twelve near neighbours). We selected dilute tin alloys to avoid Sn-Sn proximity so that the effect of the host atom surroundings could be clearly seen.

3.2 Experimental

For these reasons following dilute tin alloys have been studied:

$Pb_{98}Sn_2$, $Ag_{95}Sn_5$, $Cu_{95}Sn_5$,
$Sb_{95}Sn_5$, $In_{95}Sn_5$, $Cd_{99.6}Sn_{0.4}$

These alloys were prepared by the standard metallurgical techniques and characterized by the powder X-ray diffraction (Philips 1730) method as described in the previous Chapter.

X-ray photoelectron spectra were recorded using an ESCA-3, Mk II electron spectrometer (VG Scientific Ltd., U.K.) equipped with a MgK_{α} anode (1253.6 eV) with analyzer energy set at 50 eV and entrance slit width at 4 mm. The pressure in the spectrometer was maintained at $< 10^{-10}$ torr. Prior to recording of the XP spectra the samples were cleaned by argon ion etching followed by annealing at $125^{o}C$ in the preparation chamber of the spectrometer. This treatment removed the sputter damage and all surface contaminants. The calibration of the spectrometer was checked by measuring the binding energy of Au $4f_{7/2}$ (84.0 eV), Ag $3d_{5/2}$ (368.3 eV) and Cu $2p_{3/2}$ (932.4 eV). These binding energy values were in good agreement with the values available in the literature. The instrumental resolution obtained under these conditions for Au $4f_{7/2}$ level was 1.6 eV (FWHM). The experimental binding energy throughout this investigation is given in relation to the Fermi level. The estimated accuracy of these binding energies is about $\pm$ 0.2 eV.

3.3 Results and discussion :

3.3.1 X-ray diffraction (XRD) study

The diffraction patterns confirmed that all the alloys were homogeneous and had the correct lattice constants. Table 3.1 gives the structure and lattice constants of these alloys and of α-Sn and β-Sn.

Allotropes of tin

Tin has two forms. Above 18°C the stable form is the so called β or white tin and below 18°C the stable form is the so called α or grey tin.

α-tin crystallizes in the diamond structure with lattice constant a = 6.4600 Å. In α-tin each atom has four equidistant neighbours at a distance of 2.804 Å. Whereas β-tin crystallizes in the tetragonal structure with lattice constants a = 5.8569 Å and b = 3.1487 Å. In β-tin each atom has four nearest neighbours at 3.016 Å and two further neighbours at 3.175 Å.

$Pb_{98}Sn_2$ alloy

It crystallizes in the face centred cubic structure. The X-ray diffraction patterns of the alloy show that the lattice parameter of Pb is lowered by addition of Sn from

Table 3.1 : The structure and lattice constants of the alloys used

Sample	Type	Structure	Lattice constants (Å)
Sn (β)	Metal	Tetragonal	a - 5.8569 b - 3.1487
Sn (α)	Metal	Diamond	a - 6.4600
Sn_2Pb_{98}	Solid solution	F.C.C.	a - 4.9167
Sn_5Ag_{95}	Solid solution	F.C.C.	a - 4.1271
Sn_5Cu_{95}	Solid solution	F.C.C.	a - 3.6152
Sn_5In_{95}	Solid solution	Tetragonal (distorted F.C.C.)	a - 3.2381 c - 4.9874
Sn_5Sb_{95}	Solid solution	Rhombohedral	a - 6.1380 α - 89.38°
$Sn_{0.4}Cd_{99.6}$	Solid solution	H.C.P.	a - 2.9711 c - 5.5992

a = 4.9506 Å (Pb) to a = 4.9167 Å ($Pb_{98}Sn_2$), in accordance with the earlier observation[237]. Thus in the Pb-Sn alloy each atom has twelve equidistant neighbours (i.e. coordination number is 12) at a distance of 3.495 Å.

$Ag_{95}Sn_5$ alloy

This alloy crystallizes in the face centred cubic structure with lattice constant a = 4.1271 Å. The X-ray diffraction patterns of the alloy indicate that the lattice constant of Ag is increased by addition of Sn from a = 4.0862 Å (Ag) to a = 4.1271 Å ($Ag_{95}Sn_5$). This is in good agreement with the earlier observation of Rothery et al.[238]. Thus in this alloy each atom has twelve equidistant neighbours at a distance of 2.918 Å.

$Cu_{95}Sn_5$ alloy

It exists in the face centred cubic structure with a lattice constant a = 3.6152 Å. So in the $Cu_{95}Sn_5$ alloy each atom has twelve equidistant neighbours at a distance of 2.556 Å.

$Sb_{95}Sn_5$ alloy

It crystallizes in the rhombohedral hexagonal type, (with lattice constant a = 6.1380 Å and $\alpha = 89.38^\circ$) in

which atoms are arranged in double layers so that each has three close neighbours at a distance of 2.898 Å and three at a somewhat greater distance of 3.357 Å [239].

$In_{95}Sn_5$ alloy

It crystallizes in the face centred tetragonal structure with lattice constants a = 3.2381 Å and c = 4.9874 Å. So that in the In-Sn alloy each atom has twelve near neighbours in an approximate close packing. The neighbours fall into two groups, one of four at a distance of 3.24 Å and the other group of eight at 3.37 Å [239].

$Cd_{99.6}Sn_{0.4}$ alloy

It crystallizes in close packed hexagonal structure with lattice constants a = 2.9711 Å and c = 5.5992 Å. In this structure each atom has six close neighbours lying in one plane and at a greater distance three in a similar plane above and three below. Thus in the $Cd_{99.6}Sn_{0.4}$ alloy each atom has twelve neighbours at an approximate distance of 2.973 Å.

3.3.2 X-ray photoelectron spectroscopic (XPS) study

Fig. 3.1 shows the XP spectra of the Sn 3d core levels for β-Sn (at room temperature and at liquid nitrogen

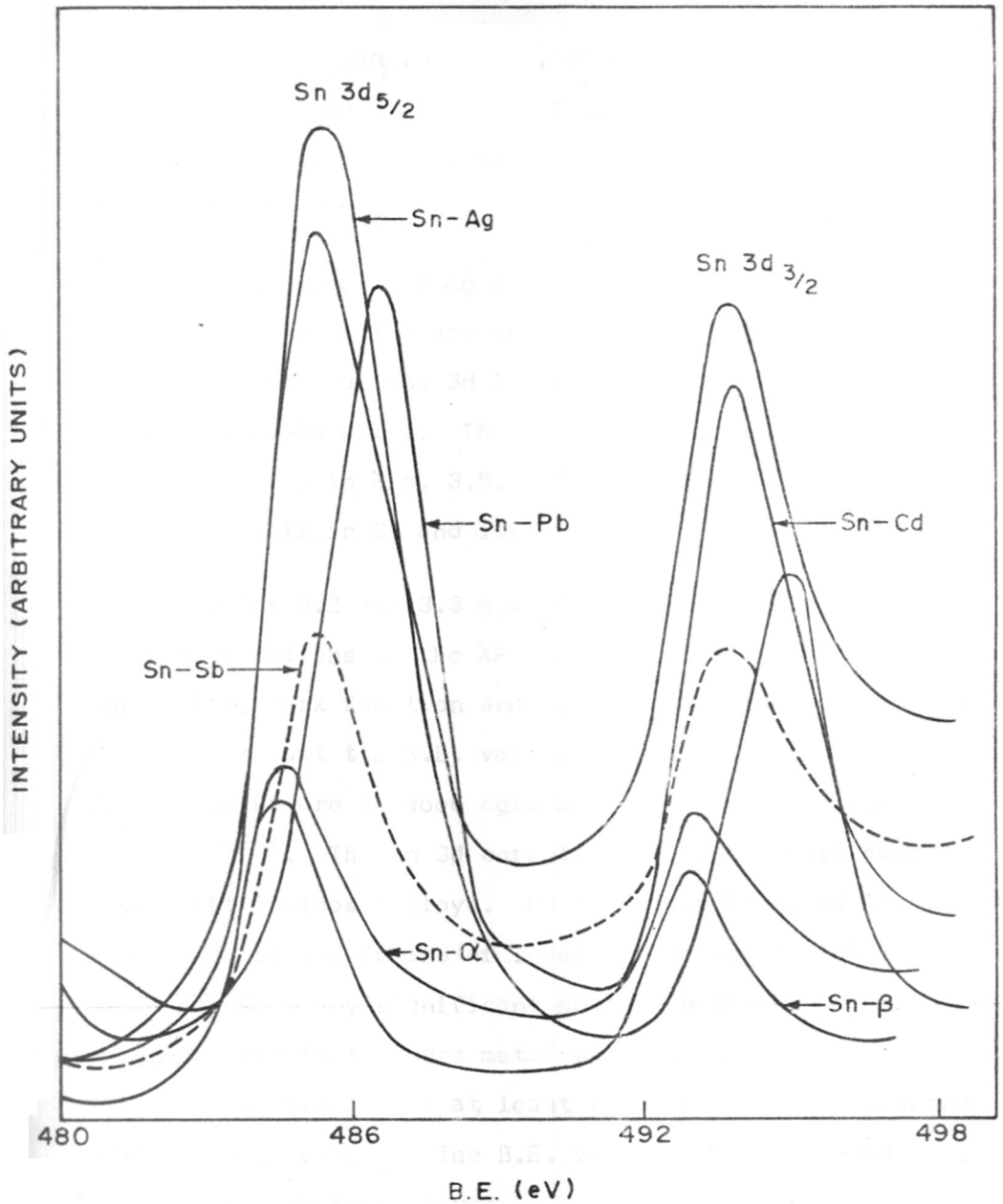

FIG. 3·1. XP SPECTRA OF Sn 3d LEVELS

temperature), $Pb_{98}Sn_2$, $Ag_{95}Sn_5$, $Sb_{95}Sn_5$ and $Cd_{99.6}Sn_{0.4}$. Fig. 3.2 shows the XP spectra of the Sn 3d core levels for β-Sn (at room temperature and at liquid nitrogen temperature), $Cu_{95}Sn_5$ and $In_{95}Sn_5$.

The 3d levels of Ag and its Sn alloy and the 4f levels of Pb and its Sn alloy are shown in Fig. 3.3. Fig. 3.4 shows XP spectra of the 3d levels of Cd and its Sn alloy and of the Sb-Sn alloy. The 3d levels of In and its Sn alloy are given in Fig. 3.5. Fig. 3.6 shows the XP spectra of Cu 2p levels in Cu and its Sn alloy.

Tables 3.2 and 3.3 give B.E. values derived from the line positions in the XP spectra, along with the electronegativity, work function and heat of sublimation data. It can be seen that the B.E. values for pure β-Sn, Cd, Ag, In, Sb, Cu and Pb are in good agreement with the reported values[240,241]. The Sn 3d core lines showed significant B.E. shift in these alloys. On the other hand, 3d levels of Ag, Cd, Sb and In and 4f levels of Pb and 2p levels of Cu did not show any significant change in the binding energy when compared to the pure metal values. Here each B.E. value is the result of at least three repetitive measurements on each sample. The B.E. values are calibrated relative to the Fermi level.

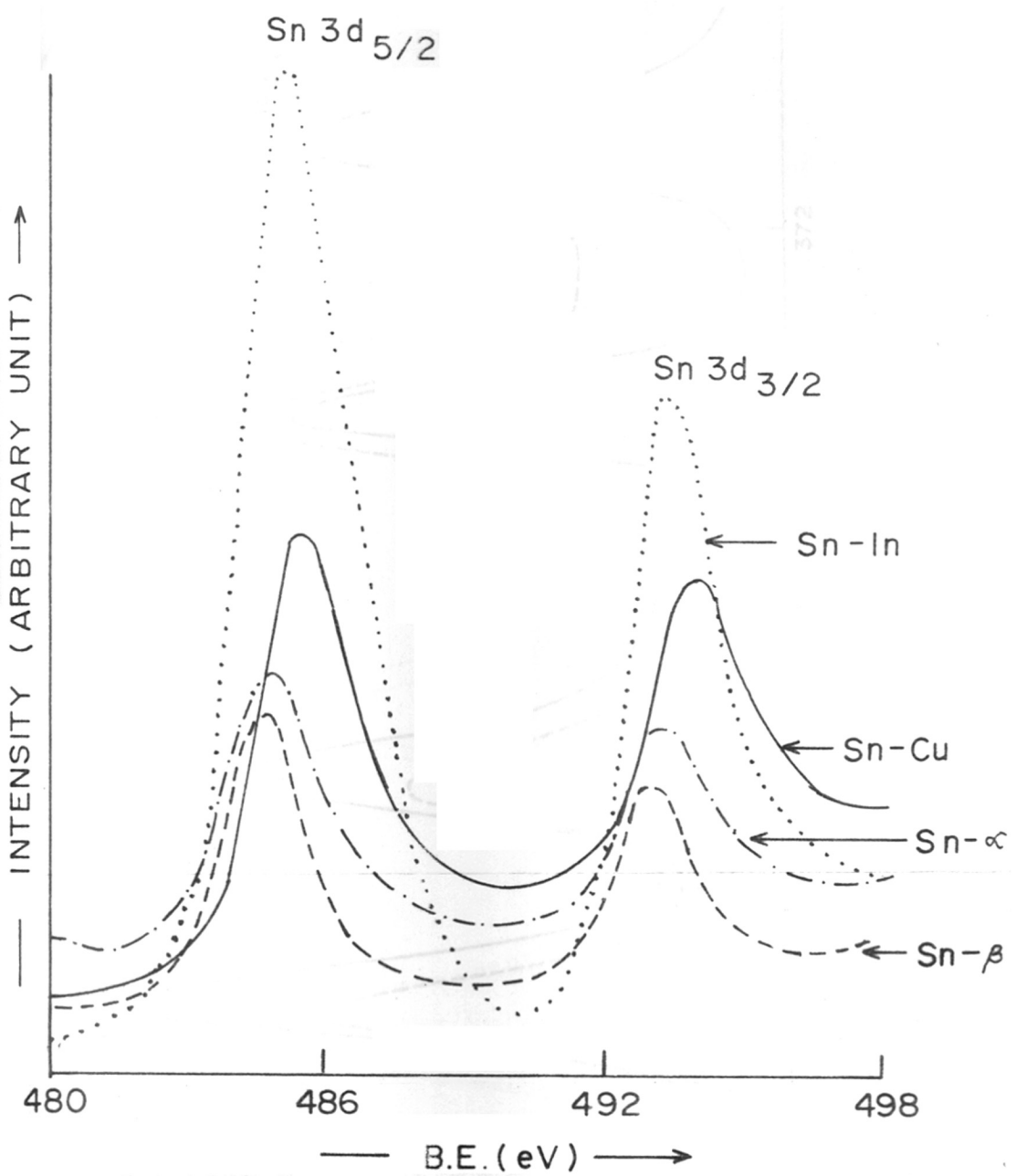

FIG 3·2: XP SPECTRA OF Sn3d LEVELS

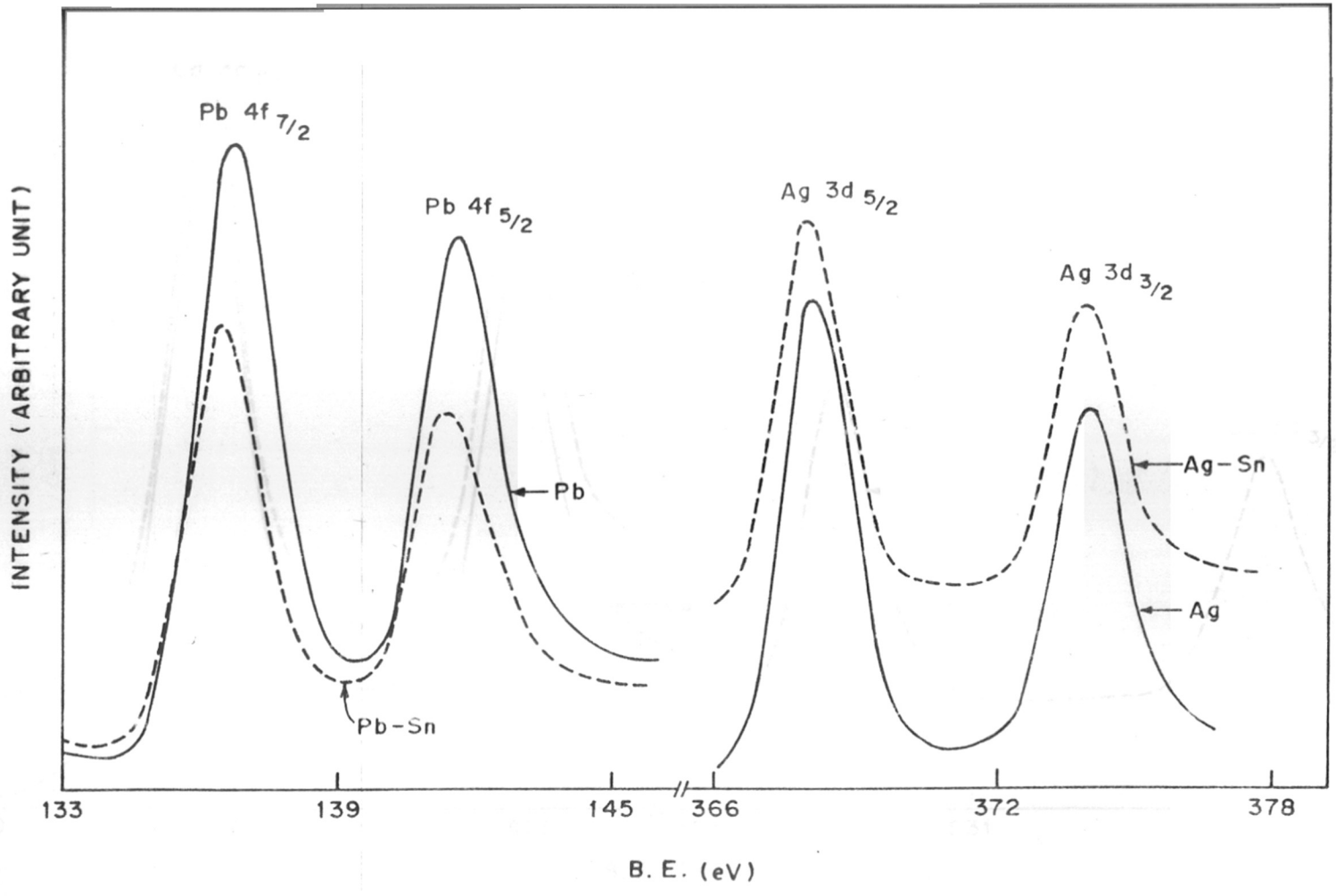

FIG. 3·3. XP SPECTRA OF Pb 4f AND Ag 3d LEVELS

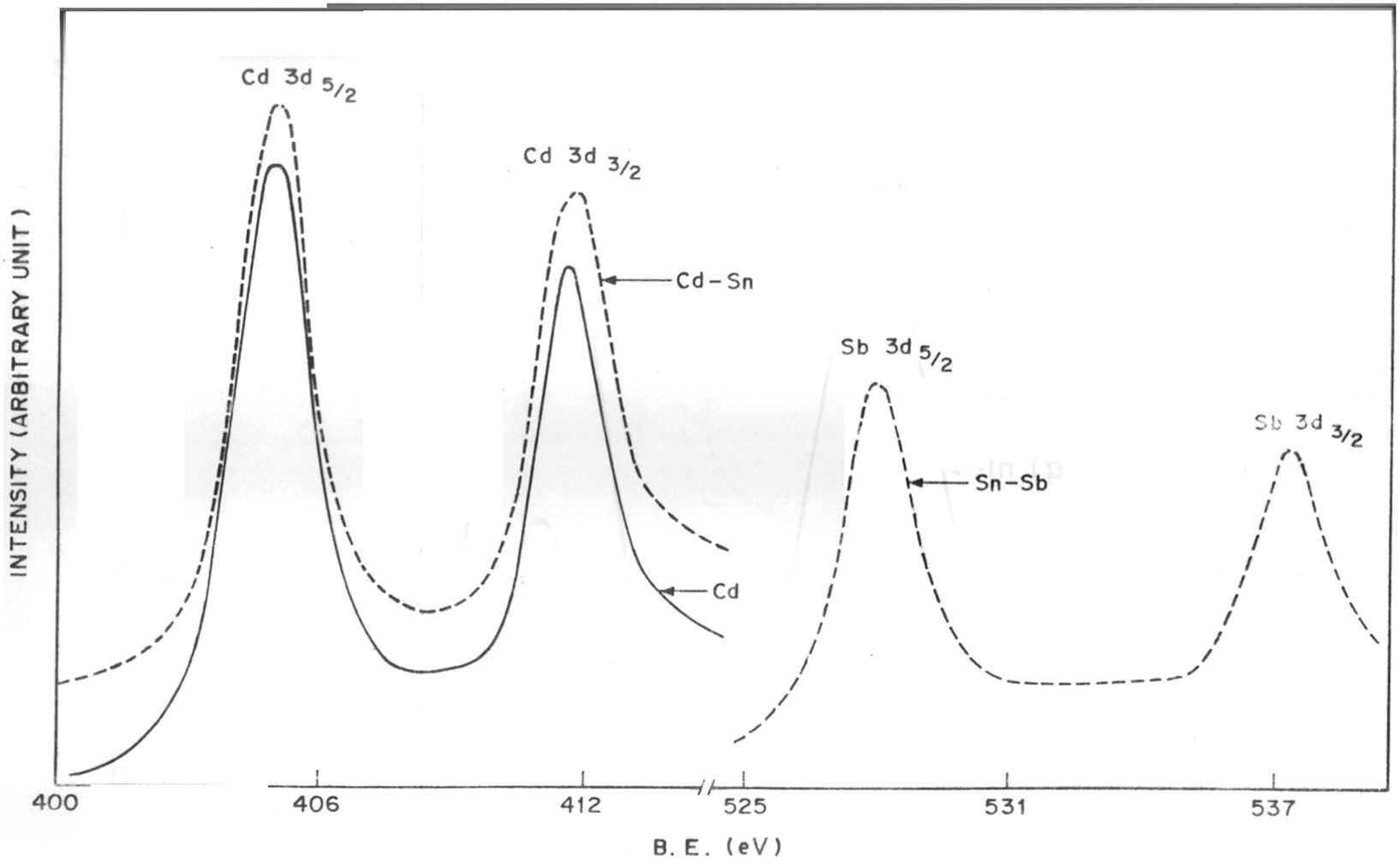

FIG. 3·4. XP SPECTRA OF Cd 3d AND Sb 3d LEVELS

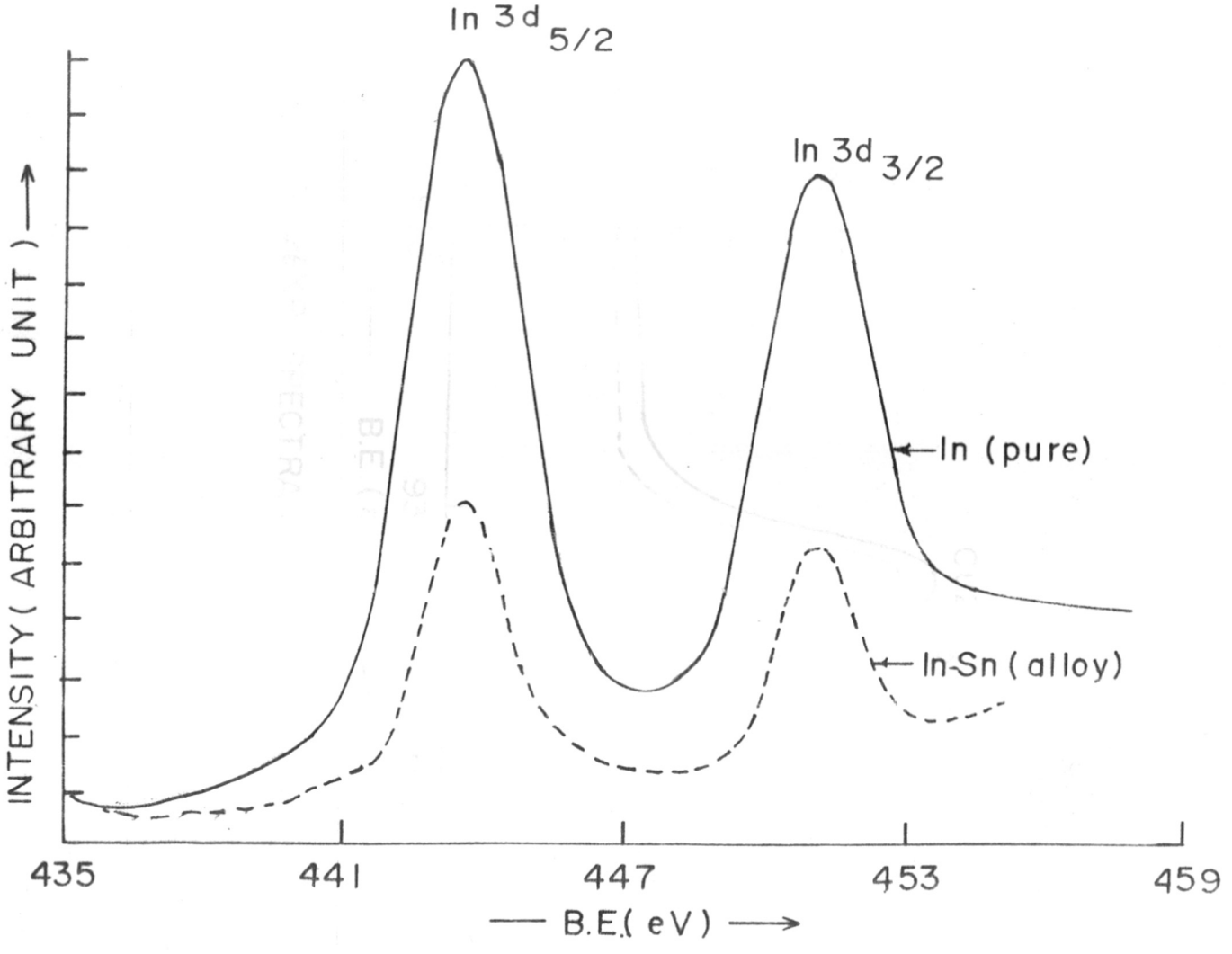

FIG.3.5:XP SPECTRA OF In 3d LEVELS

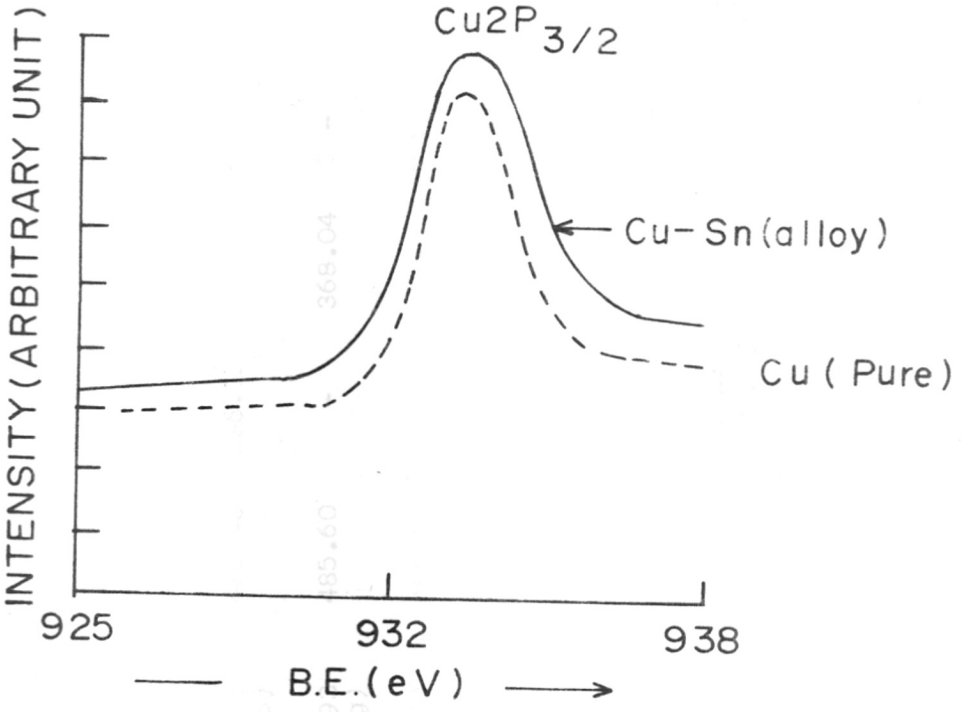

FIG.3.6:XP SPECTRA OF $Cu2p_{3/2}$ LEVEL

Table 3.2 : Binding energy values as derived from the line position in the photoelectron spectra along with electronegativity, work function and heat of sublimation data

System	Coordination No. (η)	Electronegativity (λ)	$Sn3d_{5/2}$ eV	$Pb4f_{7/2}$ eV	$Ag3d_{5/2}$ eV	$Cd3d_{5/2}$ eV	$Sb3d_{5/2}$ eV	ΔE eV	Work function* ϕ eV	Heat of sublimation kcals/mole
β-Sn	4+2	1.96	484.60	-	-	-	-	0	4.1	72.0
α-Sn	4	1.96	485.00	-	-	-	-	0.4	4.1	72.0
$Pb_{98}Sn_2$	12	2.33 (Pb)	486.40	136.72	-	-	-	1.8	4.0	46.34 (Pb)
$Ag_{95}Sn_5$	12	1.93 (Ag)	485.60	-	368.04	-	-	1.0	4.1	69.12 (Ag)
$Cd_{99.6}Sn_{0.4}$	12	1.69 (Cd)	485.30	-	-	404.92	-	0.7	4.1	26.97 (Cd)
$Sb_{95}Sn_5$	3+3	2.05 (Sb)	485.20	-	-	-	528.00	0.6	4.1	60.80 (Sb)
Pure metals	-	-	-	136.96	368.20	405.04	528.00	-	-	-
Sn-oxidized	-	-	487.10	-	-	-	-	2.5	-	-

* Work function derived from the UPS study as described in the text.

Table 3.3 : Binding energy values as derived from line positions in the photoelectron spectra, along with electronegativity, work function and heat of sublimation data

System	Coordination No. (η)	Electronegativity (λ)	$Sn3d_{5/2}$ eV	$Cu2p_{3/2}$ eV	$In3d_{5/2}$ eV	ΔE eV	Work function* ϕ eV	Heat of sublimation kcals/mole
β-Sn	4+2	1.96	484.60	-	-	-	4.1	72.0
α-Sn	4	1.96	485.00	-	-	0.4	4.1	72.0
$In_{95}Sn_5$	4+8	1.78 (In)	485.20	-	443.60	0.6	4.0	58.2 (In)
$Cu_{95}Sn_5$	12	1.90 (Cu)	485.60	932.5	-	1.0	4.1	81.5 (Cu)
In	4+8	1.78	-	-	443.60	-	4.0	58.2
Cu	12	1.90	-	932.4	-	-	4.3	81.5

* Work function derived from the UPS study as described in the text.

Calibration of binding energy relative to the Fermi level as determined from the valence electron spectra of the sample

Procedure :

1. Measure valence band spectrum of the sample viz. Sn metal (see Fig. 3.7).
2. Extrapolate background intensity measured above Fermi level to higher binding energies under valence band peak.
3. Measure height of valence-band maximum from this background and mark 50% point.
4. From the 50% point draw a line parallel to the energy axis to intercept measured curve.
5. Read energy scale corresponding to intercept.

This method[242] yields a unique Fermi level which is considered as the zero of binding energy on the instrumental B.E. scale. The same procedure is used to find out zero B.E. of Sn in all the alloys studied here.

3.3.2A Sn allotropes (α-Sn and β-Sn)

On cooling β-tin to liquid nitrogen temperature the tin structure changes from tetragonal to diamond. The difference in the B.E. (ΔE) values between β-tin at room temperature and at liquid nitrogen temperature is 0.4 eV.

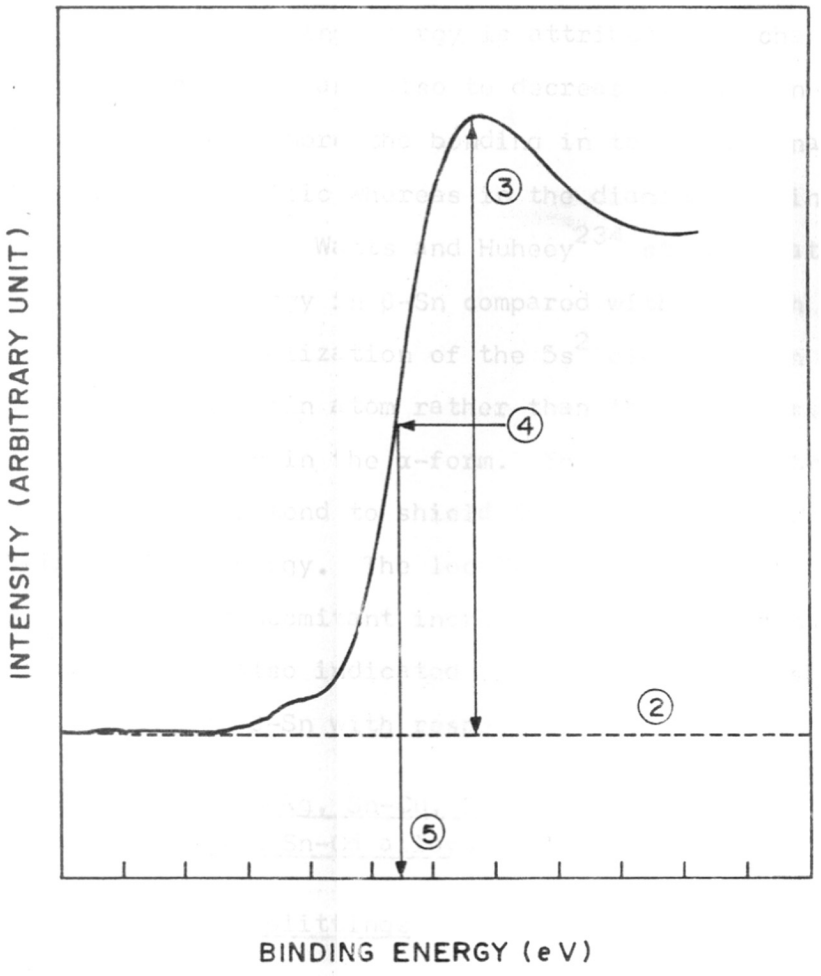

FIG. 3·7. ① VALENCE BAND SPECTRUM OF TIN METAL

This is 0.2 eV less than the difference reported earlier[234]. This change in binding energy is attributed to change in the coordination number and also to decrease in the Sn-Sn distance. Furthermore the bonding in the tetragonal (β-tin) structure is metallic whereas in the diamond (α-tin) structure is covalent. Watts and Huheey[234] stated that the lower binding energy in β-Sn compared with that in α-Sn is due to the localization of the $5s^2$ electrons in atomic orbitals on each tin atom rather than their participation in the bonding as in the α-form. The highly penetrating s electrons will tend to shield the 3d electrons and lower their binding energy. The localization of the Sn $5s^2$ electrons and concomitant increased s electron density at the nucleus is also indicated by the positive Mossbauer isomer shift of β-Sn with respect to α-Sn[243-246].

3.3.2B Sn-Pb, Sn-Ag, Sn-Cu, Sn-Sb, Sn-In and Sn-Cd alloys

(i) Spin-orbit splittings

The Sn $3d_{5/2}$ and Sn $3d_{3/2}$ binding energies have been measured in all these alloys (Table 3.4). The Sn $3d_{5/2}$ - $3d_{3/2}$ doublet was found in the present investigation to exhibit an intensity ratio of 3:2 as predicted from a simple free atom model in which the relative intensity of

Table 3.4 : Sn 3d binding energies in various samples.

Sample	Sn $3d_{5/2}$ eV	Sn $3d_{3/2}$ eV	ΔE_{3d} eV	FWHM eV
Sn (β)	484.60	493.00	8.40	1.9
Sn (α)	485.00	493.40	8.40	1.9
$Pb_{98}Sn_2$	486.40	494.80	8.40	2.2
$Ag_{95}Sn_5$	485.60	494.00	8.40	2.2
$Cu_{95}Sn_5$	485.60	494.00	8.40	2.1
$Sb_{95}Sn_5$	485.20	493.60	8.40	2.2
$In_{95}Sn_5$	485.20	493.50	8.30	2.1
$Cd_{99.6}Sn_{0.4}$	485.30	493.70	8.40	2.0
Sn oxidized	487.10	495.50	8.40	2.1

the two lines is derived from the statistical weights of the two final states i.e. [2(5/2) + 1]:[2(3/2) + 1] . Additionally a constant energy separation ($\Delta E_{3d} = E_{3d_{5/2}} - E_{3d_{3/2}}$) of 8.4 ± 0.10 eV was observed for these two peaks over the entire range of the dilute tin alloys.

It is also observed that the relative intensities of the two levels (of host atoms) in each of these alloys is proportional to the statistical weights (2J + 1) of the two final states. The 3d spin-orbit splittings (ΔE_{3d}) for Ag, Cd, In, Sn and Sb in their alloys have been measured (see Table 3.5). In these alloys the spin-orbit splittings (ΔE_{3d}) for Ag, Cd, In, Sn and Sb are linearly related (see Fig. 3.8) to the atomic number Z, of the host atom as

$$\Delta E_{3d} = mZ + C.$$

This indicates that there is strong deviation from the spherical coulombic potential[247].

(ii) Line widths

As can be seen from Table 3.4, there is no significant change in the Sn 3d line width over the entire range of the dilute tin alloys. The broadening of the Sn 3d level can be ascribed to change in vacancy life time. The valence electron density influences these life times through its

Table 3.5 : Relation between spin-orbit splitting and atomic number

Sample	Atomic number Z	Core levels		Spin-orbit splitting
		$E_{3d_{5/2}}$ eV	$E_{3d_{3/2}}$ eV	ΔE_{3d} eV
$Ag_{95}Sn_5$	47 (Ag)	368.28	374.28	5.9
$Cd_{99.6}Sn_{0.4}$	48 (Cd)	405.00	411.80	6.8
$In_{95}Sn_5$	49 (In)	443.60	451.20	7.6
Sn_{100}	50 (Sn)	484.60	493.00	8.4
$Sb_{95}Sn_5$	51 (Sb)	528.00	537.40	9.4

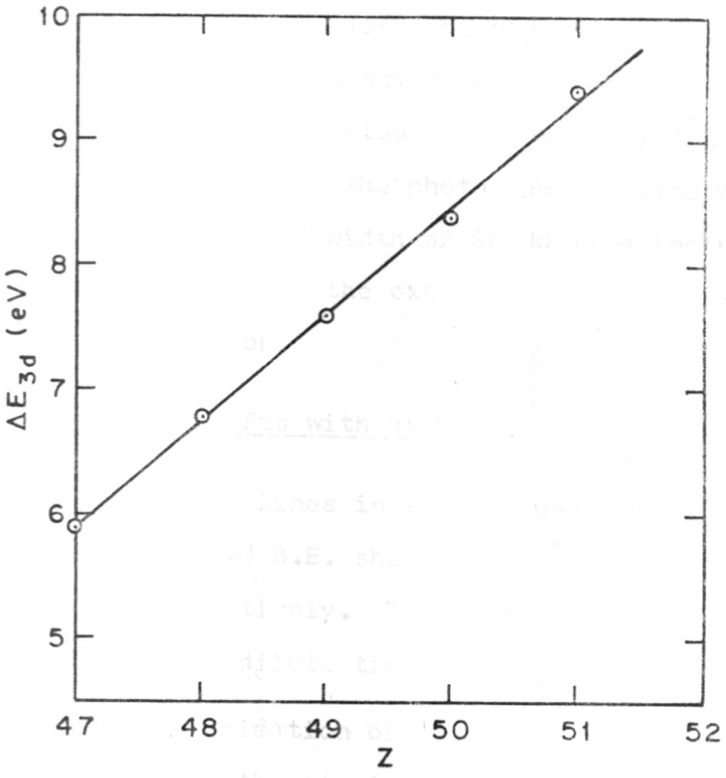

FIG. 3·8. PLOT OF THE SPIN-ORBIT SPLITTINGS ΔE_{3d} IN DILUTE TIN ALLOYS vs. ATOMIC NUMBER Z

effect on Auger transition rates. The Auger processes are usually responsible for filling the vacancies. Variation in valence-shell electron density associated with bonding differences should be reflected in the Auger rates and thus the vacancy life times and the photoelectron line width. In addition, the measured width of Sn 3d line include contributions from the width of the exciting radiation and the spectrometer resolution.

(iii) Core level shifts with alloying

The Sn 3d core lines in Pb-Sn, Cu-Sn, Ag-Sn, Cd-Sn, Sb-Sn and In-Sn showed B.E. shifts of 1.8, 1.0, 1.0, 0.7, 0.6 and 0.6 eV respectively. The Sn 3d core level binding energy shifts in the dilute tin alloys may be due to

(a) surface oxidation of the tin,

(b) change in the atomic volume during the formation of the alloy,

(c) difference in the work function of the metals,

(d) difference in the electronegativity and

(e) change in the coordination number.

The B.E. shifts in the Sn 3d levels can not be attributed to the surface oxidation of Sn in these alloys, because these alloys were cleaned and polished to a mirror finish and preserved properly to avoid any surface oxidation

until they were used for recording the XP spectra. Secondly, each sample was cleaned by Ar-ion etching, before recording the spectra. The O1s signal was found to be totally absent, or its intensity had diminished to such an extent that we could not detect it. Further, as a test case, the Pb-Sn alloy was deliberately oxidized by heating in air at $\sim 150^{\circ}C$. The XP spectrum of the oxidized surface was recorded. The shift in the B.E. value of the Sn $3d_{5/2}$ level was found to be 2.5 eV, corresponding to the formation of SnO_2. The B.E. shift obtained in the case of the alloys was much less than this.

The 'molecular' volumes of the ordered compounds Ag-Sn, Pb-Sn, Cu-Sn, Sb-Sn, In-Sn and Cd-Sn are almost exactly the sum of the volumes of the two pure metals according to the equation :

$$V(A_xB_y) \simeq xV(A\text{-metal}) + yV(B\text{-metal})$$

Hence the change in the energy level shifts is attributed to change in the charge distribution rather than to change in the atomic volume.

Experimentally the core level binding energies for the alloys are measured relative to the Fermi level. If the alloy sample and the spectrometer are in electrical

contact, the Fermi levels must be at equal energies. So the measured binding energy depends only on the work function of the spectrometer material (see Fig. 1.1), presumably a constant, even when different samples are used. Thus it is clear that the differences in work function of the alloys (the experimental determination of which is most difficult) are of no importance for the binding energies as long as the work function of the spectrometer material is constant. Moreover, the work functions of these alloys were determined by measuring the position of the zero-kinetic energy cut-off of the usually very intense secondary electron peak in the UPS studies. This procedure for determining the work functions has been shown in Fig. 3.9 for metallic Sn. The work functions of the alloys measured in this way are very nearly equal (given in Tables 3.2 and 3.3) and hence the energy level shifts due to the differences in work function can be ruled out.

The electronegativities of Sn, Ag, Cu, Pb, Sb, In and Cd are given in Tables 3.2 and 3.3. It can be seen that Pb has the highest electronegativity[248] and correspondingly the Sn 3d level in the Pb-Sn system has the largest B.E. Considering the alloys Sn-Pb, Sn-Ag, Sn-Cu, Sn-Cd and Sn-In which have twelve-fold coordination, the Sn 3d B.E. shift (ΔE) decreases with decrease in electronegativity

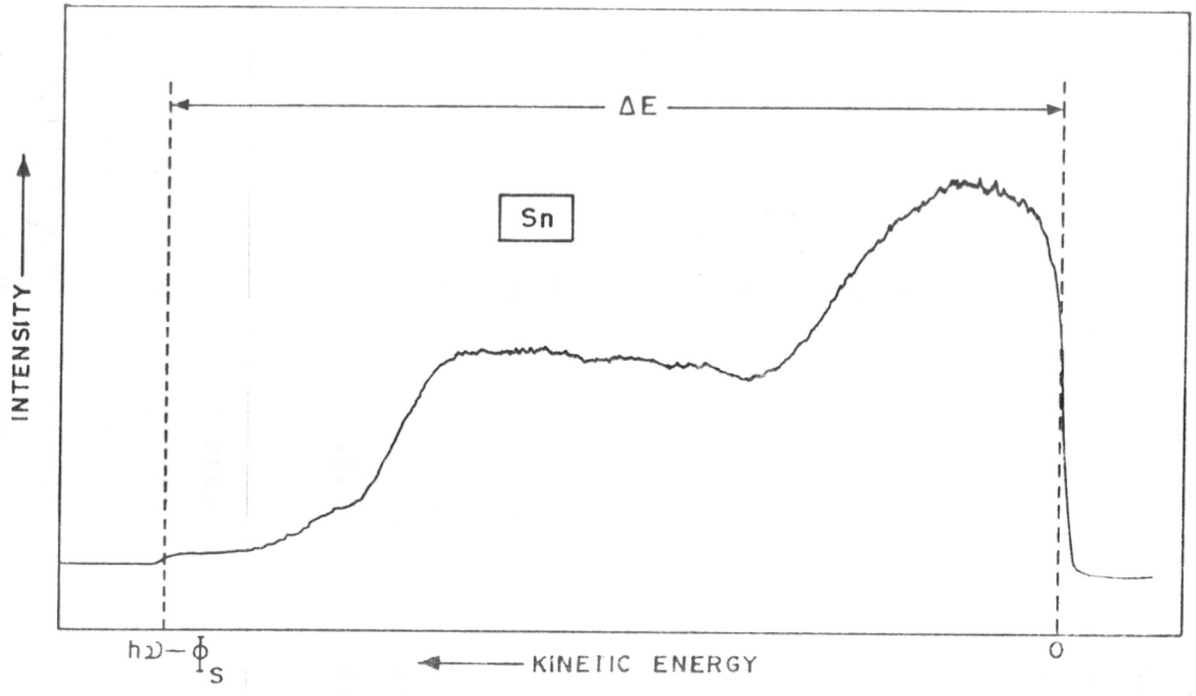

FIG. 3·9. FULL UPS SPECTRAL SCAN FOR A POLYCRYSTALLINE Sn METAL, SHOWING BOTH THE CUT-OFF OF THE SECONDARY ELECTRON PEAK AT ZERO KINETIC ENERGY AND THE HIGH-ENERGY CUT-OFF FOR EMISSION FROM LEVELS AT THE METAL FERMI LEVEL. THE MEASURABLE DISTANCE ΔE THUS EQUALS $h\nu - \Phi_S$, FOR THIS CASE, $h\nu$ WAS 21·2 eV AND Φ_S WAS 4·1 eV

as shown in Table 3.6. Thus in the dilute alloy systems where the near neighbour coordination is the same, the chemical shift (ΔE) increases in the same direction as the electronegativity of the near neighbours (see Fig. 3.10).

The electronegativities of Sn, Ag, Cu and Sb are nearly the same, but if one compares the B.E. shifts of Sn 3d level in α-tin with that of Sn-Ag, Sn-Cu and Sn-Sb, the B.E. shift (ΔE) as can be seen from Table 3.7 increases with the number of Sn coordinating atoms. Thus the plot of Sn 3d chemical shift (ΔE) versus the number of coordinating atoms of the Sn for the dilute tin alloys gives a straight line, as shown in Fig. 3.11.

It is possible that the entire increase in B.E. in the cases of Sn-Pb, Sn-Cu and Sn-Ag is due not only to the increased coordination number, but to the combined effect of both electronegativity and coordination number. However, the trend of increase in B.E. with coordination number appears clear.

Antimony has an electronegativity of 2.05. Accordingly a B.E. should be expected slightly lower than that of Pb, which has an electronegativity of 2.33. But the Sn 3d level in the Sb-Sn system has a B.E. shift of 0.6 eV, which is lowest B.E. in the present series. The Sb-Sn

Table 3.6 : Sn 3d binding energy shift (ΔE) as a function of near neighbour electronegativity (λ)

System	Coordination number (η)	Electro-negativity (λ)	ΔE eV
Sn_2Pb_{98}	12	2.33	1.8
Sn_5Ag_{95}	12	1.96	1.0
Sn_5Cu_{95}	12	1.90	1.0
$Sn_{0.4}Cd_{99.6}$	12	1.69	0.7
Sn_5In_{95}	12	1.78	0.6

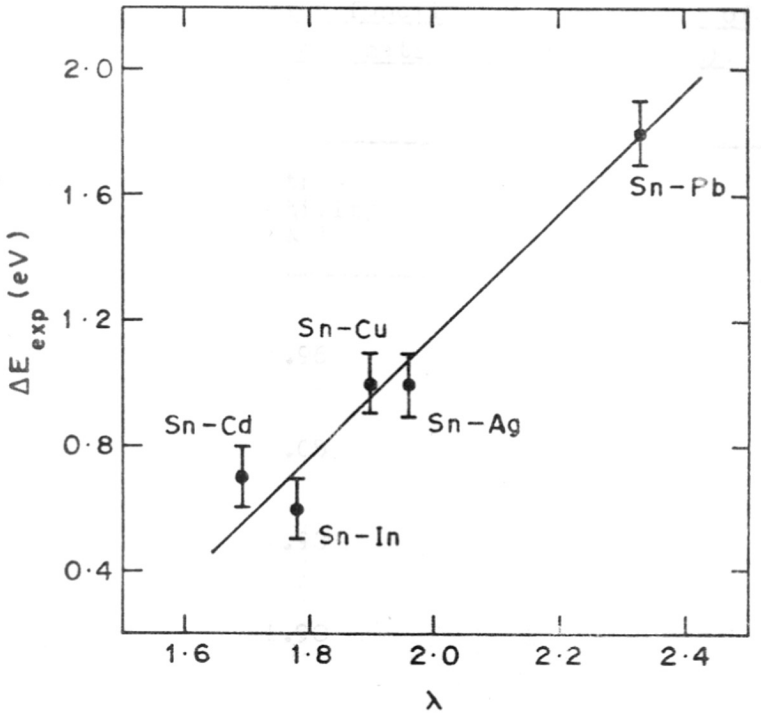

FIG. 3·10. PLOT OF THE Sn3d BINDING ENERGY SHIFT ΔE_{exp} IN DILUTE TIN ALLOYS vs. NEAR NEIGHBOUR ELECTRONEGATIVITY (λ)

Table 3.7 : Sn 3d binding energy shift (ΔE) as a function of the number of coordinating atoms of Sn (η).

System	Electro-negativity (λ)	Coordination number (η)	ΔE eV
Sn (α)	1.96	4	0.4
Sn_5Sb_{95}	2.05	6	0.6
Sn_5Ag_{95}	1.93	12	1.0
Sn_5Cu_{95}	1.90	12	1.0

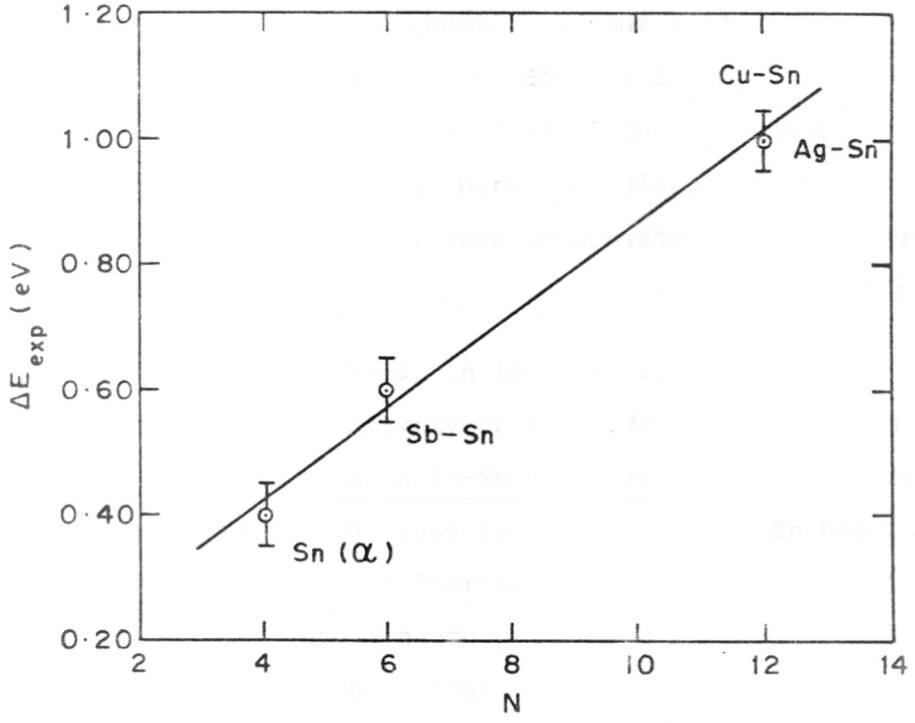

FIG. 3·11. PLOT OF THE Sn3d BINDING ENERGY SHIFT ΔE_{exp} IN DILUTE TIN ALLOYS vs. N THE NUMBER OF COORDINATING ATOMS OF Sn

alloy[239] crystallizes in the rhombohedral hexagonal type, in which the atoms are arranged in double layers so that each has three close neighbours and three at a somewhat greater distance. Thus in the Sb-Sn alloy Sn has a (3+3) coordination, whereas in the rest of the systems Sn has a twelve-fold coordination. Hence the effect of higher electronegativity is very much compensated by the lower coordination number.

On the other hand, in the case of In-Sn system the electronegativity of In (1.78) is lower than that of β-Sn, but still Sn in In-Sn alloy shows a B.E. increase of 0.6 eV. This is because in In-Sn alloy[239] Sn has the twelve neighbours in an approximate close packing. The neighbours fall into two groups, one of four at a distance of 3.24 Å and the other group of eight at 3.37 Å. Thus Sn has (4+8) coordination in In-Sn alloy, whereas in β-Sn it has (4+2) coordination. So here the effect of lower electronegativity is compensated by higher coordination number. In a similar way the Sn 3d core level shift in Cd-Sn alloy can be explained on the basis of higher coordination number of Sn, even though the electronegativity of Cd (1.69) is much less than that of β-Sn (1.96).

Literature on core level binding energy shifts in dilute alloys is very scarce. Table 3.8 gives the obtained B.E. shifts (ΔE) of Sn 3d level in some dilute tin alloys relative to the position in the pure β-Sn.

From the above results, it is clear that the binding energy shift (ΔE) depends on the electronegativity difference, the coordination number and also the interatomic distance. The following empirical equation was arrived at to get the best fit with the experimental data.

Consider a dilute AB alloy, where A is a metallic impurity in a host metallic matrix B. Here, we assume that (i) there is no A-A proximity and (ii) A is completely surrounded by B such that the effect of host metal surroundings is clearly seen. Thereby one arrives at the following relation for the chemical shift ΔE_{cal} :

$$\Delta E_{cal} \simeq K\eta\lambda^3[1+(r_A/r_B)]$$

where K is a proportionality constant, η is the near neighbour coordination number of A, which affects the electrostatic potential at A atoms, λ is the electronegativity of the near neighbour B atoms, which is a measure of charge transfer, r_A and r_B the atomic radii of A and B atoms respectively. The term in the bracket is a function of

Table 3.8 : Core level binding energy shifts in dilute tin alloys

Sample	$\Delta E_{exp.}$ eV	$\Delta E_{calc.}$ eV	η	λ	λ^3	r_A Å	r_B Å
$Pb_{98}Sn_2$	1.8	1.64	12	2.33	12.65	1.58	1.75
$Ag_{95}Sn_5$	1.0	1.03	12	1.93	7.19	1.58	1.44
$Cu_{95}Sn_5$	1.0	1.03	12	1.90	6.86	1.58	1.28
$Sb_{95}Sn_5$	0.6	0.59	6 (3+3)	2.05	8.62	1.40	1.36
$In_{95}Sn_5$	0.6	0.73	12 (4+8)	1.78	5.64	1.58	1.67
$Cd_{99.6}Sn_{0.4}$	0.7	0.66	12	1.69	4.83	1.58	1.52
Sn (α)	0.4	0.34	4	1.96	7.53	1.40	1.40

$$\Delta E_{exp.} = E_{alloy}(A) - E_{pure}(A)$$

$$\Delta E_{calc.} \simeq K\eta\lambda^3 [\, 1 + (r_A/r_B)]$$

The value of K = 0.0057

changes in the atomic volume.

The linear dependence on the atomic coordination number (η) is understandable as is the dependence on r_B, the radius of the host atom. The strong dependence on electronegativity difference (third power) is interesting.

The results obtained from the calculations using the above equation are given in Table 3.8. The value of the constant K (0.0057) was chosen so as to give the best fit with the experimental data. The degree of agreement between the calculated and experiment can be seen from Fig. 3.12, where we have plotted the calculated versus the measured binding energy shifts. The agreement is quite encouraging and so the usefulness of XPS to get information about the geometry, structure or coordination of the atoms is brought out.

3.4 Conclusions

From the above studies we conclude firstly that the chemical shift not only depends on the electronegativity of the near neighbours but also on the interatomic distances. In addition, the binding energy shifts give information on the atomic coordination number.

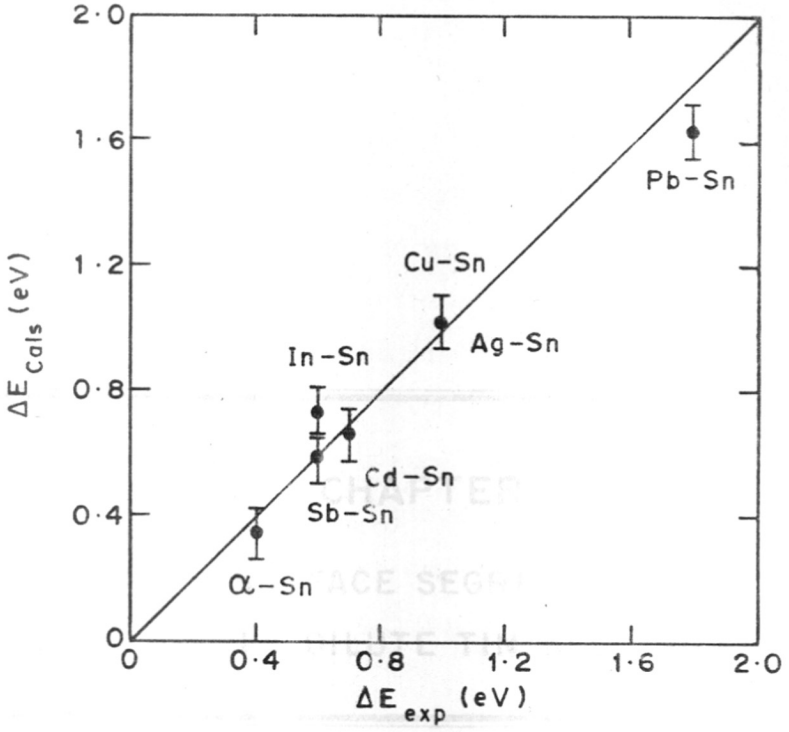

6.3·12. EXPERIMENTAL Sn3d CORE LEVEL BINDING ENERGY SHIFTS IN DILUTE ALLOYS AS COMPARED TO THOSE OBTAINED FROM THE SIMPLE EMPIRICAL CALCULATIONS.

CHAPTER IV

SURFACE SEGREGATION IN DILUTE TIN ALLOYS

SURFACE SEGREGATION IN DILUTE TIN ALLOYS

4.1 Introduction

It is well known that the equilibrium surface composition at the surface of an alloy often differs from that in the bulk[1,19]. This is because the creation of a surface requires work and results in an increase in the surface free energy. The component with the lower surface energy segregates to the surface in order to lower the surface free energy and establish equilibrium. For dilute binary alloys the surface concentration is related to the bulk concentration through the following relation[1,19,107].

$$\frac{X_A^S}{X_B^S} = \frac{X_A}{X_B} e^{(Q/RT)} \qquad \ldots\ldots \qquad [4.1]$$

where X_A and X_B are the concentrations in the bulk of the two components constituting the alloy ($X_A + X_B = 1$) and X_A^S and X_B^S are those on the surface. It has been assumed here that X_A is the minor component (i.e. $X_A << X_B$) and Q is its heat of segregation.

This equation [4.1] shows that for positive values of Q the element A will segregate to the surface and its

concentration will be higher on the surface than in the bulk. It also shows that with increasing temperature the segregation decreases and ultimately reaches the bulk value at high temperatures. On the other hand, for negative values of Q the reverse is true.

At present, there is a substantial gap between surface segregation theory and the corresponding experimental results. Accurate data of heat of segregation for well defined systems can help in bridging this gap.

From this point of view the surface analysis techniques such as AES, XPS/ESCA can play a very important role in experimentally determining the surface composition at various temperatures from where the heat of segregation can be extracted.

XPS/ESCA has been preferred over AES because this technique provides more quantitative chemical information than AES, though analysis times are slower. This technique is non-destructive and no selective sputtering occurs in the case of multi-component systems as ours. Moreover vacuum requirements to XPS are less stringent than to AES.

We have studied the surface of polycrystalline Cu-Sn, Ag-Sn and Sb-Sn alloys containing small amounts (5 wt %) of Sn using ESCA as the technique. Our main aim

is to see whether equation [4.1] correctly describes the temperature dependence of Sn concentration on the alloy surface and if so, to determine the heat of segregation. We choose these alloys for several reasons.

According to the bond breaking approach Ag should segregate to the Ag-Sn alloy surface since Ag has lower heat of sublimation compared to Sn, on the other hand, lattice strain theory predicts the segregation of Sn, since Sn has a higher atomic radius than Ag in Ag-Sn alloy. In case of Cu-Sn alloy both theories predict the segregation of Sn. In fact Ferrante[163] has reported that Sn does segregate to the Cu-Sn alloy surface. On the other hand Sn does not segregate to the surface in the case of Sb-Sn alloy.

An investigation of the composition of the alloys: Cu_3Sn Cu_4Sn and Cu_5Sn shows that the observed XPS signal intensity ratio is proportional to the corresponding atomic ratio of the elements present, which would suggest that matrix effects do not play an important role when one considers the ratio of the XPS signals. This result enables a quantitative determination of the average surface composition of the dilute tin alloys under various conditions of treatment such as annealing in ultrahigh vacuum etc.

4.2 Experimental

(a) Preparation of sample

The dilute tin alloys, namely, Cu-5% Sn, Ag-5% Sn, and Sb-5% Sn alloys and the intermetallics: Cu_3Sn, Cu_4Sn and Cu_5Sn were prepared from spectroscopically pure elements by the usual metallurgical technique as described in Chapter-II.

X-ray diffraction patterns confirmed that the alloys were homogeneous and had the correct lattice constants. The structure and lattice constants of the dilute tin alloys are given in Table 3.1 and that of the three intermetallics in Table 4.1.

(b) X-ray photoelectron spectroscopic analysis

X-ray photoelectron spectra were recorded using ESCA-3, Mk II electron spectrometer (VG Scientific Ltd., U.K.) equipped with a AlK_α anode (1486.6 eV), with analyzer energy set at 50 eV and entrance slit width at 4 mm. The pressure in the spectrometer was maintained at $< 10^{-10}$ torr. Prior to the recording of XP spectra the samples were cleaned by Ar-ion etching followed by annealing at $\sim 150^{\circ}C$ in the preparation chamber of the spectrometer. This treatment removed the sputter damage and all surface

Table 4.1 : The structure and lattice constants of the intermetallics used

System	Type	Structure	Lattice constants (Å)
Cu_3Sn	ϵ-phase	orthorhombic	a = 4.33 b = 4.78 c = 5.52
Cu_4Sn	γ-phase	b.c.c.	a = 17.95
Cu_5Sn	β-phase	b.c.c.	a = 4.24

contaminants. The instrument was calibrated using the Au $4f_{7/2}$ peak as 84.0 eV.

For comparative study the spectrometer parameters were kept constant while analysing the samples heated at different temperatures. After a clean alloy surface was obtained, the surface composition was measured using XPS as a function of the alloy surface temperature. The sample was first heated to the desired temperature at which it was held for 30 min. then the spectrum was recorded. The XP spectrum for the Cu-Sn alloy was recorded at various temperatures starting from room temperature to 500°C, from room temperature to 400°C for the Ag-Sn alloy and from room temperature to 300°C for the Sb-Sn alloy.

(c) Measurements of surface composition using XPS

XPS is considered as a semi-quantitative technique (< ± 50% relative error)[249-251]. This large error is introduced because spectral intensities[22-24] are strongly influenced by several sample matrix dependent factors such as changes in peak shape, sputtering, atomic density, surface roughness, escape depth, backscattering etc. So to make it quantitative analysis requires elaborate calibration procedures.

We developed an internal calibration method. It has three important characteristics:

(i) It makes use of an elemental yield ratio of two elements present in one matrix.

(ii) The reference compounds have a known surface composition.

(iii) The instrumental parameters do not fluctuate during the time of analysis.

The calibration is based on the assumption that the surface of the alloy will contain the elements in amounts given by the stoichiometric formula. The information about the elemental yield ratio of the two alloy partners in that particular matrix is obtained from the XP spectrum.

Calibration method was carried out with three intermetallic compounds: Cu_3Sn, Cu_4Sn and Cu_5Sn. The XPS peak intensity of Cu $2p_{3/2}$ and Sn $3d_{5/2}$ in these compounds are given in Table 4.2. When the ratio of XPS peak heights I of Cu $2p_{3/2}$ line and Sn $3d_{5/2}$ line are plotted against the Cu/Sn bulk atomic ratio, a straight line is obtained as shown in Fig. 4.1. The line passes correctly through the origin, while the reproducibility of the measurements is very good. We therefore concluded from the proportionality between peak height ratio and atomic ratio that a variation in the atomic ratio does not involve matrix

Table 4.2 : The XPS peak intensities from the three Cu-Sn intermetallics

Sample	Intensity of XPS peak (x 10^5 counts s^{-1})		Intensity ratio $Cu2p_{3/2}/Sn3d_{5/2}$
	Sn $3d_{5/2}$	Cu $2p_{3/2}$	
Cu_3Sn	3.7	10.8	2.92
Cu_4Sn	3.2	12.3	3.84
Cu_5Sn	2.4	11.1	4.63

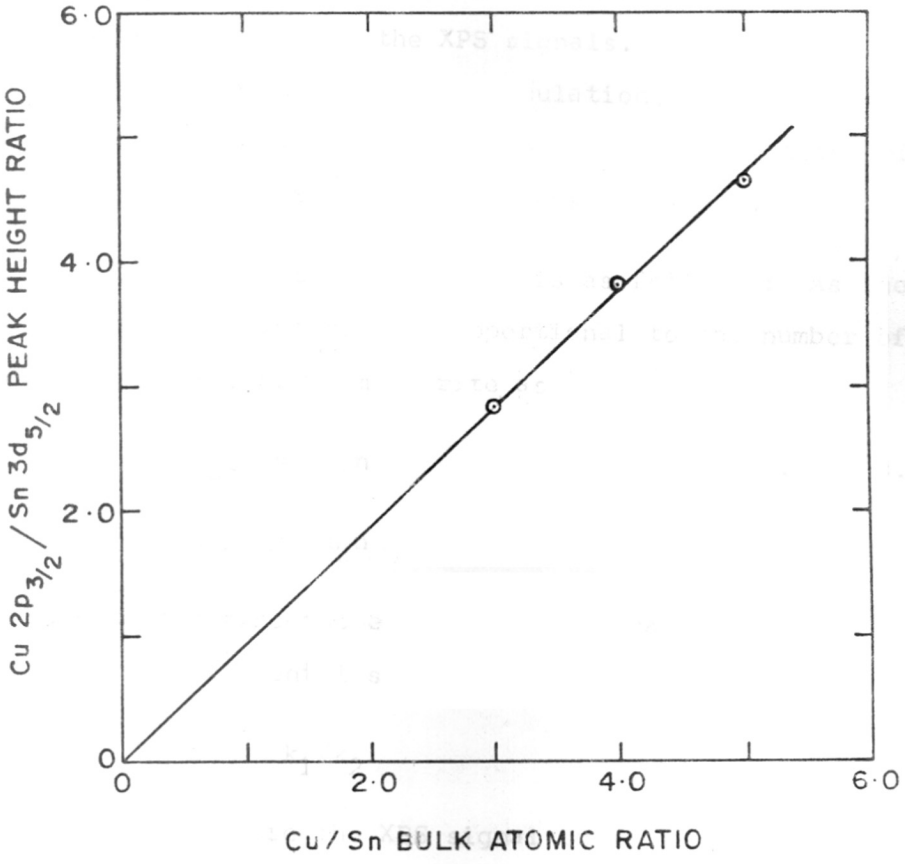

FIG. 4·1. CALIBRATION PLOT OF Cu/Sn ALLOYS OBTAINED AT CONSTANT INSTRUMENTAL PARAMETERS

effects, or to be precise, that any effect caused by a change in the chemical composition is neutralized when one considers the ratio of the XPS signals. The calibration plot can now be used for the calculation, from any spectrum in our experiment, of the ratio of the concentrations of tin and copper in the alloy surfaces under study.

The calculation procedure is as follows : As the XPS signal I is apparently proportional to the number of emitting atoms, n, we may write as

$$I_{Sn} = k_1 n_{Sn} \quad \ldots\ldots \quad [4.2]$$

$$I_{Cu} = k_2 n_{Cu} \quad \ldots\ldots \quad [4.3]$$

We may then define the elemental yield ratio constant or the relative elemental sensitivity factor α as

$$\alpha = k_1/k_2 \quad \ldots\ldots \quad [4.4]$$

where k_1 and k_2 are the XPS signal intensities obtained under identical conditions from pure Sn $3d_{5/2}$ and Cu $2p_{3/2}$ lines respectively. These expressions can be introduced into the expression of the surface composition:

$$X_{Sn} = \frac{n_{Sn}}{[n_{Cu} + n_{Sn}]}$$

$$= \frac{I_{Sn}/k_1}{[I_{Cu}/k_2 + I_{Sn}/k_1]} \quad \ldots\ldots \quad [4.5]$$

$$X_{Sn} = \frac{I_{Sn}}{[I_{Sn} + \alpha I_{Cu}]} \quad \ldots\ldots \quad [4.6]$$

$$X_{Sn}(wt\ \%) = \frac{I_{Sn}}{[I_{Sn} + \alpha I_{Cu}]} \times 100 \ \ldots\ldots \quad [4.7]$$

wherein I_{Sn} and I_{Cu} are the peak intensities of the spectrum of an arbitrary Cu/Sn alloy. This expression suggests that at least for alloy systems the concept of an elemental yield ratio or relative elemental sensitivity factor α is a useful one.

The results of this calibration enables a quantitative determination of the average surface composition of the dilute tin alloys as a function of temperature.

Surface composition of Cu-5% Sn alloy

Alloy composition for Cu-Sn alloy can be calculated from the relative intensity of Cu $2p_{3/2}$ and Sn $3d_{5/2}$ peaks, since $2p_{3/2}$ and $3d_{5/2}$ are the intense XPS peaks for Cu and Sn respectively. The alloy composition of Sn, X_{Sn} can be calculated using the equation [4.7].

In the present investigation of Cu-Sn alloy surface, signal intensities were measured from the Sn $3d_{5/2}$ and Cu $2p_{3/2}$ peak heights rather than areas, after taking a straight line background subtraction[252] which corrects

for inelastically scattered electrons. Relative elemental sensitivity factor α was taken from the ratios of identically assigned pure element peak heights and was found to give $\alpha \simeq 0.9$ for the Sn $3d_{5/2}$:Cu $2p_{3/2}$ peaks. Then the expression for the surface composition becomes

$$X_{Sn}(\text{wt }\%) = \frac{I_{Sn}}{[I_{Sn} + (0.9)\, I_{Cu}]} \times 100 \quad \ldots \quad [4.8a]$$

Surface composition for Ag-5% Sn alloy

In a similar way the expression for Sn surface concentration on Ag-Sn alloy can be shown to be

$$X_{Sn}(\text{wt }\%) = \frac{I_{Sn}}{[I_{Sn} + (1.4)\, I_{Ag}]} \times 100 \quad \ldots \quad [4.8b]$$

since $\alpha = \dfrac{I_{Sn}\ (\text{pure})}{I_{Ag}\ (\text{pure})} \simeq 1.4.$

Surface composition for Sb-5% Sn alloy

The expression for Sn surface composition on Sb-Sn alloy can be shown to be

$$X_{Sn}(\text{wt }\%) = \frac{I_{Sn}}{[I_{Sn} + (0.9)\, I_{Sb}]} \times 100 \quad \ldots \quad [4.8c]$$

since $\alpha = \dfrac{I_{Sn}\ (\text{pure})}{I_{Sb}\ (\text{pure})} \simeq 0.9.$

4.3 Results and discussion

4.3.1 Cu-5% Sn alloy

Fig. 4.2 shows the XP spectra of the Cu-Sn alloy heated at various temperatures. The peaks have been identified and assigned to Cu $2p_{3/2}$, Cu $2p_{1/2}$ and Sn $3d_{5/2}$, Sn $3d_{3/2}$ states. It can be seen clearly that the intensity of Sn 3d level increases upto a certain temperature, then decreases considerably at high temperature. Secondly, the Sn $3d_{5/2}$ binding energy obtained for the Cu-Sn alloy was 485.6 eV which remains constant for all the temperatures studied. This Sn $3d_{5/2}$ binding energy shift has been interpreted by the authors[1,16-19] as due to the effect of coordinating atoms of Sn on the core level electrons and not due to the surface oxidation of Sn. The intensity ratio of Sn $3d_{5/2}$/Cu $2p_{3/2}$ provides a measure of the surface composition of the Cu-Sn alloy (see Table 4.3). This ratio increases with increasing temperature as shown in Fig. 4.3, and then at high temperature it starts decreasing and reaches the bulk value at very high temperature. This behaviour is in accordance with the Arrhenius equation [4.1]. This clearly predicts the segregation of Sn in Cu-Sn alloy supporting both theories of surface segregation (i.e. bond breaking theory and lattice strain theory).

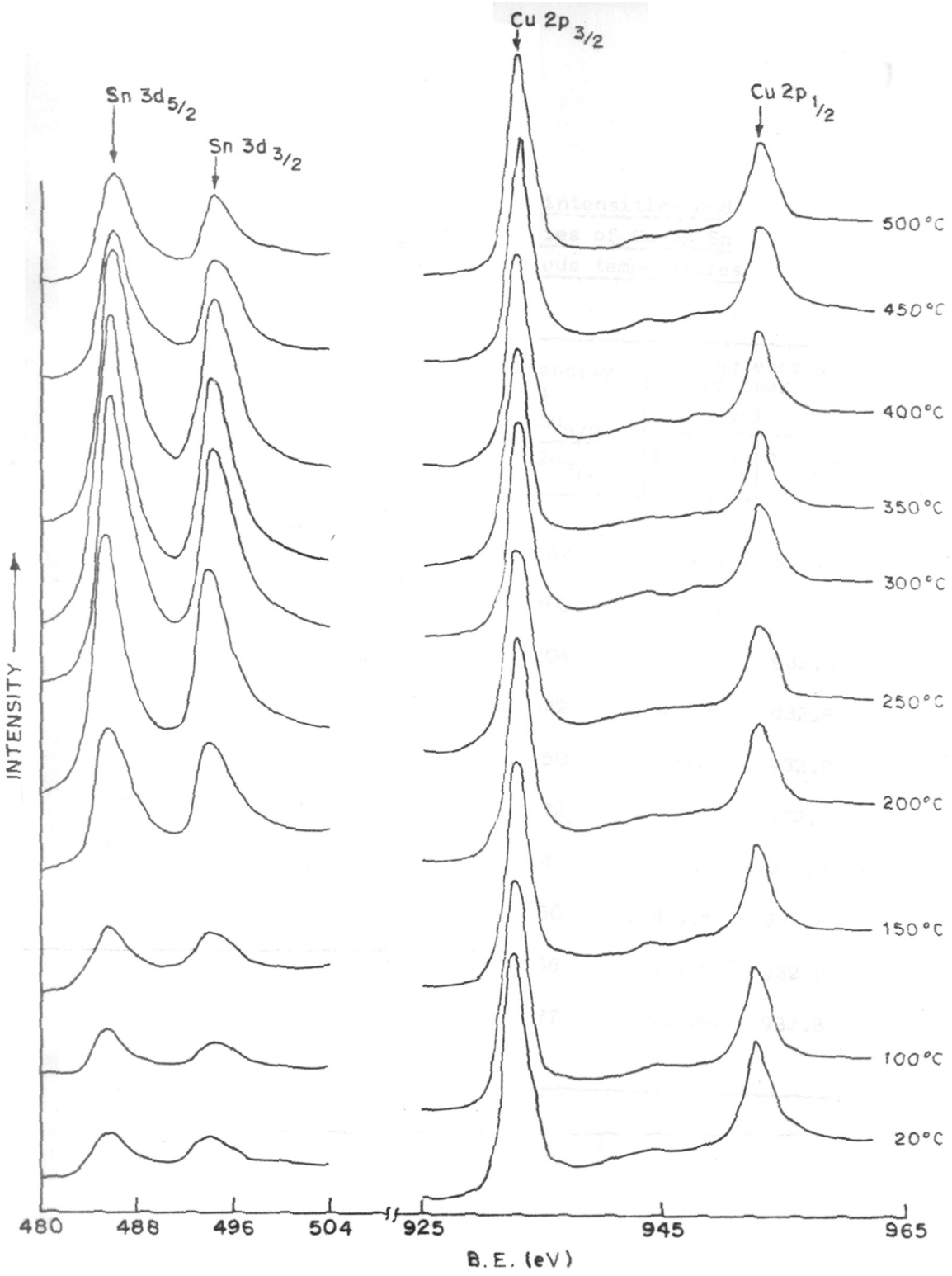

FIG. 4·2. XPS OF Cu – 5% Sn ALLOY HEATED AT DIFFERENT TEMPERATURES

Table 4.3 : The XPS peak intensities and binding energies of Cu-5% Sn alloy at various temperatures

Temperature °C	Intensity of XPS peak ($\times 10^5$ counts s^{-1})		Intensity ratio $\frac{Sn\ 3d_{5/2}}{Cu\ 2p_{3/2}}$	Binding energy of XPS peak (eV)	
	Sn $3d_{5/2}$	Cu $2p_{3/2}$		Sn $3d_{5/2}$	Cu $2p_{3/2}$
20	0.10	5.9	0.0169	485.6	932.8
100	0.11	5.5	0.0200	485.6	932.8
150	0.11	5.4	0.0204	485.6	932.8
200	0.34	5.3	0.0642	485.6	932.8
250	0.60	4.8	0.1250	485.6	932.8
300	0.70	5.1	0.1372	485.6	932.8
350	0.70	5.2	0.1346	485.6	932.8
400	0.65	5.2	0.1250	485.6	932.8
450	0.36	5.4	0.0666	485.6	932.8
500	0.20	5.3	0.0377	485.6	932.8

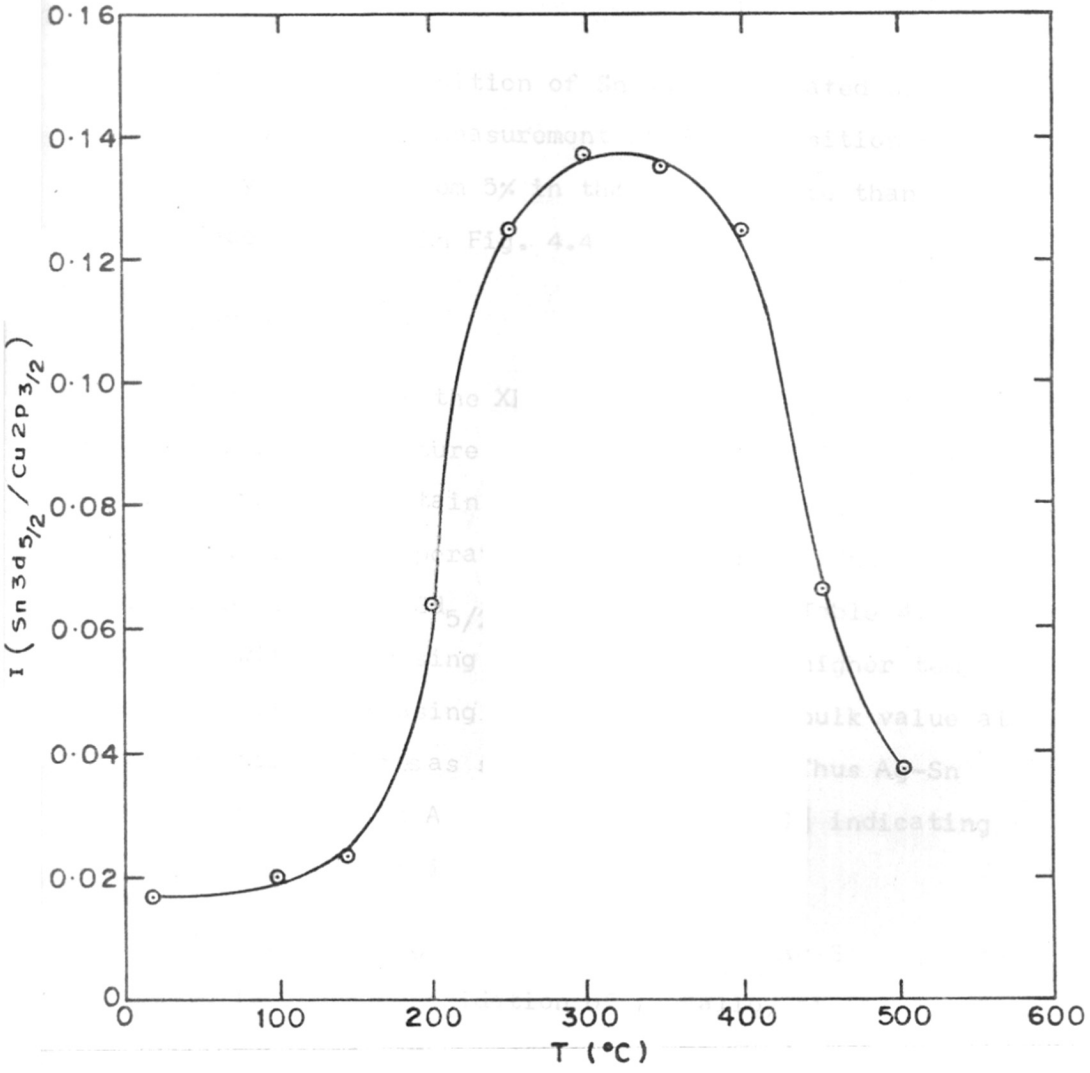

FIG. 4·3. XPS PEAK HEIGHT RATIO, $Sn\ 3d_{5/2}$ / $Cu\ 2p_{3/2}$, OF Cu-5% Sn ALLOY AS A FUNCTION OF TEMPERATURE

The alloy composition of Sn was calculated using the equation [4.8a]. The measurement of Sn composition of the Cu-Sn alloy varied from 5% in the bulk to more than 35% on the surface as shown in Fig. 4.4

4.3.2 Ag-5% Sn alloy

Fig. 4.5 shows the XP spectra of the Ag-Sn alloy as a function of temperature . The intensity of Sn $3d_{5/2}$ increases up to a certain temperature and then starts decreasing as the temperature becomes higher. The intensity ratio of Sn $3d_{5/2}$/Ag $3d_{5/2}$ which is given in Table 4.4, increases with increasing temperature and at higher temperature it starts decreasing and approaches the bulk value at very high temperatures as shown in Fig. 4.6. Thus Ag-Sn system also obeys the Arrhenius equation [4.1] indicating the segregation of Sn in the alloy surface.

The surface segregation of Sn on the Ag-Sn alloy may be due to (a) surface oxidation of the alloy or (b) due to the lattice effect.

Surface segregation of Sn may be due to the formation of SnO_2 [which is more thermodynamically favourable[253] compared to SnO, AgO or Ag_2O (see Table 4.5)] giving rise to more Sn-O bonds on the surface and decreases the surface free energy.

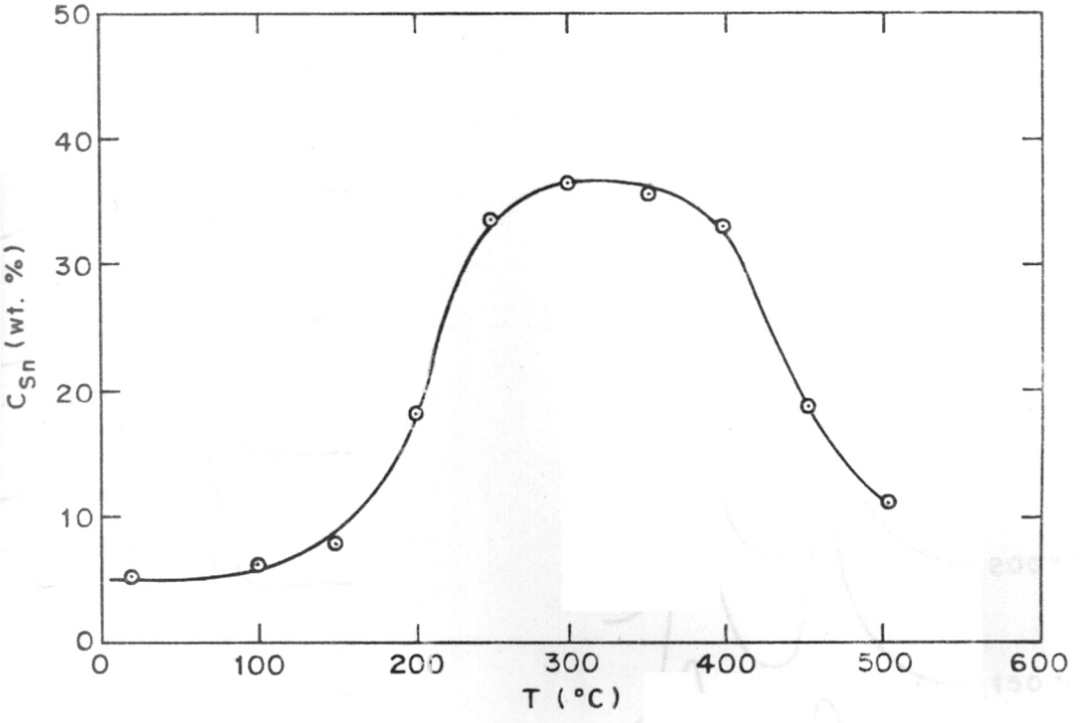

FIG. 4·4. Sn SURFACE CONCENTRATION IN Cu–5% Sn ALLOY AS A FUNCTION OF TEMPERATURE

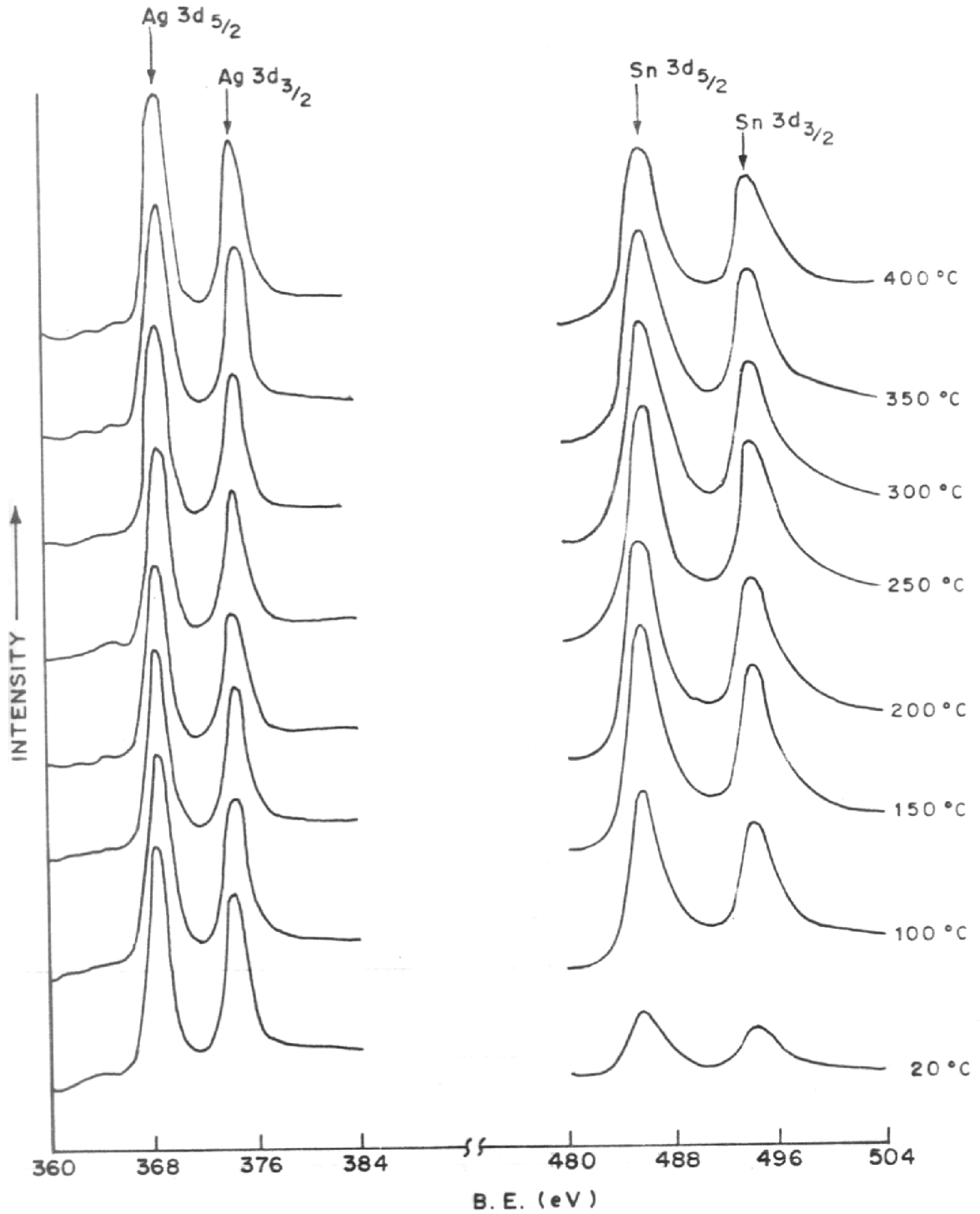

FIG. 4·5. XPS OF Ag–5% Sn ALLOY HEATED AT DIFFERENT TEMPERATURES

Table 4.4 : The XPS peak intensities and binding energies of Ag-5% Sn alloy at various temperatures

Temperature °C	Intensity of XPS peak (x 10^5 counts s^{-1})		Intensity ratio $\frac{Sn\ 3d_{5/2}}{Ag\ 3d_{5/2}}$	Binding energy of XPS peak (eV)	
	Sn $3d_{5/2}$	Ag $3d_{5/2}$		Sn $3d_{5/2}$	Ag $3d_{5/2}$
20	0.14	5.4	0.0259	485.6	368.4
100	0.39	4.9	0.0796	485.6	368.4
150	0.50	4.8	0.1042	485.6	368.4
200	0.48	4.5	0.1066	485.6	368.5
250	0.50	4.6	0.1087	485.6	368.5
300	0.48	4.8	0.1000	485.6	368.5
350	0.40	5.2	0.0769	485.6	368.5
400	0.37	5.4	0.0685	485.6	368.5

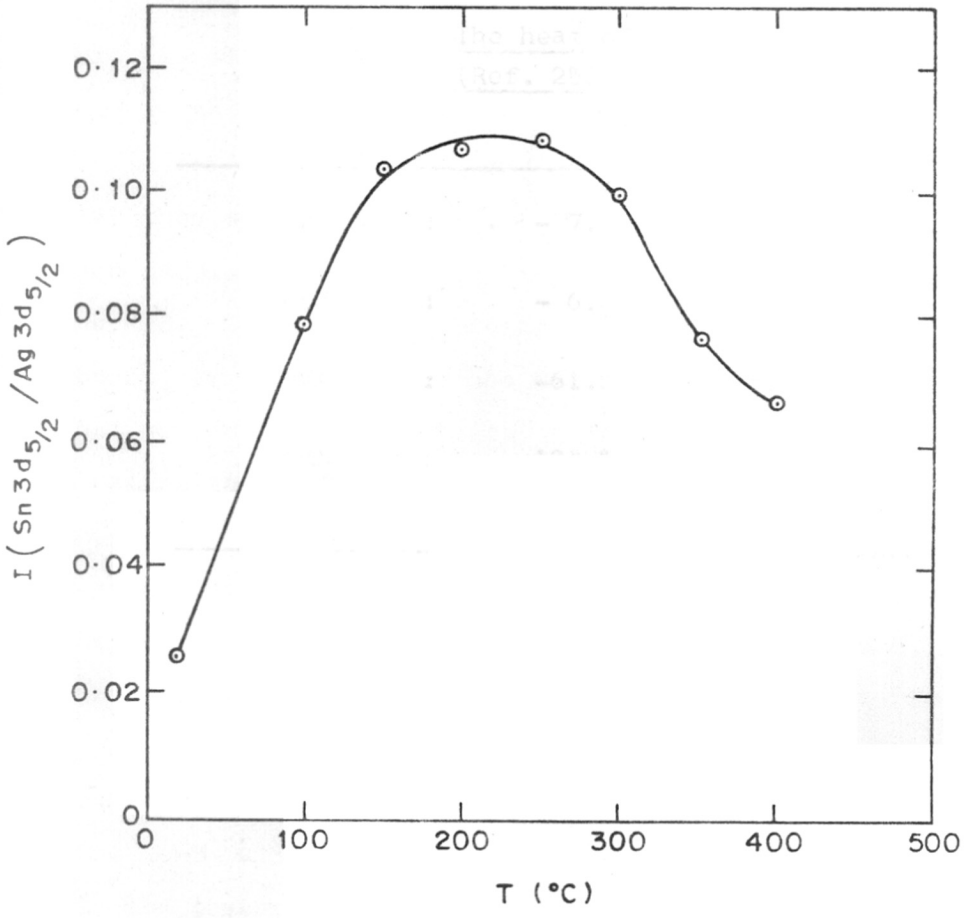

FIG. 4·6. XPS PEAK HEIGHT RATIO, Sn $3d_{5/2}$ / Ag $3d_{5/2}$, OF Ag-5 % Sn ALLOY AS A FUNCTION OF TEMPERATURE

Table 4.5 : The heat of formation data (Ref. 253)

AgO	:	- 7.3 kcals/mole
Ag_2O	:	- 6.3 kcals/mole
SnO	:	-61.5 kcals/mole
SnO_2	:	-124.5 kcals/mole

The possibility of the Ag-Sn alloy surface becoming enriched with Sn in the form of SnO_2 can be ruled out, because the alloy was cleaned and polished to a mirror finish and preserved properly to avoid any surface oxidation till they were used for recording the XP spectra. Secondly, each sample was cleaned by Ar-ion etching, before recording the XPS. The oxygen 1s signal was found to be totally absent, or its intensity had deminished to such an extent that we could not detect it. In addition, the oxygen contamination level is found to be below the detection limit at the various temperatures of study. Further, the Ag-Sn alloy was deliberately oxidized by heating in air at $\sim 150^{\circ}C$. The XP spectrum of the oxidized surface was recorded. The shifts in the B.E. values of the Sn $3d_{5/2}$ level was found to be 2.5 eV, corresponding to the formation of SnO_2. However, the Sn $3d_{5/2}$ binding energy shift obtained for the pure Ag-Sn alloy was only 1.0 eV which remained constant at all the temperatures studied.

The segregation of Sn on the Ag-Sn alloy surface is based on elastic strain energy effects. Since the solute atoms (Sn) having a size different from that of the solvent atoms (Ag) exert a stress on the lattice. Interchanging the solute (Sn) atoms with a surface atom reduces this stress in the lattice. Thus the Sn (having higher

atomic radius than Ag) segregates on the Ag-Sn alloy surface. So it seems atomic radius is a reliable index for Sn segregation on Ag-Sn alloy surface. The measurement of Sn composition of the Ag-Sn alloy using equation [4.8b] varies from 5 % in the bulk to more than 20 % on the surface (see Fig. 4.7).

4.3.3 Sb-5% Sn alloy

The intensity ratio of Sn $3d_{5/2}$/Sb $3d_{5/2}$ provides a measure of the surface composition of the Sb-Sn alloy, decreases with increasing temperature as shown in Fig. 4.8 and then starts increasing and reaches the bulk value at 300°C. This clearly predicts that Sn does not segregate to Sb-Sn alloy supporting the bond breaking theory of surface segregation.

4.3.4 Time dependence of surface segregation

It is possible to produce a wide range of surface compositions with time owing to the slowness of diffusion at low temperatures. In fact Burton et al.[142] have obtained a wide range of surface compositions for Ni(Au) alloys at low temperatures.

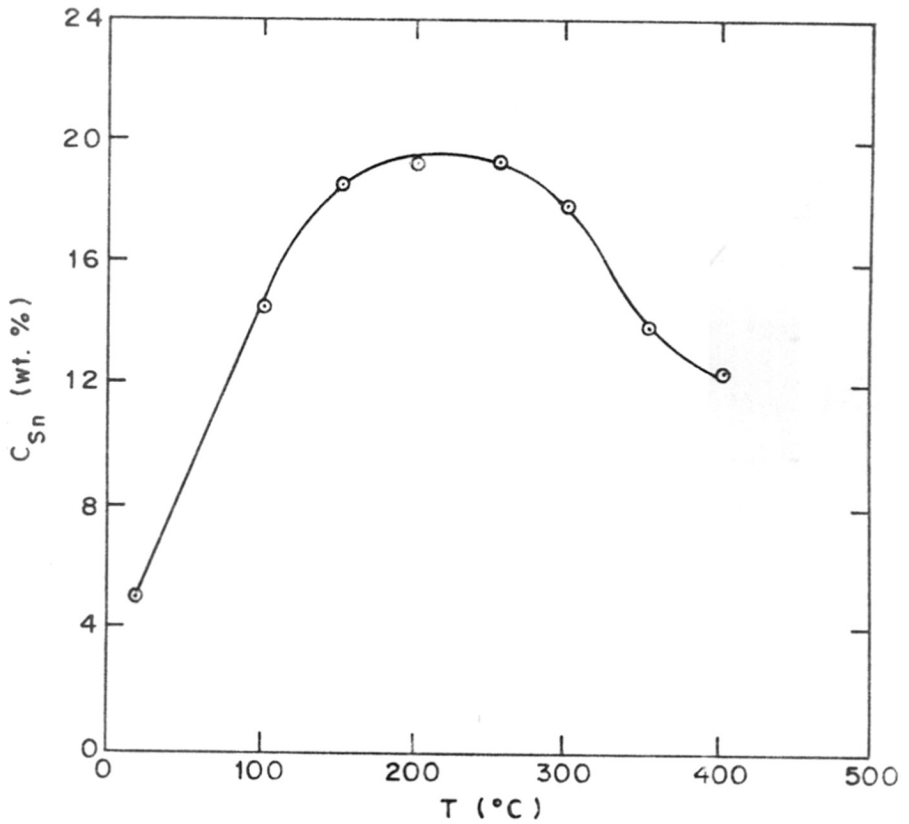

FIG. 4·7. Sn SURFACE CONCENTRATION IN Ag–5% Sn ALLOY AS A FUNCTION OF TEMPERATURE

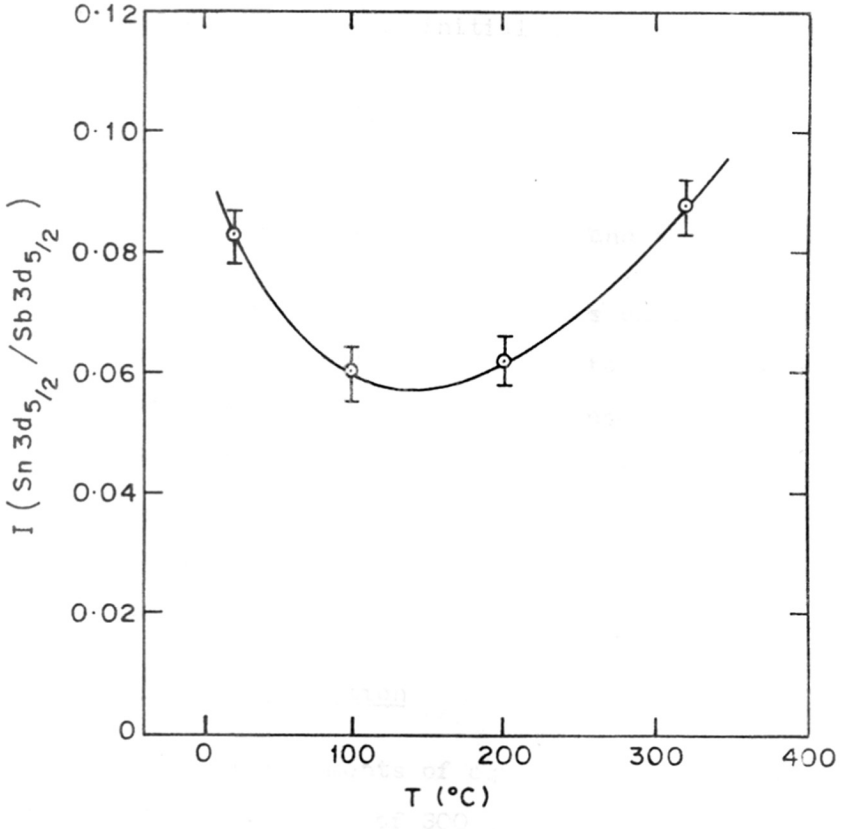

FIG. 4·8 XPS PEAK HEIGHT RATIO, $Sn\ 3d_{5/2}$ /$Sb\ 3d_{5/2}$ OF Sb-5% Sn ALLOY AS A FUNCTION OF TEMPERATURE

If the segregation of Sn to the alloy surface is diffusion limited, the surface concentration should increase with time according to the initial segregation kinetics[254].

$$C_X^S = 2C_X^B \left(\frac{D_X t}{\pi}\right)^{1/2} \quad \ldots\ldots \quad [4.9]$$

where D_X is the bulk diffusivity of X and t the ageing time.

We performed several experiments on the time dependence of surface composition in order to investigate to ensure that equilibrium had been attained. Fig. 4.9 shows the time dependence of the surface composition of the alloys heated at 400°C. It is clear that after half an hour of equilibration the surface concentration is independent of time at temperatures of study.

4.3.5 Heats of segregation

For the measurements of equilibrium surface composition a temperature range of 300 to 500°C was chosen in case of Cu-Sn alloy. From a series of repeated primary runs it was established that equilibrium surface composition can be obtained by heating the sample in this temperature range for a sufficiently long time (30 minutes). Further heat treatment was found to cause no change in the monitored composition.

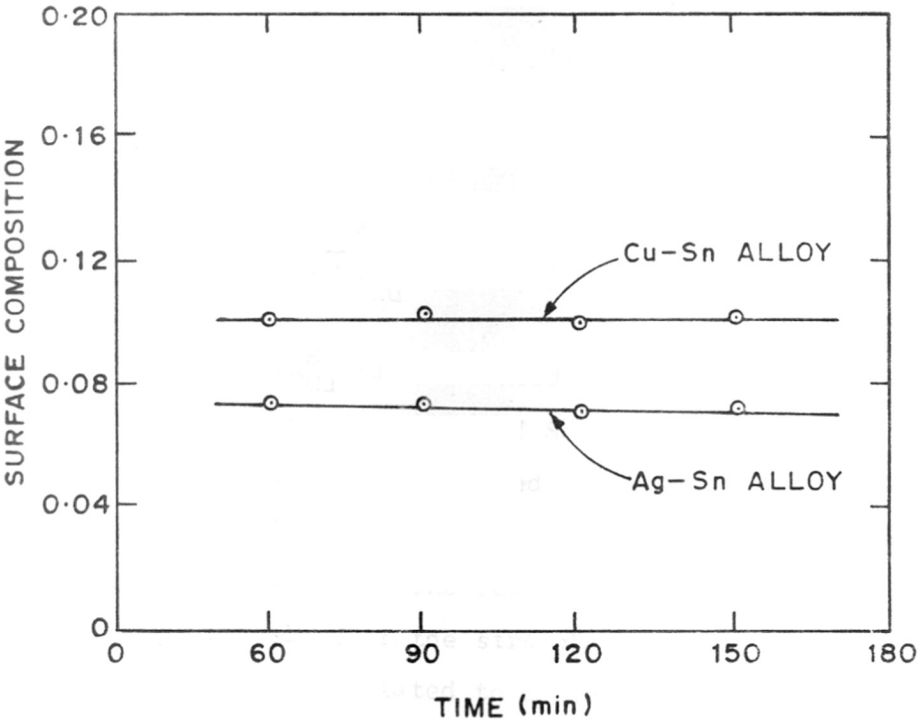

4·9. TIME DEPENDENCE OF SURFACE COMPOSITION OF THE Cu-5 % Sn AND Ag-5 % Sn ALLOYS HEATED AT 400 °C

The surface composition of the Cu-Sn alloy at a temperature of T (K) can be related to its bulk composition as

$$\frac{X^S_{Sn}}{1 - X^S_{Sn}} = \frac{X^B_{Sn}}{1 - X^B_{Sn}} e^{Q/RT} \quad \ldots\ldots \quad [4.10]$$

i.e. $$\frac{X^S_{Sn}}{X^S_{Cu}} = \frac{X^B_{Sn}}{X^B_{Cu}} e^{Q/RT} \quad \ldots\ldots \quad [4.11]$$

The ratio of X^S_{Sn}/X^S_{Cu} can be considered to be proportional to the ratio of the peak heights of Sn $3d_{5/2}$ and Cu $2p_{3/2}$ XPS signals. In Fig. 4.10 we plotted log $I(Sn3d_{5/2})/I(Cu2p_{3/2})$ against 1/T. Only the results above 573 K and below 773 K are shown in Fig. 4.10. The results do fall on a straight line. From the slope of the straight line the heat of segregation Q was calculated to be 12.0 ± 1.0 kcal/mole, indicating Sn segregation on the alloy surface.

In a similar way, we plotted log $I(Sn3d_{5/2})/I(Ag3d_{5/2})$ against 1/T. The data above 473 K and below 673 K are shown in Fig. 4.11. From the slope of the straight line the heat of segregation Q was calculated to be 3.5 ± 1.0 kcals/mole indicating Sn segregation on the alloy surface.

In case of Sb-Sn alloy, we plotted log $I(Sn3d_{5/2})/I(Sb3d_{5/2})$ against 1/T. The data above 373 K and below 573 K are shown in Fig. 4.12. From the slope of the

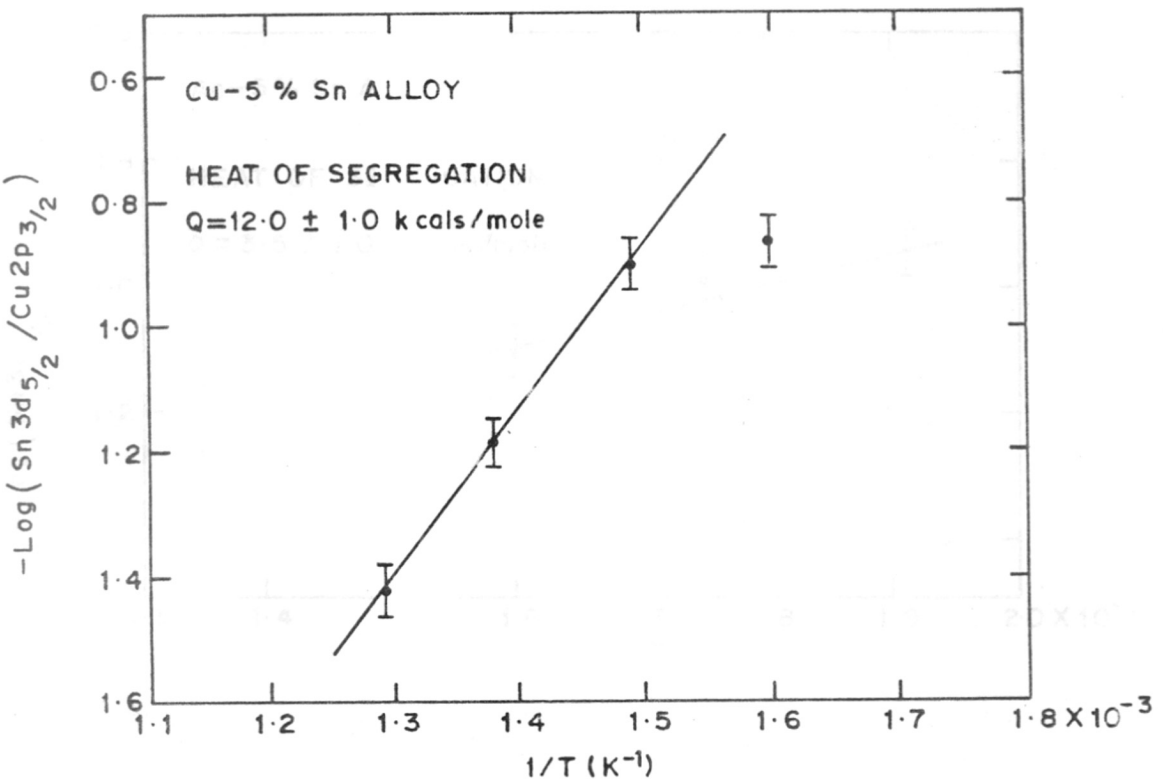

FIG. 4·10. ARRHENIUS PLOT OF $-\text{LOG}\,(\text{Sn}\,3d_{5/3}/\text{Cu}\,2p_{3/2})$ XPS PEAK HEIGHT RATIO vs. TEMPERATURE. HEAT OF SEGREGATION 'Q' IS CALCULATED FROM THE SLOPE OF THE STRAIGHT LINE TO BE 12·0 ± 1·0 k cals/mole.

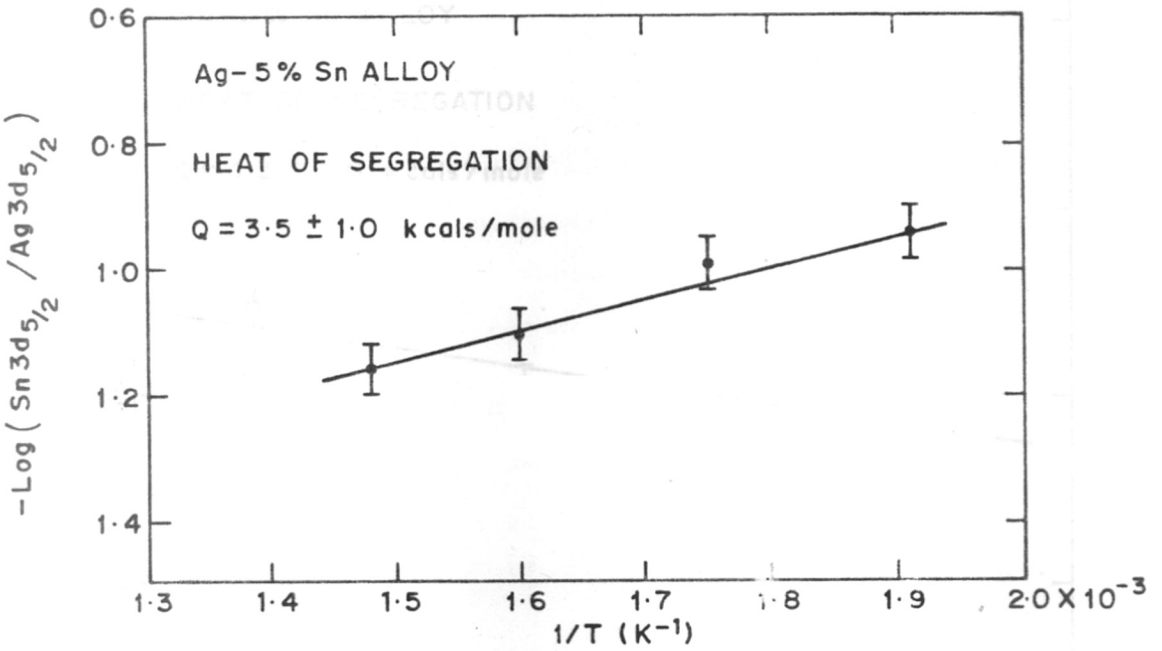

FIG. 4·11. ARRHENIUS PLOT OF -LOG ($Sn\,3d_{5/2}/Ag\,3d_{5/2}$) XPS PEAK HEIGHT RATIO vs. TEMPERATURE. HEAT OF SEGREGATION 'Q' IS CALCULATED FROM THE SLOPE OF THE STRAIGHT LINE TO BE 3·5 ± 1·0 k cals/mole

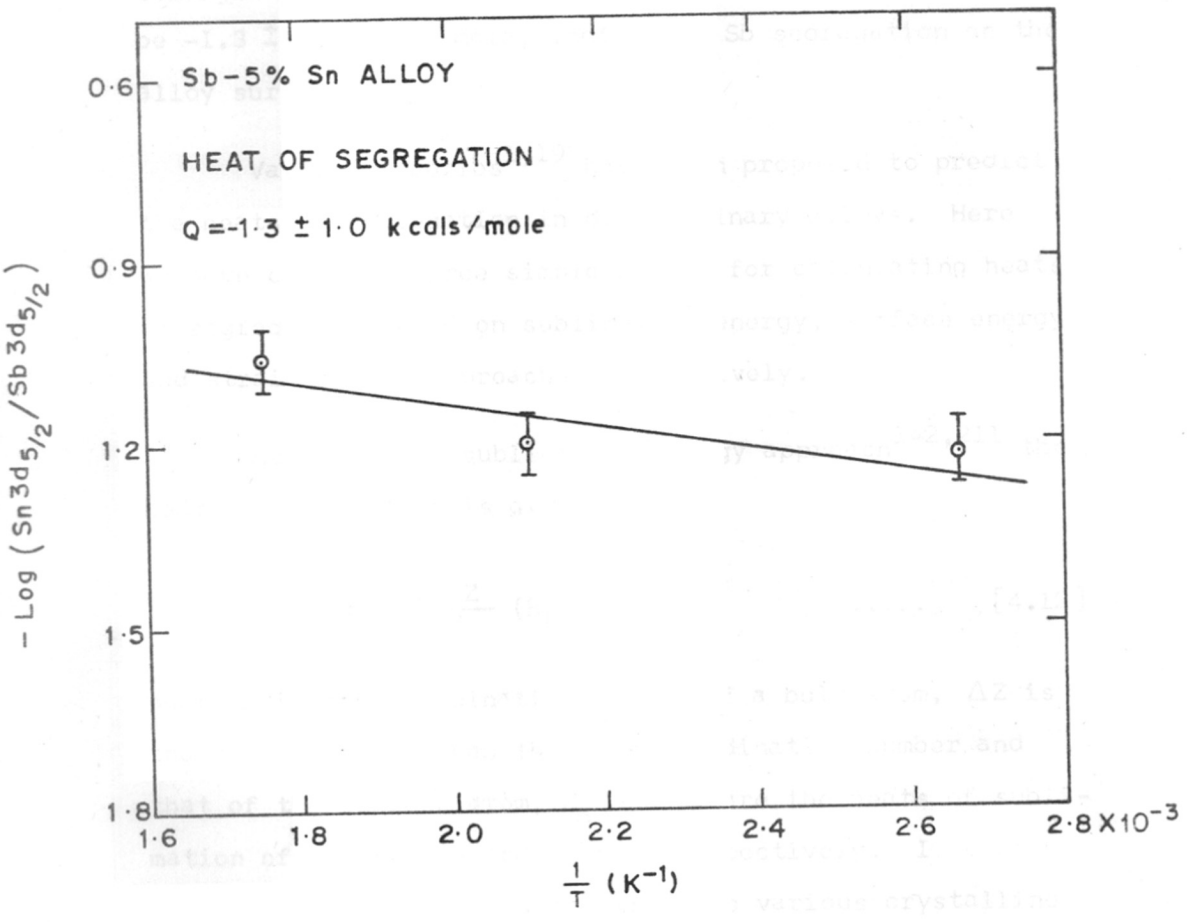

FIG. 4·12. ARRHENIUS PLOT OF -LOG ($Sn\,3d_{5/2}/Sb\,3d_{5/2}$) XPS PEAK HEIGHT RATIO vs. TEMPERATURE. HEAT OF SEGREGATION 'Q' IS CALCULATED FROM THE SLOPE OF THE STRAIGHT LINE TO BE 1·3 ± 1·0 k cals/mole.

straight line the heat of segregation Q was calculated to be -1.3 ± 1.0 kcals/mole, indicating Sb segregation on the alloy surface.

Various theories[1,19] have been proposed to predict the heats of segregation in dilute binary alloys. Here we have compared three simple models for calculating heats of segregation based on sublimation energy, surface energy and strain energy approaches respectively.

According to sublimation energy approach[142,211] the heat of segregation is given by

$$Q = \frac{\Delta Z}{Z} (H_B - H_A) \quad \ldots\ldots \quad [4.12]$$

where Z is the coordination number of a bulk atom, ΔZ is the difference between the bulk coordination number and that of the surface atom, H_A and H_B are the heats of sublimation of the solute and solvent respectively. In a polycrystalline alloy, ΔZ is not known as various crystalline planes comprise the surface. However $\Delta Z/Z < 1$, so $Q < (H_B - H_A)$.

The surface energy approach[104,142] predicts

$$Q = \sigma_A a_A - \sigma_B a_B \quad \ldots\ldots \quad [4.13]$$

where σ_A and σ_B are the surface energies of the solute and solvent respectively, a is the area per surface atom.

The heat of segregation can also be calculated as an elastic lattice strain energy[107] as,

$$Q = \frac{24\pi KGr^3 \epsilon^2}{3K + 4G} \quad \ldots\ldots \quad [4.14]$$

where K is the bulk modulus of the solute, G is the shear modulus of the solvent, r is the average radius of a solvent and a solute atom, $(r_{solute} + r_{solvent})/2$ and ϵ is $(r_{solute} - r_{solvent})/r_{solute}$.

However, a modified Seah's expression for the heat of segregation has been reported recently by Berry et al.[166], which includes terms such as surface energies of the constituents, their enthalpy of mixing and the strain energy effects.

$$Q = 24(T_B^m - T_A^m) + 1.86\Omega + M \times 4.64 \times 10^7 \, r_B(r_A - r_B)^2 \text{ J/mole}$$

$$\ldots\ldots \quad [4.15]$$

where T_B^m and T_A^m are the melting temperatures of solvent and solute respectively. Ω = alloy parameter = $\Delta H_m / Z X_A^B X_B^B$, r = atomic radius in nm and M = 1 for $r_A > r_B$ and M = 0 for $r_A < r_B$.

If we assume that the heat of mixing (ΔH_m) = O in the case of Cu-Sn, Ag-Sn and Sb-Sn alloys, (which is reasonable assumption in the case of dilute alloys) the equation [4.15] reduces to

$$Q = 24(T_B^m - T_A^m) + M \times 4.64 \times 10^7 \, r_B \, (r_A - r_B)^2 \text{ J/mole} \quad \ldots\ldots \quad [4.16]$$

We have used the equations [4.12, 4.13 and 4.16] to calculate the heat of segregation of Sn in Cu-Sn, Ag-Sn and Sb-Sn alloys. The predicted values are compared with our experimental results (see Tables 4.6, 4.7 and 4.8).

Surprisingly none of the theories give satisfactory agreement with the experiment in case of Cu-Sn alloy. This discrepancy could arise either due to some deficiency in the theory, or some error in the values of the parameters, e.g. heat of sublimation, surface area and surface energy that we have used for the calculation (see Table 4.9).

In case of Ag-Sn alloy the sublimation energy approach gives the heat of segregation to be < -2.9 kcals/mole. This is not in agreement with the experimental value. This discrepancy may be due to the fact that the sublimation energy approach entirely neglects the strain energy

Table 4.6 : Comparison of the heats of segregation of Sn to the Cu-5% Sn alloy surface predicted by various theories and measured experimentally using XPS technique

Experimental (XPS technique)	:	12.0 ± 1.0 kcals/mole
Sublimation energy approach [Eqn. 4.12]	:	< 9.5 kcals/mole
Surface energy approach [Eqn. 4.13]	:	4.2 kcals/mole
Modified Seah's expression [Eqn. 4.16]	:	6.0 kcals/mole

Table 4.7 : Comparison of the heats of segregation of Sn to the Ag-5% Sn alloy surface predicted by various approaches and measured experimentally using XPS technique

Experimental (XPS technique)	:	3.5 ± 1.0 kcals/mole
Sublimation energy approach [Eqn. 4.12]	:	< -2.9 kcals/mole
Surface energy approach [Eqn. 4.13]	:	2.4 kcals/mole
Modified Seah's expression [Eqn. 4.16]	:	4.5 kcals/mole

Table 4.8 : Comparison of the heats of segregation of Sb to the Sb-5% Sn alloy surface predicted by various approaches and measured experimentally using XPS technique

Experimental (XPS technique)	:	1.3 ± 1.0 kcals/mole
Sublimation energy approach [Eqn. 4.12]	:	< 11.2 kcals/mole
Surface energy approach [Eqn. 4.13]	:	3.0 kcals/mole
Modified Seah's expression [Eqn. 4.16]	:	2.3 kcals/mole

Table 4.9 : The data used to calculate 'Q' values in Cu-Sn, Ag-Sn and Sb-Sn.

	Sn	Cu	Ag	Sb
Heat of sublimation[a] (kcals/mole)	72.00	81.50	69.10	60.80
Melting temperature (^{o}C)	232	1083	961	631
Atomic radius (nm)	0.158	0.128	0.144	0.160
Surface energy[b] (ergs/cm^2)	541	1484	1064	369
Surface area[b] (cm^2/mole)	6.89×10^8	3.70×10^8	4.30×10^8	6.67×10^8

a - Ref. 253
b - Ref. 96

released on segregation. The surface energy approach gives the heat of segregation for Ag-Sn alloy as 2.4 kcals/mole. This is in close agreement with the experimental value inspite of neglecting the strain energy effects while calculating the heat of segregation using equation [4.13]. However on using equation [4.16] the heat of segregation for Ag-Sn alloy turns out to be 4.5 kcals/mole. This is also quite close to the experimental value.

In case of Sb-Sn alloy the experimental heat of segregation of Sb is too low (Q = 1.3 $\pm$ 1.0 kcals/mole). But still this value is comparable with the values calculated from surface energy approach (Q = 3.0 kcals/mole) and modified Seah's expression (Q = 2.3 kcals/mole).

4.3.6 Comparison of heats of segregation in Cu-Sn and Ag-Sn alloys

The experimental Q values for Ag-Sn alloy is very low (Q = 3.5 $\pm$ 1.0 kcals/mole) as compared to that of Cu-Sn alloy (Q = 12.0 $\pm$ 1.0 kcals/mole). For Q values low in magnitude we expect less segregation. On the other hand, considerable segregation is expected to occur for higher values of Q. In fact this is confirmed by our experiment.

The major contributions to the heat of segregation in alloys are (1) due to the difference in heats of sublimation of the constituents and (2) due to the difference in the atomic radii of the constituents. The difference in heats of sublimation and the difference in the atomic radii. of Cu and Sn is considerably large as compared to the corresponding values for the Ag-Sn couple, so one can expect a higher Q value in Cu-Sn alloy as compared to Ag-Sn alloy.

4.4 Conclusions

(a) For the Cu-5% Sn alloy, Sn is found to segregate to the surface with a heat of segregation of 12.0 ± 1.0 kcals/mole in the temperature range of 300-500°C, whereas for the Ag-5% Sn alloy Sn is found to segregate to the surface with a heat of segregation of 3.5 ± 1.0 kcals/mole in the temperature range of 200-400°C.

On the other hand, in case of Sb-5% Sn alloy, Sb segregates to the surface with a very low heat of segregation of 1.3 ± 1.0 kcals/mole in the temperature range of 100-300°C.

(b) None of the existing theories of surface segregation give satisfactory agreement with the experimental value of Q for Cu-Sn alloy. On the other hand two of the existing theories (surface energy approach and modified

Seah's expression) of surface segregation give close agreement with the experimental value of Q for both Ag-Sn and Sb-Sn alloys.

(c) The concentration of Sn in Cu-Sn alloy varied from 5% in the bulk to more than 35% on the surface. However, the measurement of Sn composition on the Ag-Sn alloy varied from 5% in the bulk to more than 20% on the surface. On the other hand, in case of Sb-Sn alloy, there is only little variation in the concentration of Sb on the surface.

REFERENCES

1. R.I. Hegde and A.P.B. Sinha, Appl. Spectrosc. Rev., 19, (1983).

2. K. Siegbahn, C. Nordling, A. Fahlman, R. Nordberg, K. Hamrin, J. Hedman, G. Johansson, T. Bergmark, S.E. Karlsson, I. Lindgren and B. Lindberg, 'ESCA Atomic, Molecular and Solid State Structure Studies by Means of Electron Spectroscopy', Nova Acta Regiae Soc. Sci. Ups., Ser. IV, Vol. 20. Almqvist and Wiksell, Stockholm (1967).

3. K. Siegbahn, C. Nordling, G. Johansson, J. Hedman, P.F. Heden, K. Hamrin, U. Gelius, T. Bergmark, L.O. Werme, R. Manne and Y. Baer, 'ESCA Applied to Free Molecules', North-Holland Publ., Amsterdam (1969).

4. M.E. Schwartz, Chem. Phys. Lett., 6, 631 (1970).

5. M.E. Schwartz, J.D. Switalski and R.E. Stronski, in Electron Spectroscopy (ed. D.A. Shirley), North Holland, Amsterdam (1972) p. 605.

6. H. Basch, Chem. Phys. Lett., 5, 337 (1970).

7. W.L. Jolly and D.N. Hendrikson, J. Am. Chem. Soc., 92, 1836 (1970).

8. J.M. Hollander and W.L. Jolly, Acc. Chem. Res., 3, 193 (1970).

9. W.L. Jolly, in Electron Spectroscopy (ed. D.A. Shirley), North-Holland, Amsterdam (1972) p. 629.

10. D.W. Davis and D.A. Shirley, Chem. Phys. Lett., 15, 185 (1972).

11. D.A. Shirley, Chem. Phys. Lett., 16, 220 (1972).

12. W.L. Jolly, Faraday Discuss. Chem. Soc., 54, 13 (1972).

13. H. Siegbahn, R. Medeiros and O. Goscinski, J. Electron Spectrosc. Relat. Phenom., 8, 149 (1976).

14. P. Kelfve, B. Blomster, H. Siegbahn, K. Siegbahn, E. Sanhueza and O. Goscinski, Phys. Scr., 21, 75 (1980).

15. U. Gelius, P.F. Heden, J. Hedman, B.J. Lindberg, R. Manne, R. Nordberg, C. Nordling and K. Siegbahn, Phys. Scr., 2, 70 (1970).

16. R.I. Hegde, S.R. Sainkar, S. Badrinarayanan and A.P.B. Sinha, J. Electron Spectrosc. Relat. Phenom., 24, 19 (1981).

17. R.I. Hegde, S.R. Sainkar and S. Badrinarayanan, Proceedings of the Symposium on Surface and Interface Properties in Materials Sciences, University of Roorkee, India (1980) p. 125.

18. R.I. Hegde, Surf. Interface Anal., 4, 204 (1982).

19. R.I. Hegde and A.P.B. Sinha, Surf. Sci., (In Press).

20. P. Wynblatt and R.C. Ku, Interfacial Segregation (eds., W.C. Johnson and J.M. Blakely), American Society for Metals, Ohio (1979).

21. M.P. Seah, J. Catal., 57, 450 (1979).

22. M.P. Seah, Analusis, 5, 171 (1981).

23. C.J. Powell, Appl. Surf. Sci., 4, 492 (1980).

24. P.M. Hall and J.M. Morabito, Surf. Sci., 83, 391 (1979).

25. S.D'Ageostino, Hist. Stud. Phys. Sci., 6, 261 (1975).

26. A. Einstein, Ann. Phys. (Leipzig), 17, 132 (1905).

27. E. Rutherford and H. Robinson, Philos. Mag., 26, 717 (1913).

28. J.G. Jenkin, R.C.G. Leckey and J. Liesegang, J. Electron Spectrosc. Relat. Phenom., 12, 1 (1977).

29. R.G. Steinhardt, Jr., 'An X-ray Photoelectron Spectrometer for Chemical Analysis', Ph.D. Thesis, Lehigh Univ., Bethleham, Pennsylvania (1950).

30. R.G. Steinhardt and E.J. Surfass, Anal. Chem., 25, 697 (1953).

31. C.J. Powell, Surf. Sci., 44, 29 (1974).

32. I. Lindau and W.E. Spicer, J. Electron Spectrosc. Relat. Phenom., 3, 409 (1974).

33. J. Hedman, P.F. Heden, C. Nordling and K. Siegbahn, Phys. Lett., 29A, 178 (1969).

34. C.S. Fadley, D.A. Shirley, A.J. Freeman, P.S. Bagus and J.V. Mallow, Phys. Rev. Lett., 23, 1397 (1969).

35. J.C. Carver, G.K. Schweitzer and T.A. Carlson, J. Chem. Phys., 57, 973 (1972).

36. R.N. Dixon, Mol. Phys., 20, 113 (1971).

37. S. Evans, J.C. Green, P.J. Joachim, A.F. Orchard, D.W. Turner and J.P. Maier, J. Chem. Soc. Faraday Trans. II, 68, 905 (1972).

38. J.H.D. Eland, 'Photoelectron spectroscopy', Halsted Press, Wiley and Sons, New York (1975).

39. T.A. Carlson, Phys. Rev., 156, 142 (1967).

40. M.O. Krause, T.A. Carlson and R.D. Dismukes, Phys. Rev., 170, 37 (1968).

41. T.A. Carlson, M.O. Krause and W.E. Moddeman, J. de. Phys., 32, C4 76 - C4 84 (1971).

42. C.D. Wagner, J. Electron Spectrosc. Relat. Phenom., 10, 305 (1977).

43. A. Rosencwaig, G.K. Wertheim and H.J. Guggenheim, Phys. Rev. Lett., 27, 479 (1971).

44. W.J. Pardee, G.D. Mahan, D.E. Eastman, R.A. Pollak, L. Ley, F.R. McFeely, S.P. Kowalczyk and D.A. Shirley, Phys. Rev., B11, 3614 (1975).

45. K. Siegbahn, D. Hammond, H. Fellner-Feldegg and E.F. Barnett, Science, 176, 245 (1972).

46. R.E. Watson and M.L. Perlman, in Structure and Bonding, Vol. 24, (ed. J.D. Dunitz), Springer, Berlin (1975).

47. J. Hedman, M. Klasson, R. Nilsson, C. Nordling, M.F. Sorokina, O.I. Kljushnikov, S.A. Nemnonov, V.A. Trapeznikov and V.C. Zyryanov, Phys. Scr., 4, 1 (1971).

48. S. Hufner, G.K. Wertheim and J.H. Wernick, Solid State Commun., 11, 259 (1972).

49. S. Hufner, G.K. Wertheim and J.H. Wernick, Solid State Commun., 17, 1585 (1975).

50. J.A. Nicolson, J.D. Riley, R.C.G. Leekey, J.G. Jenkin and J. Liesegang, J. Electron Spectrosc. Relat. Phenom., 15, 95 (1979).

51. Photoemission in Solid I and II Topics in Applied Physics, edited by M. Cardona and L. Ley (Springer, Berlin, 1978) Vols. 26 and 27.

52. R.M. Friedman, J. Hudis, M.L. Perlman and R.E. Watson, Phys. Rev., B8, 2433 (1973).

53. R.E. Watson, J. Hudis and M.L. Perlman, Phys. Rev., B4, 4139 (1971).

54. R. Bouwman and P. Biloen, Anal. Chem., 46, 136 (1974).

55. C.L. Kanekar, K.R.P. Mallikarjuna Rao and V. Udaya Shankar Rao, Phys. Lett., 19, 95 (1965).

56. G.G. Kleiman, V.S. Sundaram, C.L. Barrets and J.D. Rogers, Solid State Commun., 32, 919 (1979).

57. V.S. Sundaram, C.L. Barreto, T.D. Rogers and G.G. Kleiman, Physica Stat. Sol., 94, XXXX (1979).

58. K.S. Kim and N. Winograd, Chem. Phys. Lett., 30, 91 (1975).

59. P.H. Citrin and D.R. Hamann, Chem. Phys. Letters, 22, 301 (1973).

60. P.H. Barett, R.W. Grant, M. Kaplan, D.A. Keller and D.A. Shirley, J. Chem. Phys., 39, 1035 (1963).

61. L.D. Roberts, R.L. Becker, F.E. Obenshain and J.O. Thomson, Phys. Rev., 137A, 895 (1965).

62. T.J. Kirthlink Jr., G.P. Hurray and J.O. Thomson, Bull. Am. Phys. Soc., 16, 606 (1971).

63. R.L. Cohen, Y. Yafet and K.W. West, Phys. Rev., B3, 3872 (1971).

64. P. Steiner, S. Hufner, N. Martensson and B. Johansson, Solid State Commun., 37, 73 (1981).

65. N. Martensson and B. Johansson, Solid State Commun., 32, 791 (1979).

66. B. Johansson and N. Martensson, Phys. Rev., B21, 4427 (1980).

67. A.R. Miedema, J. Less Common Metals, 46, 67 (1976).

68. A.R. Miedema, J. Less Common Metals, 32, 117 (1973).

69. N. Martensson, R. Nyholm, H. Calen and J. Hedman, Phys. Rev., B24, 1725 (1981).

70. P. Steiner and S. Hufner, Solid State Commun., 37, 79 (1981).

71. R. Hultgren et al., 'Selected Values of Thermodynamic Properties of Metals and Alloys', John Wiley and Sons, New York (1963).

72. A.R. Miedema, P.F. de Chatel and F.R. de Boer, Physica 100 B, 1 (1980).

73. P. Fulde, A. Luther and R.E. Watson, Phys. Rev., B8, 440 (1973).

74. J.E. Houston, R.L. Park and G.E. Laramore, Phys. Rev. Lett., 30, 846 (1973).

75. B. Johansson, Phys. Rev., B19, 6615 (1979).

76. M.C. Desjonqueres, D. Spanjaard, Y. Lassailly and C. Guillot, Solid State Commun., 34, 807 (1980).

77. A. Rosengren and B. Johansson, Phys. Rev., B22, 3706 (1980).

78. B. Johansson and N. Martensson, Phys. Rev., B21, 4427 (1980).

79. P. Heimann, J.F. van der Veen and D.E. Eastman, Solid State Commun., 38, 595 (1981).

80. A. Rosengren, Phys. Rev., B24, 7393 (1981).

81. D. Chadwick and M.A. Karolewski, J. Electron Spectrosc. Relat. Phenom., 24, 181 (1981).

82. P.H. Citrin, G.K. Wertheim and Y. Baer, Phys. Rev. Lett., 41, 1425 (1978).

83. T.M. Duc, C. Guillot, Y. Lassailly, J. Lecante, Y. Jugnet and J.C. Verdrine, Phys. Rev. Lett., 43, 789 (1979).

84. J.F. van der Veen, P. Heimann, F.J. Himpsel and D.E. Eastman, Solid State Commun., 37, 555 (1981).

85. S.F. Alvarado, M. Compagna and W. Gudak, J. Electron Spectrosc. Relat. Phenom., 18, 43 (1980).

86. J.F. van der Veen, F.J. Himpsel and D.E. Eastman, Phys. Rev. Lett., 44, 189 (1980).

87. F.J. Himpsel, P. Heimann, T.C. Chiang and D.E. Eastman, Phys. Rev. Lett., 45, 1112 (1980).

88. S. Brennan, J. Stohr, R. Jaeger and J.E. Rowe, Phys. Rev. Lett., 45, 1414 (1980).

89. P. Steiner and S. Hufner, Solid State Commun., 37, 279 (1981).

90. D.E. Eastman, T.C. Chiang, P. Heimann and F.J. Himpsel, Phys. Rev. Lett., 45, 656 (1980).

91. J.W. Davenport, R.E. Watson, M.L. Perlman and T.K. Sham, Solid State Commun., 40, 999 (1981).

92. R.E. Watson, M.L. Perlman, J.W. Davenport and T.K. Sham, Solid State Commun., 41, 151 (1982).

93. R.E. Watson, J.W. Davenport, M.L. Perlman and T.K. Sham, Phys. Rev., B24, 1791 (1981).

94. J.W. Gibbs, Trans. Conn. Acad. Arts Sci., 3, 103 (1875/1876) and 3, 343 (1877/1878).

95. T. Takeuchi and M. Sakaguchi, Bull. Chem. Soc. Japan, 30, 177 (1957).

96. S.H. Overbury, P.A. Bertrand and G.A. Somorjai, Chem. Rev., 75, 547 (1974).

97. W.M.H. Sachtler and R.A. van Santen, Adv. Catal., 26, 69 (1977).

98. M.P. Seah, Surf. Sci., 80, 8 (1979).

99. G.A. Somorjai, Principles of Surface Chemistry, Prentice-Hall, New York (1972).

100. D. Kumar, A. Mukherjee and V. Kumar, J. Phys., F6, 725 (1976).

101. G. Kerker, J.L. Moran-Lo'pez and K.H. Bennemann, Phys. Rev., B15, 638 (1977).

102. F.F. Abraham, N.H. Tsai and G.M. Pound, Surf. Sci., 83, 406 (1979).

103. J.L. Meijering, Acta Metall., 14, 251 (1966).

104. R.A. van Santen and M.A.M. Boersma, J. Catal., 34, 13 (1974).

105. F.L. Williams and D. Nason, Surf. Sci., 45, 377 (1974).

106. R. Bouwman, L.H. Toneman, M.A.M. Boersma and R.A. van Santen, Surf. Sci., 59, 72 (1976).

107. D. McLean, 'Grain Boundaries in Metals', Clarendon Press, Oxford, (1957).

108. R. Bouwman and W.M.H. Sachtler, J. Catal., 19, 127 (1972).

109. J.J. Burton and E.S. Machlin, Phys. Rev. Lett., 37, 1433 (1976).

110. N.H. Tsai, F.F. Abraham and G.M. Pound, J. Catal., 50, 200 (1977).

111. R.P. Gupta and B. Perraillon, Surf. Sci., 103, 397 (1981).

112. Ph. Dumoulin, J.L. Caillerie and M. Guttmann, Surf. Sci., 104, 559 (1981).

113. K. Wandelt and C.R. Brundle, Phys. Rev. Lett., 46, 1529 (1981).

114. R. Holm and S. Storp, J. Electron Spectrosc. Relat. Phenom., 8, 139 (1976).

115. J.C. Hamilton, Phys. Rev. Lett., 42, 989 (1979).

116. C.A. Balseiro and J.L. Moran Lopez, Phys. Rev., B21, 349 (1980).

117. Ph. Lambin and J.P. Gaspard, J. Phys. F10, 2413 (1980).

118. F.F. Abraham, Phys. Rev. Lett., 46, 546 (1981).

119. F.F. Abraham and C.R. Brundle, J. Vac. Sci. Technol., 18, 506 (1981).

120. C.C. Chang, Surf. Sci., 25, 53 (1971).

121. G.C. Nelson, J. Vac. Sci. Technol., 13, 512 (1976).

122. G.C. Nelson, Surf. Sci., 59, 310 (1976).

123. A. Benninghoven, Surf. Sci., 35 427 (1973).

124. J.E. Holliday and R.P. Frankenthal, J. Electrochem. Soc., 119, 1190 (1972).

125. W.M.H. Sachtler, G.I.H. Dorgelo and R. Jongepier, J. Catal., 4, 100 (1965).

126. W.M.H. Sachtler and G.I.H. Dorgelo, J. Catal., 4, 645 (1965).

127. W.M.H. Sachtler and R. Jongepier, J. Catal., 4, 665 (1965).

128. D.A. Cadenhead and N.J. Wagner, J. Catal., 27, 475 (1972).

129. R. Bouwman, G.T.M. Lippits and W.M.H. Sachtler, J. Catal., 25, 350 (1972).

130. S.C. Fain, Jr., and J.M. McDavid, Phys. Rev., B9, 5099 (1974).

131. S.H. Overbury and G.A. Somorjai, Surf. Sci., 55, 209 (1976).

132. B.E. Sundquist, Acta Metal., 12, 585 (1964).

133. P. Braun and W. Farber, Surf. Sci., 47, 57 (1975).

134. J.M. McDavid and S.C. Fain Jr., Surf. Sci., 52, 161 (1975).

135. H.C. Potter and J.M. Blakely, J. Vac. Sci. Technol., 12, 635 (1975).

136. B.J. Wood and H. Wise, Surf. Sci., 52, 151 (1975).

137. G. Maire, L. Hilaire, P. Legare, F.G. Gault and A.O. Cinneide, J. Catal., 44, 293 (1976).

138. A. Jablonski, S.H. Overbury and G.A. Somorjai, Surf. Sci., 65, 578 (1977).

139. T. Khikawa, Phys. Stat. Sol. (a), 32, 369 (1975).

140. S.H. Overbury and G.A. Somorjai, J. Chem. Phys., 66, 3181 (1977).

141. F.L. Williams and M. Boundart, J. Catal., 33, 438 (1973).

142. J.J. Burton, C.R. Helms and R.S. Polizzotti, J. Chem. Phys., 65, 1089 (1976).

143. J.J. Burton, C.R. Helms and R.S. Polizzotti, J. Vac. Sci. Technol., 13, 204 (1976).

144. V. Kumar, Surf. Sci., 84, L 231 (1979).

145. P. Wynblatt and R.C. Ku, Surf. Sci., 65, 511 (1977).

146. A.I. Saadoon, W. Richard, Joyner and M.W. Roberts, J. Chem. Soc. Faraday Trans. I, 72, 540 (1976).

147. S. Thomas, Appl. Phys. Lett., 24, 1 (1974).

148. W.K. Hall, J. Catal., 6, 314 (1966).

149. D.A. Cadenhead and N.J. Wagner, J. Phys. Chem., 72, 2775 (1968).

150. J. Takasu, S. Maru, J. Matsuda and H. Shimizu, Bull. Chem. Soc.Japan, 48, 219 (1975).

151. P.R. Webber, C.E. Rojas, P.J. Dobson and D. Chadwick, Surf. Sci., 105, 20 (1981).

152. C.R. Helms and K.Y. Yu, J. Vac. Sci. Technol., 12, 276 (1976).

153. P.S. Ho, J.E. Lewis and J.K. Howard, J. Vac. Sci. Technol., 14, 322 (1977).

154. K. Nakayama, M. Ono and H. Shimizu, J. Vac. Sci. Technol., 9, 749 (1972).

155. H. Shimizu, M. Ono and K. Nakayama, Surf. Sci., 36, 817 (1973).

156. M.L. Tarng and G.K. Wehner, J. Appl. Phys., 42, 2449 (1971).

157. K. Watanabe, M. Hashiba and T. Yamashina, Surf. Sci., 61, 483 (1976).

158. K. Watanabe, M. Hashiba and T. Yamashina, Surf. Sci., 69, 721 (1977).

159. T.L. Barr, Chem. Phys. Lett., 43, 89 (1976).

160. K. Hirokowa and M. Oku, Talanta, 25, 539 (1978).

161. J. Ferrante, Acta Met., 19, 743 (1971).

162. D. Tomanek, S. Mukherjee, V. Kumar and K.H. Bennemann, Surf. Sci., 114, 11 (1982).

163. J. Ferrante, NASA TND - 6982 (1973).

164. J.C. Shelton, H.R. Patil and J.M. Blakely, Surf. Sci., 43, 493 (1974).

165. K. Wandelt and G. Ertl, Z. Naturforsch., 31, 205 (1976).

166. C. Berry, D. Majumdar and Y.W. Chung, Surf. Sci., 94, 293 (1980).

167. G.D. Parks, Appln. Surf. Sci., 5, 92 (1980).

168. W.E. Baitinger et al., Am. Proc. Reliab. Phys., 12, 1 (1974).

169. V. Krasevec and B. Navinsek, Surf. Sci., 45, 39 (1974).

170. P. Biloen, R. Bouwman, R.A. van Santen and H.H. Brongersma, Appln. Surf. Sci., 2, 532 (1979).

171. H.J. Grabke, W. Paulitschke, G. Tauber and H. Veifhaus, Surf. Sci., 63, 377 (1977).

172. A. Joshi, P.W. Palmberg and D.F. Stein, Metal. Trans., 6A, 2160 (1975).

173. K. Wandelt and G. Ertl, J. Phys., F6, 1607 (1976).

174. R.A. Pollak and C.H. Bajorek, J. Appl. Phys., 46, 1382 (1975).

175. R.S. Polizzotti and J.J. Burton, J. Vac. Sci., 14, 347 (1977).

176. C. Leygraf, G. Hultquist, S. Ekelund and J.C. Eriksson, Surf. Sci., 46, 157 (1974).

177. M.P. Seah and C. Lea, Philos. Mag., 31, 627 (1975).

178. D.H. Buckley, NASA TND - 6359 (1971).

179. R.L. Moss and D.H. Thomas, J. Catal., 8, 151 (1967).

180. J.J. Burton, Surf. Sci., 69, 712 (1977).

181. J.A. Schwarz, R.S. Polizzotti and J.H. Burton, J. Vac. Sci. Technol., 14, 457 (1977).

182. J.H. Anderson Jr., P.J. Conn and S.G. Brandenberger, J. Catal., 16, 326 (1970).

183. J.J. Burton and R.S. Polizzotti, Surf. Sci., 66, 1 (1977).

184. J.C. Hamilton and J.M. Blakely, J. Vac. Sci. Tech., 15, 559 (1978).

185. J.C. Hamilton and J.M. Blakey, Surf. Sci., 91, 199 (1980).

186. F.L. Williams and G.C. Nelson, Appl. Surf. Sci., 3, 409 (1979).

187. R. Bouwman, L.H. Tonemann and A.A. Holscher, Surf. Sci., 35, 8 (1973).

188. R. Bouwman and P. Biloen, Surf. Sci., 41, 348 (1974).

189. J.H. Anderson, Jr., P.J. Conn and S.G. Brandenberger, J. Catal., 16, 404 (1970).

190. R.J. Bird, Metal Sci. J., 7, 109 (1973).

191. S. Berglund and G.A. Somorjai, J. Chem. Phys., 59, 5537 (1973).

192. G.L. Powell, R.E. Clausing and G.E. McGuire, Surf. Sci., 49, 310 (1975).

193. P.E.C. Franken and V. Ponec, J. Catl., 35, 417 (1974).

194. L.C. Isett and J.M. Blakey, Surf. Sci., 58, 397 (1976).

195. D.T. Quinto, V.S. Sundaram and W.D. Robertson, Surf. Sci., 28, 504 (1971).

196. M.C. Tarmg and G.K. Wehner, J. Appl. Phys., 42, 2449 (1971).

197. M. Ono, Y. Lakasu, K. Nakayama and T. Yamashina, Surf. Sci., 26, 313 (1971).

198. M. Kundo et al., Bunseki Kagaku, 26, (3), 173 (1977).

199. G.J. Slusser and N. Winograd, Surf. Sci., 84, 211 (1979).

200. G. Betz, J. Dudonis and P. Braun, Surf. Sci., 104, L 185 (1981).

201. J.W. Coburn, Thin Solid Films, 64, 371 (1979).

202. R.P. Frankenthal and D.J. Siconolfi, Surf. Sci., 104, 205 (1981).

203. P.S. Ho and J.E. Lewis, Surf. Sci., 55, 335 (1976).

204. P.H. Holloway, Surf. Sci., 66, 479 (1977).

205. A. Van Oostram, J. Vac. Sci. Technol., 13, 224 (1976).

206. Z.L. Liau, W.L. Brown, R. Homer and J.M. Poati, Appl. Phys. Lett., 30, 626 (1977).

207. P.H. Holloway and R.S. Bhattacharya, Surf. Interface Anal., 3, 118 (1981).

208. A.W. Adamson, Physical Chemistry of Surfaces, Wiley, New York (1967).

209. J.J. Burton and E. Hyman, J. Catal., 37, 114 (1975).

210. R.A. van Santen and W.M.H. Sachtler, J. Catal., 33, 202 (1974).

211. J.J. Burton, E. Hyman and D. Fedak, J. Catal., 37, 106 (1975).

212. J.J. Burton, C.R. Helms and R.S. Polizzotti, J. Chem. Phys., 65, 1089 (1976).

213. V.S. Sundaram and P. Wynblatt, Surf. Sci., 52, 569 (1975).

214. A.R. Miedema, Z. Metallk., 69, 455 (1978).

215. R.A. van Santen, L.H. Toneman and R. Bouwman, Surf. Sci., 47, 64 (1975).

216. M. Guttmann, Surf. Sci., 53, 213 (1975).

217. M. Guttmann, Mater. Sci. Eng., 42, 227 (1980).

218. M. Guttmann, Phil. Trans. Roy. Soc. London, A295, 169 (1980).

219. M. Guttamann and D. McLean, Interfacial Segregation, (ASM, Metals Park, Ohio, 1979) p. 261.

220. Ph. Dumoulin and M. Guttmann, Mater. Sci. Eng., 42, 249 (1980).

221. R. Bouwman, G.J.M. Lippists and W.M.H. Sachtler, J. Catal., 25, 350 (1972).

222. L. Hilaire, P. Legare, Y. Holl and G. Maire, Surf. Sci., 103, 125 (1981).

223. M. Bettini and H.J. Richter, Surf. Sci., 80, 334 (1979).

224. A. Yanagisawa and M. Namba, Japan J. Appl. Phys., 12, 748 (1973).

225. L.D. Huelett, A.L. Bacarella, L. LiDonnici and J.C. Griess, J. Electron Spectrosc. Relat. Phenom., 1, 169 (1972).

226. J.E. Castle, Nature Phys. Sci., 93, 234 (1971).

227. J.E. Castle and M. Narserian, Corr. Sci., 15, 537 (1975).

228. R. Bouwman, Gold Bull., 11, 81 (1978).

229. V.M. Gryaznov, Proc. Int. Congr. Catal. 6th 1976 (Pub. 1977) 2, 894 (Eng.).

230. K. Asami et al., Corrs. Sci., 17, 713 (1977).

231. M.O. Krause and J.G. Ferreira, J. Phys., B8, 2007 (1975).

232. N. Winograd and S.W. Gaarenstroom, X-ray Photoelectron Spectroscopy in Physical Methods in Modern Chemical Analysis, ed. Theodore Kuwana, Academic Press, N.Y. (1980) p. 122.

233. G. Johansson, J. Hedman, A. Berndtsson, M. Klasson and R. Nilsson, J. Electron Spectrosc. Relat. Phenom., 2, 295 (1973).

234. P.H. Watts and J.E. Huheey, Inorg. Nucl. Chem. Lett., 10, 287 (1974).

235. L. Porte and J.C. Maire, Solid State Commun., 33, 481 (1980).

236. C.R. Brundle, T.J. Chaung and K. Wandelt, Surf. Sci., 68, 459 (1977).

237. C. Tyzack and G.V. Raynor, Acta Cryst., 7, 505 (1954).

238. W.H. Rothery, G.F. Lewin and P.W. Reynolds, Proc. Roy. Soc. (London), A157, 167 (1936).

239. W.H. Rothery and G.V. Raynor, The Structure of Metals and Alloys, Institute of Metals, London (1962) p. 56.

240. R. Holm and S. Storp, J. Electron Spectrosc. Relat. Phenom., 6, 459 (1976).

241. R. Nyholm and N. Martensson, J. Phys. C., 13, L279 (1980).

242. C.J. Powell, N.E. Erickson and T.E. Madey, J. Electron Spectrosc. Relat. Phenom., 17, 311 (1979).

243. M.C. Hayes, J. Inorg. Nucl. Chem., 26, 915 (1964).

244. J.P. Bocquet, Y.Y. Chu, O.C. Kistner, M.L. Perlman and G.T. Emery, Phys. Rev. Lett., 17, 809 (1966).

245. J.K. Lees and P.A. Flinn, J. Chem. Phys., 48, 882 (1968).

246. R.H. Herber and H.S. Cheng, Inorg. Chem., 8, 2145 (1969).

247. D.D. Sarma and C.N.R. Rao, J. Electron Spectrosc. Relat. Phenom., 20, 25 (1980).

248. H.B. Gray, Chemical Bonds, An Introduction to Atomic and Molecular Structure, W.A. Benjamin Inc., U.S.A. (1973) p. 56.

249. D. Briggs, (ed.) Handbook of X-rays and Ultraviolet Photoelectron Spectroscopy (Heyden, London 1977).

250. M.P. Seah and W.A. Dench, Surface and Interface Anal., 1, 1 (1979).

251. C.J. Powell, Appl. Surf. Sci., 4, 492 (1980).

252. S. Badrinarayanan, R.I. Hegde, I. Balakrishnan, S.B. Kulkarni and P. Ratnasamy, J. Catal., 71, 439 (1981).

253. F.D. Rossini (ed.) Selected Values of Chemical Thermodynamic Properties, Circular 500, issued by National Bureau of Standards (1952).

254. J. Crank, The Mathematics of Diffusion, Clarendon, Oxford (1967).

*****